PhD Thesis in Physics

Local Stimulation of Cell Signals in Single Cells

Written by

Haleh Ebrahimian

Department of Physics
Bielefeld University
November 2012

تقدیم به امیر

مهربان فرشته زندگی ام

Dedicated to Amir

My loving angel

Examining Committee:

Prof. Dr. Guenter Reiss

Prof. Dr. Walter Pfeiffer

Prof. Dr. Peter Reimann

Prof. Dr. Thomas Huser

Submitted to Bielefeld University

Printed, Nov 2012

Declaration

I hereby declare that this thesis is written by me and used none but the indicated resources.

Haleh Ebrahimian

Acknowledgments

I am grateful for being accepted to work in Local stimulation of cell signals in single cells project, for the interesting topic of the thesis that has been attributed to me. Without the continuous help from all the coworkers in the D2 group, this thesis could not be possible. I would like to thank especially to my supervisors **Prof. Dr. Günter Reiss, Prof. Dr. Karl-Josef Dietz** and **Dr. Simone Herth**. Particularly, I would like to thank **Dr. Karsten Rott** for introducing me in the lab work and for his perpetual patience with me. His knowledge and thrust offer me the foundation for the work done throughout this thesis.

Moreover, I would like to thank to **A.G.Venkatesh** for his helpful and suggestive comments during my work. Notably I would like to thank **Miriam Giesguth** and **Martina Holt** for the atmosphere they introduced in the biology group. I would like to thank to all the persons responsible for the machines that had to be utilized for the work of the thesis. Without their great care and proper maintenance a lot from this work could not be done. I would like to thank for all D2 members.

Last, but not least I would like to thank my spouse, family and friends for their permanent reinforcements they provide throughout the years.

List of Publications

Articles

Submitted

"New setup of a magnetic tweezer to determine viscosities of cell interiors" ***Haleh Ebrahimian***, Günter Reiss, Karl-Josef Dietz, Simone Herth (Submitted)

"*Thermo capillaries as temperature biosensor in single cells and generator of local temperature stimuli in cell signaling".** Simone Herth, Miriam Giesguth, ***Haleh Ebrahimian, Günter Reiss and Karl-Josef Dietz (Submitted)

Published

"Effect of nitrogen ion implantation on corrosion Resistance of Ti films deposited on steel 304 by ion beam sputtering" ***H. Ebrahimian****, M. Ghoranneviss, A.Shokouhy, M. Yari, M. Eshghabadi and D.Hanifeh published in" plasma and fusion research series" journal (Vol.8 , 30 September 2009)

Conferences

"Molecular Sensor for H_2O_2 Stress in Single Cells", Miriam Giesguth, ***Haleh Ebrahimian***, Simone Herth, Günter Reiss, and Karl-Josef Dietz SFB 613 – International Symposium, September 27-28, 2012,Germany (poster)

"Manipulation of Particles Inside Cells for Analyzing or Triggering Local Effects" , ***Haleh Ebrahimian***, G. Reiss, K.J. Dietz, S. Herth , XI International Conference on Nanostructured materials, Rodos, August 26-31, 2012 , Greece (Oral)

"Manipulation of magnetic particles in living cells" ***H. Ebrahimian****,* M. Giesguth, J.R. Schubert, G. Reiss, K-J. Dietz, S. Herth**,** DPG spring meeting 2011, Dresden, Germany (poster)

"Thermal measurement in single cells" Simone Herth, Miriam Giesguth, ***Haleh Ebrahimian****,* Günter Reiss and Karl-Josef Dietz**,** DPG spring meeting 2011, Dresden, Germany (oral)

"**Thermocapillaries As Sensors and Actors in Cell Biology",** Miriam Giesguth, Simone Herth, ***Haleh Ebrahimian***, Günter Reiss and Karl-Josef Dietz Botaniker Tagung 2011 18-23 September, Berlin, Germany (poster)

"**Thermocapillaries As Sensors and Actors in Cell Biology"** Miriam Giesguth, Simone Herth, ***Haleh Ebrahimian***, Günter Reiss and Karl-Josef Dietz Photosynthese Workshop 2011, 11-12 August, Munchen, Germany

"**Effect Of nitrogen ion implantation on corrosion Resistance of Ti films deposited on steel 304 by ion beam sputtering"** ***H. Ebrahimian***, M. Ghoranneviss, A. Shokouhy , M. Yari, M. Eshghabadi, Conference icpp 2008, Fokouka, Japan

Table of Contents

List of Figures

Abstract

Magnetic tweezers gained increasing interest in recent years especially for applications in biology. In this thesis, a new setup of a magnetic tweezer is introduced using micropatterned conducting lines on a transparent glass slide and magnetic particles with a diameter of 1 µm injected into the vacuole of barley protoplast using a microinject system and controlled through an inverse fluorescent microscope.

The setup enables a precise localization of the particles, which can be functionalized or fluorescently labeled at their surface, and the determination of forces in viable cells. The setup was utilized to determine the viscosity of vacuolar sap of barley (Hordeum vulgare) and compare it with the viscosity of water and the vacuolar fluid outside the cell. The viscosity of the vacuolar sap in living cells was about 5 times higher than that of water, and this compared to a 2-fold higher viscosity of extracted vacuolar fluid.

Also local heating inside the A. thaliana cell was done by means of applying electric voltage to a ThermoMicroCapillary in order to detect ROS generation as a sign of cell response to the heat stress. In addition chemical oxidative stress studied by injecting the functionalized particle inside the A. thaliana cell.

Furthermore, the marker dicarboxy fluorescein diacetate (DCF-DA) fed to the cell to detect DCF light emitted as a reporter of (ROS) heat stress or chemical oxidative stress.

Chapter 1: Introduction

"Biological sciences are entering a completely new phase. Genomics, proteomics, and metabolomics have provided us a long list of components such as physical and chemical reactions that occur in a living cell."[1]

"A variety of techniques have been developed to investigate and study the localization, dynamics, and physical or chemical interactions of molecules inside the living cells."[1] In recent years, the Lab-On-a-Chip (LOC) systems have been developed and miniaturized for hand held applications.[2] This system also can be extended for the analysis of heat or chemical stress in a living cell.

Research interests in manipulation and positioning of magnetic particles inside living cells has been growing in recent years in various biophysics experiments with single cells, DNA, enzymes or proteins. The proposed solution of this work provides new opportunities for cell signaling and functionalized particle studies. The main goal for such experiments is to study the ability of cells in receiving and responding to environmental stress like heat stress, chemical oxidative stress, heavy metals etc. Environmental stress in a biosystem could cause severe damages and generate strong molecular response. The importance of such experiments to provide studies of the behavior of different cells in different environments because stress and diseases often cause disturbances in cell metabolism with concomitant cellular redox imbalances and production of reactive oxygen species (ROS).

Contactless effects of the magnetic forces on the magnetic particle inside the cell can be manipulated distantly, without damaging the cell, these providing realistic mechanical or physical characteristics of the cell.

According to the most recent model on heat shock mechanism, the activation occurs by trimerisation[3] of monomers called heat shock factors, which can then enter the nucleus to start the gene expression of heat shock proteins. Heat shock proteins are (HSPs) also involved in protein folding i.e., help other proteins to fold again in the correct way and they can be tagged with fluorescent proteins as reporter for heat stress.[4]

The aim of this thesis is to activate the cell signals locally by means of heat or chemical stress using a magnetic or functionalized particle or Thermomicrocapillary (TMC).

This thesis consists of three main parts:

- Injection and positioning of magnetized particles in a specific location inside a living cell by magnetic force.
  Three major activities were involved in this part: (I) trapping the cell using a holding capillary, (II) injection of the magnetic particle by Intra Cytoplasmic Sperm Injection (ICSI) capillary and (III) positioning of the particle inside the cell by means of high magnetic field generated by electrodes. The results of this experiment could be used to determine viscosity of the cell vacuole's inner-space and to deduce characteristic diffusion times through a vacuole for various molecules and proteins as well.

- Temperature stimulation in cell signaling
  The ThermoMicroCapillary (TMC) used to induce the local heat shock stimulation into *A. thaliana* single cell fed with 2',7'-dichlorodihydrofluorescein diacetate (H_2DCF-DA). Activities in this step were preparation and calibration of thermomicrocapillary (TMC) as a stable heat generator. Negative control experiments were done to prove the results of the heating experiments are due to heat shock stimulation by TMC inside the cell.

- Local stimulation of cell signals by functionalized particle
  The intention of this step is to study the oxidative stress with a functionalized magnetic particle. This experiment includes preparation of the functionalized particle and implementation of several positive and negative control experiments to prove that the results of the experiment are due to chemical oxidative stress.

This work is presented in five chapters, starting with this chapter as the introduction to the work. Some information regarding the background of the work are gathered in the second chapter and present along with basic information about the principles and the concepts of the work also a brief description of the hardware facilities and various systems used during the experiments. Specifications and functions of each system are also described in details for easier understanding of methodology of each experiment. Details of the materials, instruments and the methods utilized in various experiments are provided in the third chapter. Results of the experiments are presented and described in chapter four, and finally analysis and discussions of the results are covered in chapter five.

Summary of each work and future plans are very important topics in presentation of any type of research work, therefore a description about each of these subjects are provided in separate sections after the fifth chapter, briefing the whole scope of the research along with expected developments in this field.

Chapter 2: Background

This chapter covers an overview of the basic concepts, relevant knowledge, principles and the background behind various methods utilized for different experiments. Physical knowledge is necessary for various calculations including magnetic force and heat generation calculations as well as biological background for preparation of the cells and understanding of cell signaling.

2.1 *Cell signaling*

"Cell signaling is a core biological process. The survival of an organism whether single cell or multi cellular, plant or animal, strongly depends on its ability to receive and respond to stimuli such as oxidative stress, heavy metals and heat stress together with cell damaging agents and pathogens presented by the environment."[105] "Stress responses of plants are studied experimentally since the middle of the 19th century (Sachs 1864; Müller-Thurgau 1980)."[5]

"Plants show a great ability to adapt their metabolism to rapid changes in the environment. For this purpose, they are equipped with complex processes, such as perception transduction and transmission of stress stimuli.[6]In their adaptation to the environment, plants have a specific mechanism increasing their reaction to the action of a stress stimulus. It induces their proper defense even when the initial strength of the stress is small, e.g. by a puncture or virus infection, which, in further perspective can be a great threat to their existence. Such a mechanism, related to the perception of stimuli and their expansion in cells, between organs and organisms, is composed of biochemical processes intensifying the action of particular signaling pathways. In any plant, species exist in more than one form of enzymes involved in biosynthesis of particular signaling molecules enhancing the stress reaction response."[7]

"Signal transduction pathways in plants are very well developed while at the same time they are extremely complex to reveal all the cross talks. The simple reason behind these complexities is that the plants are sessile and experiences all cue, biotic or abiotic being stationed at one position. Signaling pathways are induced in response to environmental stresses, and recent molecular and genetic studies have revealed that these pathways involve a host of diverse responses.[110,111] It has been well established that abiotic stress response is a complex trait governed by multiple genes. In the last two decades, basic biological research has taken a big leap from studying the expression of single genes or proteins to focusing on a large number of genes or gene products simultaneously, enabling genome-wide expression strategies for better understanding of these complex traits."[8]

2.1.1 ***Heat stress***

"Heat stress is one of the main abiotic stresses that limit plant biomass production and productivity, especially in tropical and subtropical countries."[9] "The photosynthetic activity of chloroplasts is considered among the most heat sensitive cell function."[10]

"There are at least three major stress-sensitive sites in the photosynthetic machinery (PM): the photosystems, mainly photosystem II (PSII) with its oxygen evolving complex (OEC), the ATP generating[11], and the carbon assimilation processes.[12,13] PSII is the critical site of damage by a variety of stress factors such as drought, salinity, low and high temperatures, high light, and UV radiation.[14] In vivo, the extent of damage under any type of stress depends on the balance between damage and repair processes during the stress; this is particularly true for PSII, and it provides the basis for acclimation and photosynthetic recovery processes[15]."[112]

"According to literature, there are two principal modes of stress-induced impairment of photosynthesis: first, a direct damage induced by the stress factor, and second inhibition of de novo protein synthesis by reactive oxygen species (ROS). Further, stresses may be referred to as a category of oxidative stresses that inhibit the repair of PSII and/or PSI.[16] A number of studies demonstrated that ROS-scavenging mechanisms have an important role in protecting plants against high temperature stresses or combination of high-light and temperature stresses.[17,18,19] See (Figure 2.1)."[112]

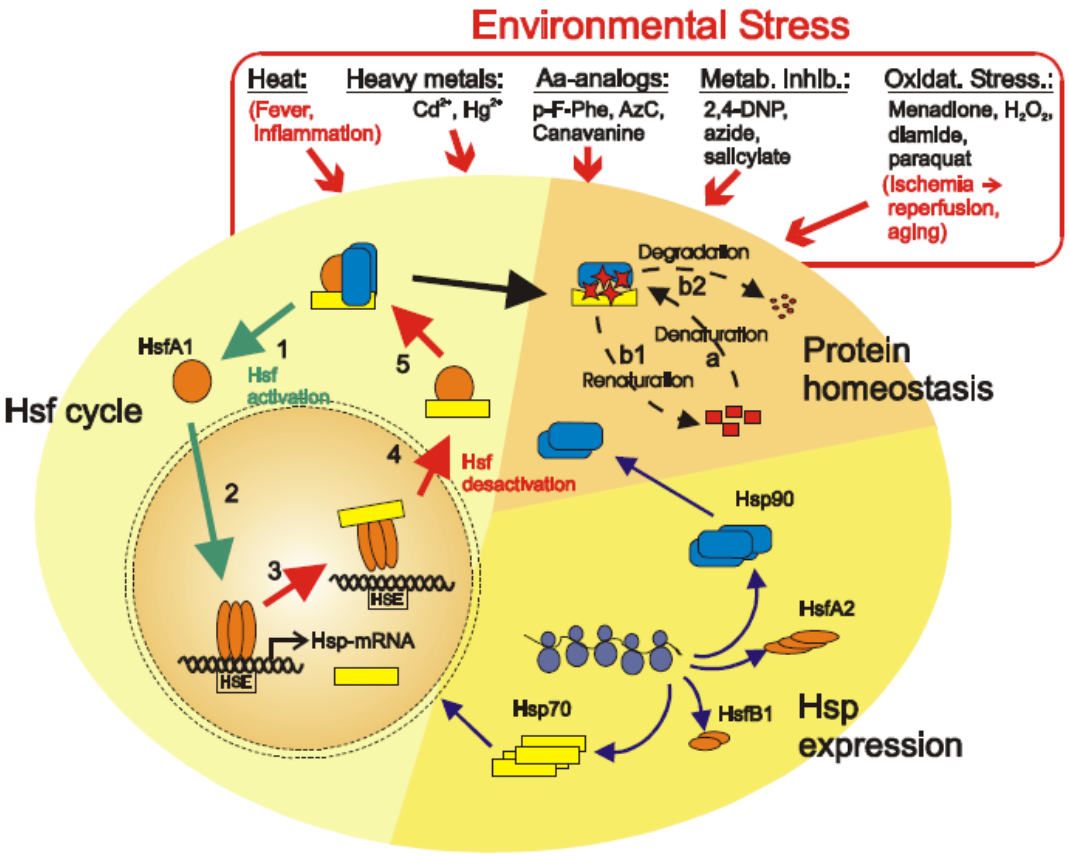

Figure 2.1: Cycle of the heat stress response. [Taken from ref (113)]

2.1.2 *Oxidative stress*

"Most types of abiotic stresses such as drought, salinity, heat and cold stresses disrupt the metabolic balance of cells, resulting in oxidative stress.[20] Oxidative stress is a term used to describe the effect of oxidation in which an abnormal level of reactive oxygen species (ROS), as it shown in (Figure 2.2), such as the free radicals (e.g., hydroxyl, nitric acid, superoxide) or the nonradicals (e.g., hydrogen peroxide, lipid peroxide) lead to damage (called oxidative damage) to specific molecules with consequential injury to cells or tissue.[21] Removal or neutralization of ROS is achieved with antioxidants, endogenous (e.g., catalase, glutathione, superoxide dismutase) or exogenous (e.g., vitamins A, C, E, bioflavonoids, carotenoids). Plants overcome oxidative stress with the production of scavenger enzymes such as catalases, which decompose H_2O_2."[8]

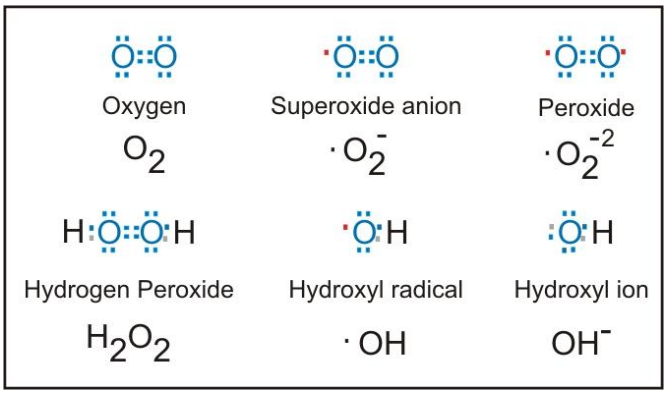

Figure 2.2: Electron structures of common reactive oxygen species. Each structure is provided with relevant name and chemical formula. [Taken from ref (104)]

"ROS such as H_2O_2 may be important during moderate heat stress. The generation of ROS was observed both in PSI and PSII[22] as well as in the Calvin-Bensoncycle.[23] In vitro experiments from several laboratories suggested that thermal stress at high enough temperatures produces ROS such as super-oxide radicals, hydroxyl radicals, and hydrogen peroxide at the PSII RC, which are scavenged by antioxidants, including superoxide dismutase (SOD).[24] The presence of antioxidant enzymes saves the organisms by limiting the formation of singlet oxygen, very toxic ROS, also produced under strong light.[25] Like singlet oxygen, hydroxyl radicals are most toxic for plant cells, and their conversion to H_2O_2 reduces their damaging effect.[26] There are observations that formation of ROS and their scavenging by antioxidants also occurs in vivo[27]."[112]

2.1.3 ***Heavy Metal***

"Higher dose of heavy metals adversely affects plant growth and development even though heavy metal ions are essential in many physiological and developmental processes. The presence of enhanced level of heavy metal ions triggers a wide range of cellular responses. In plants, higher amount of copper, cadmium and mercury ions resulted in the activation of a novel cell trapping and injection. Heavy metals have become one of the main abiotic stress agents for living organisms because of their increasing use in the developing fields of industry and agrotechnics, and high bioaccumulation and toxicity. The effect of their toxic influence on plants is largely a strong and fast inhibition of growth processes of the above and underground parts, as well as the activity decrease of the photosynthetic apparatus, often correlated with progressing senescence[28]."[7]

"Roots are usually shortened and thickened or poorly developed.[29] Growth inhibition and senescence stimulation, caused by heavy metals in excess are

intriguing effects, more so, as the knowledge of their mechanisms can have a great significance in ecophysiology and medicine."[7]

2.1.4 *Mechanism of action of DCFH-DA*

"DCFH-DA, a cell permeable, non-fluorescent precursor of 2',7'-dichlorfluorescein (DCF) can be used as an intracellular probe for oxidative stress.[106] Intracellular esterases cleave DCFH-DA at the two ester bonds, producing a relatively polar and cell membrane impermeable product, H_2DCF. This non-fluorescent molecule accumulates intracellularly and subsequent oxidation by hydrogen peroxide (or peroxynitrite) yields the highly fluorescent product of DCF[30]. The redox state of the sample can be monitored by detecting the increase in fluorescence. See (Figure 2.3). Various inhibitors can be used to elucidate the source of the oxidative stress."[31]

$$\text{D-amino acid} + H_2O + O_2 \rightarrow \text{Keto acid} + NH_4^+ + H_2O_2$$

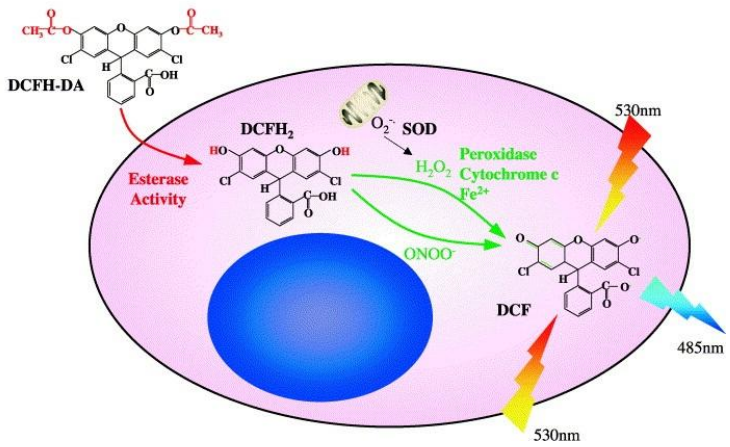

Figure 2.3: Mechanism of action of DCFH-DA. [Taken from ref (31)]

2.2 *Cell trapping*

"Conventional cell studies are conducted with large populations of cells and, therefore, measurement can only reflect average values summed over the responses of many cells. However, this approach can be a source of misinterpretation,

because it ignores the statistical nature of many cellular events. Miniaturization technology provides facilities for creating tools with feature sizes matching the dimensions of cells and enables integration of cell-handling and fluid-manipulation elements. Immobilization and separation of single cells and particles are fundamental cell-handling operations that are part of almost any microfluidic cell-based system. Cell-handling tasks such as cell sorting, pre-fractionation, filtering, isolation of individual cells, and concentration or enrichment, are based on these operations. Researchers have been very inventive in developing cell or particle-separation functionality on a chip, which are often derived from specific physical principles applied on the micro scale[32]. (Figure 2.4) shows a variety of cell immobilization[33,34,35] methods, which partly imply cell separation capability. They can be classified as contactless cell trapping or as cell immobilization on a surface."[36]

"The former class comprises optical, dielectrophoretic (nDEP)[37,38,39], acoustic[40,41,42], holding pipette [43] and magnetic trapping.[44,45] chemically driven cell attachment to a surface and hydrodynamic trapping[46,47] belong to the second class. Cell encapsulation in a polymer is regarded as being situated in between".[36]

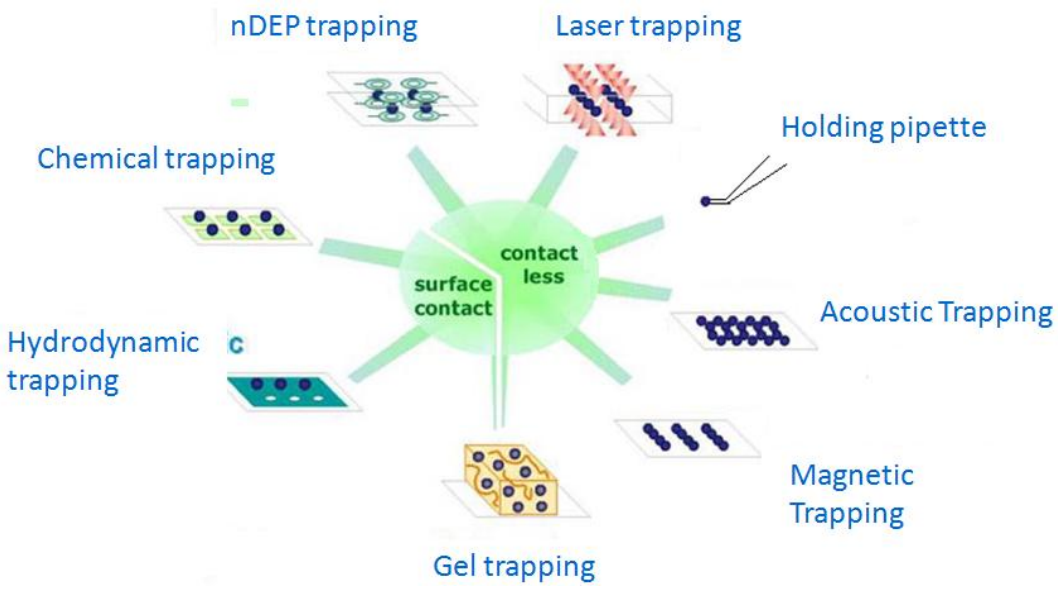

Figure 2.4: Cell trapping methods [Taken from ref (36)]

2.3 *Microinjection*

"Single-cell microinjection[48] is a powerful technique for injecting foreign materials at a microscopic level into the cells and for extracting or transferring cellular components into each other.[49] Microinjection system includes an inverted microscope, a pressure device, micromanipulators and microinjection capillaries."[50]

2.3.1 *Microscope*

"An inverted microscope with its light source on the top, above the stage, while the objectives and turret are below the stage pointing up- (Carl Zeiss Axiovert 40 CFL) is used in this thesis for microinjection purposes. One important parameter is the working distance of the condenser, which is measured from the most bottom part of the condenser to the stage, after the condenser has been adjusted correctly. A "long" or "ultra-long" working distance condenser allowing the micromanipulator headstages access and unobstructed movement is preferred. Any clash between the stage attachments (moving stages and specimen holders) and the micromanipulator motors should be avoided. In addition, a photo camera (Carl Zeiss AxioCam MRm) and a TV monitor should be provided for recording and demonstration purposes."[50]

2.3.2 *Micromanipulators*

"The micromanipulator (Patchman NP_2) is utilized to locate and move the micropipette close to the tissue to be manipulated or injected.

Micromanipulators should be securely fixed on the microscope by means of a firm adapter (supplied separately). Performance of the micromanipulator and ultimately success of any microinjection largely depends on stability of the micromanipulator mounting."[50]

2.3.3 *Microinjector*

"Microinjector (Femtojet express) is used to control the pressure level in the micropipette. Depending on the application, different pressures may be required. These applications are described below. Direct-pressure microinjection of fluids such as nucleic acid solutions, dyes and drug compounds into the cells uses a sharp hollow capillary-glass micropipette with a tip diameter typically in micron rang. Relatively high pressure (in the order of a few *hPa*) is normally applied to eject the solution out of the micropipette and into the cell. When the injection pressure is not being applied, a constant positive "base" pressure should be

applied to the tip to ensure that natural capillary action does not draw the medium in the injection chamber, up into the micropipette, and dilute the solution being injected.

The injection system must be capable of providing a pulse of high pressure to the micropipette tip to clear out the blockages that inevitably occur when injecting through the lipid cell membrane. In addition to variable pressure, the injection system should be programmable to provide pulses of pressure for defined times, usually in the order of tens of milliseconds, on command. This feature provides feasibility of multiple injections from one cell to the next cell by pressing a single switch. Finally, the desired pressure may be applied continuously as long as a control is depressed.

The first step in microinjection is defining a cell within the field as the target. Then four simultaneous actions are followed as below:

- Twisting the micromanipulator joystick in (X, Y, Z) direction, to lower the micropipette tip towards the cell.
- Penetrating the micropipette[50] tip into the cell
- Applying nitrogen pressure using the micro injector to inject the materials into the cell. Ideally, a particle no more than a few percent of the cell's volume will be introduced into the cell and will be visible as a tiny shockwave passing through the cytoplasm.
- Retracting the micropipette from the cell immediately after injection."[50]

Set up used for this thesis demonstrating in (Figure 2.5).

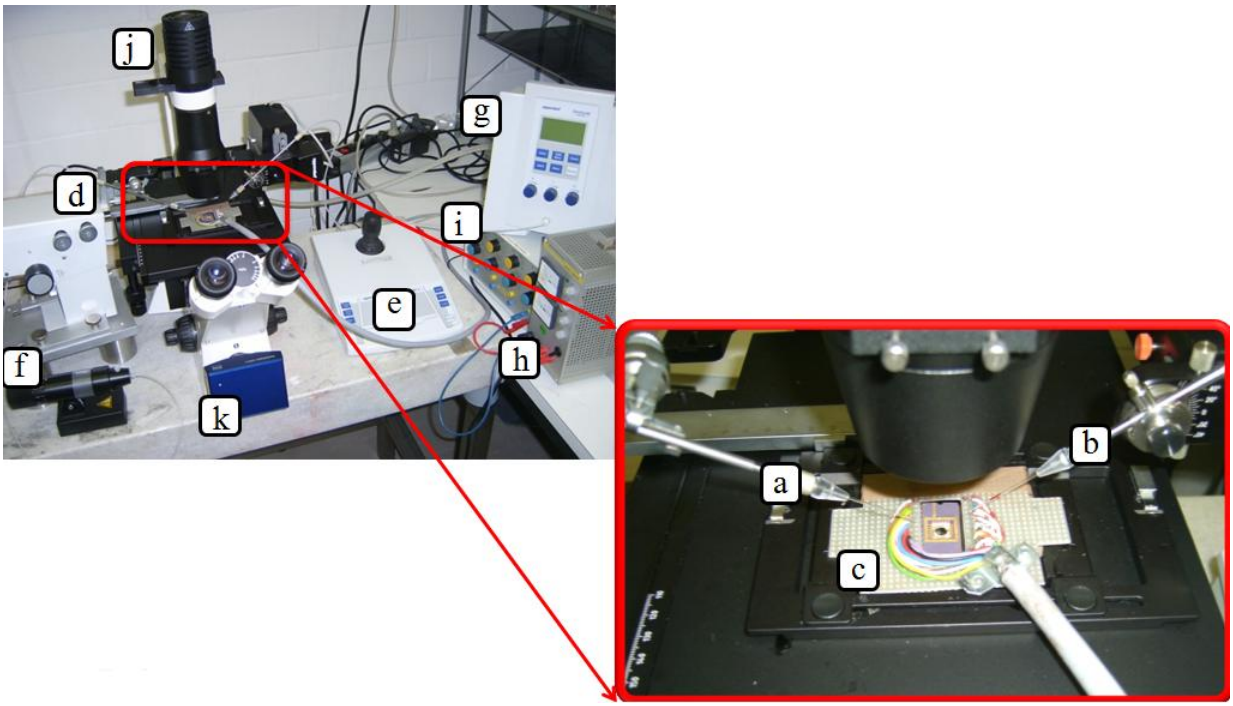

a. Holding capillary
b. ICSI capillary
c. Electrodes and electrical system
d. Joystick to adjust holding capillary in a proper position
e. Patchman NP2 for easy movement injecting capillary
f. Celltram air (pressure control) to trap the cell
g. Femtojet express to apply pressure to injection of magnetic particle
h. Power supply
i. Electrodes selector
j. Inverted microscope (Carl Zeiss Axiovert 40 CFL)
k. Photo camera (Carl Zeiss AxioCam MRm)

Figure 2.5: Set up used for manipulation experiment

2.4 *Calculation of forces acting on a superparamagnetic bead*

"Superparamagnetic beads are important in a multitude of biological and biomedical applications,[51,52,53] including manipulation[54,103] and separation[55,56,57] of cells, isolation of specific cells in immunomagnetic assays,[58] separations of proteins,[59]and application of mechanical forces to cells. Suspensions of superparamagnetic beads in biocompatible aqueous buffers are often used in conjunction with microfluidic and other types of microfabricated devices.[60]Macroscopic permanent magnets and electromagnets can produce magnetic fields sufficiently strong (>0.5 *T*) to saturate the magnetization of superparamagnetic beads; under these circumstances, the beads simply behave as permanent magnets. Magnetic fields generated by microfabricated electromagnets

are too weak (0-10 mT) to saturate the magnetization of the beads[61]but they induced some magnetization.

The internal structure of superparamagnetic beads can be very complex. Depending on the synthesis procedure, each bead may consist of iron oxide (magnetite, Fe_3O_4) particles with a functionalized coating,[62] a sphere of polymer matrix impregnated with iron oxide nanoparticles[63] or a polymer sphere coated with iron oxide[64]. In weak magnetic fields ($B = \mu_0 H \leq 3mT$), the magnetization $\vec{M}_0$ of a superparamagnetic bead has approximately a linear relation with the applied magnetic field (eqn (1)), where $\vec{M}_0$ is the initial magnetization ($A\ m^2\ kg^{-1}$) and χ_{bead} is the initial magnetic susceptibility of the bead (dimensionless).

$$\vec{M} = \vec{M}_0 + \frac{\chi_{bead}}{\rho}\vec{H} = \vec{M}_0 + \frac{\chi_{bead}}{\rho}\frac{\vec{B}}{\mu_0} \qquad (1)$$

The empirical dependence of the effective magnetic moment of an average individual bead $\vec{m}_{bead}(A\ m^2)$ on the applied magnetic field is then given by (eqn (2)).

$$\vec{m}_{bead} = \rho V\vec{M} = \rho V\left(\vec{M}_0 + \vec{M}(\vec{B})\right) = \rho V\left(\vec{M}_0 + \frac{\chi_{bead}}{\rho\mu_0}(\vec{B})\right) \qquad (2)$$

Note that since the bead can freely rotate in suspension, $\vec{M}_0$ is always parallel to the applied field $\vec{H} = \frac{\vec{B}}{\mu_0}$ as long as the bead is spherical and its magnetic response is isotropic.

The magnetic force acting on a magnetic dipole, $\vec{m}$, in an applied magnetic field, $\vec{B}$, is generally given by (eqn (3))[65,66,67]By substituting the empirical expression for the magnetic moment $\vec{m}_{bead}$ of the superparamagnetic bead (eqn (2)) into (eqn (3)), (eqn (4)) is obtained for calculating the force acting on the bead

$$\vec{F} = (\vec{m}.\nabla)\vec{B} \qquad (3)$$

$$\vec{F} = (\vec{m}_{bead}.\nabla)\vec{B} = \rho V(\vec{M}_0.\nabla)\vec{B} + \frac{V\chi_{bead}}{\mu_0}(\vec{B}.\nabla)\vec{B} \qquad (4)$$

If we neglect the effect of the magnetic properties of the suspending medium, the conventional formula for the force acting on a super-paramagnetic bead in magnetic field becomes as (eqn (5)).

$$\vec{F}_m = \frac{V\chi_{bead}}{\mu_0}(\vec{B}.\nabla)\vec{B} \qquad (5)$$

Using the expression for the magnetic field (eqn (6)) and some basic geometrical considerations (Figure 2.6.a) (eqn (7)) can be obtained for the magnetic force acting on the bead during the motion.

$$B = \frac{\mu_0 I}{2\pi\sqrt{x^2+y^2+z^2}} \tag{6}$$

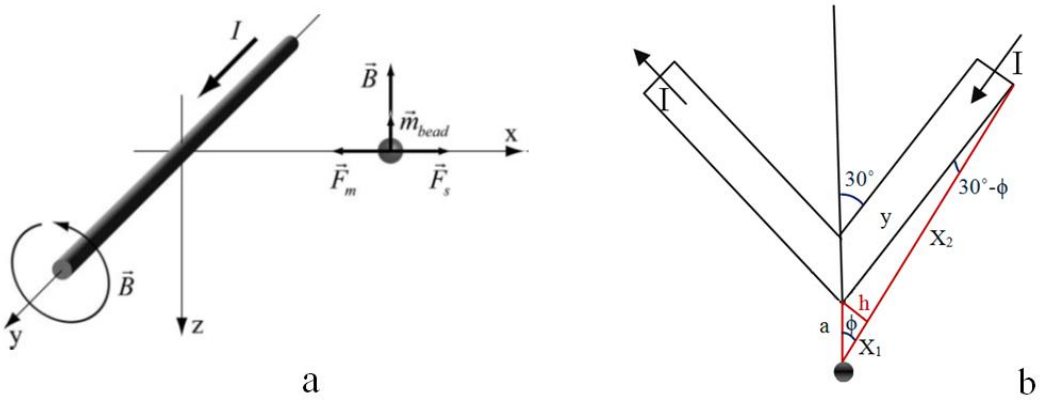

Figure 2.6: a) An idealized representation of the superparamagnetic bead in the microfluidic channel with an adjacent metal wire (electrode). The electromagnet is represented by an infinitely long, cylindrical wire carrying electrical current. [Taken from ref (69)] b) The black dot is the position of the particle to the V type electrode.

$$F_m = -\left[\frac{\chi_{bead}\, R^3 \mu_0 I^2}{3\pi x^3} + \frac{2\rho M_0\, R^3 \mu_0 I}{3x^2}\right] \tag{7}$$

I is the electrical current passing throw the electrode (*A*), x is the distance of bead from electrode (*m*), R is the radius of the bead (*m*) and, χ_{bead} is the initial magnetic susceptibility of the bead.(Mention that this is a rough estimation in x direction)"[68]

The C value introduced in (eqn (8)) was defined to develop (eqn (7)) for V type electrodes as (eqn (9)) by (eqn (8)) from geometrical considerations (Figure 2.6.b). For more details see (Appendix.1)

$$C = \frac{F_{mag.V\ shaped}}{F_{mag.\ straight}} = 0.2145 \quad (8)$$

$$F_m = -C \times \left[\frac{\chi_{bead}\, R^3 \mu_0 I^2}{3\pi x^3} + \frac{2\rho M_0\ R^3 \mu_0 I}{3x^2}\right] \quad (9)$$

Two forces act on a superparamagnetic bead during the movement between electrodes: the magnetic force, $\vec{F}_m$, due to the gradient of the applied magnetic field, $\vec{B}$, produced by the electrode, and the Stokes force, $\vec{F}_s$, due to the viscous drag exerted by the suspending medium on a moving bead (eqn (10)) (here $\vec{a}$ is the acceleration of the bead). The Stokes force is given by (eqn (11)), where η (*kg* m^{-1} s^{-1}) is the dynamic viscosity of the suspending medium, $\vec{v}$ is the velocity of the superparamagnetic bead (*m* s^{-1}), and R_H is the radius of the bead (*m*)[69].

$$\rho V\vec{a} = \vec{F}_m + \vec{F}_s \quad (10)$$

$$\vec{F}_s = -6\pi\eta R_H\vec{v} \quad (11)$$

2.5 *Electron Beam Lithography*

Electron beam lithography (often abbreviated as e-beam lithography) is performed by computer controlled scanning of a highly focused electron beam on resist-coated substrate. The lithography process is realized by using resists. The resist can be positive or negative type. The scanning electron microscope (SEM) used for this work was a LEO 1530 Gemini system with acceleration voltage comprised between 0.2-20 *kV*. SEM also used to analyze samples.[70] The energy, the aperture and the detector type (Inlens or SE2) can be adjusted to suit the investigated sample.[73,75]

2.5.1 *Magnetron Sputtering*

Sputter deposition is a physical vapor deposition (PVD)[71] method to deposit thin films. This method is used for coating the materials in, e.g., the semiconductor industry. Grove published the first article regarding sputtering in 1852.[72] This process offers the advantage of coating a homogeneous large area all at once.[73]

"In this method, a vacuum chamber is filled with argon gas. Ar^+ ions out of plasma are accelerated towards a target consisting of the material to be deposited under an applied high Direct Current (DC) voltage. Materials are detached (sputtered) from the target (source) and then deposited on a substrate (such as silicon wafer, glass etc.) in the vicinity[74]."[75]

"The deposition rate can be adjusted by increasing or decreasing the ionization density of the Argon gas. The magnetic field generated by permanent magnets, forces the electrons to follow the magnetic lines causing an increase in ion density to 10^{13} *ions/cm*^{3} due to a higher degree of collision. DC magnetron sputtering is not suitable for coating of the insulating materials. An alternative voltage current in radio frequency RF range of 13.56 *MHz* was applied to trap the positive charge in plasma zone and preventing accumulation at the cathode for a successful sputtering of insulating materials."[75]

Sputtering was used in this thesis for fabricating the electrodes, conducting lines, contact pads and protection layers.

2.5.2 ***Resist***

Resist is a thin layer of a polymer material used to transfer the lithographically defined electrode pattern to, e.g., the glass substrate that it is deposited upon during chip fabrication process.

"Resists are classified as two groups; positive and negative. In positive resist, the exposure causes a chemical breakdown of high molecular weight polymer in to lower ones (the exposed areas of resist will be dissolved in the developer solution) and in the negative resist the exposure causes a polymerization of monomers to high molecular weight polymer (the exposed areas stay after developing the sample). "Resist sensitivity of 1 to 5 $\mu C.cm^{-2}$ at 20 *kV* is required for electron-beam lithography[76]."[75]

2.5.3 ***Ion beam milling***

"Etching is the process of removing materials from the substrate by means of physical or chemical actions. When the sample is ready, physical etching is employed in combination with negative e-beam resist for patterning purpose. Incident ions of Ar^+ are accelerated towards the sample surface and eliminate the materials that are not protected by resist. The removed particles can be either neutral or charged. Charged particles pass through an energy filter and are

analyzed by a mass spectrometer attached to the etching chamber. Precise measurement of the analyzed particles provides a useful feature to define an accurate stop point for etching process."[77]

2.6 *Iron oxide based magnetic beads*

"The nanoparticles currently used in biomedicine are magnetite (Fe_3O_4)[78] or maghemite (Fe_2O_3)[79] base. The main advantages of them are their small size and non-interaction feature between nanoparticles. The magnetic properties and biocompatibility of the nanoparticles has been extensively investigated, and recognized that they could be metabolized by the human body (in liver and kidneys). Currently, they are mostly used as contrast agents in MRI techniques or as hyperthermia agents in cancer therapies. Further applications for nanoparticles are foreseen in drug delivery systems to specific location of disease, magnetic cell separation and biomolecular technology.[80] Their functionalization with biomolecules is mandatory for their use in biomedicine, but due to different biological treatments, their magnetic moment can be reduced.[81] The nanoparticles' interchange is based on dipole-dipole interaction and exchange interactions.[82] Any kind of interaction between the nanoparticles is suppressed in case the distance between the nanoparticles is larger than three times their diameter,"[77]

"The commercial magnetic beads Dynabeads® MyOne™ [1] used for manipulation experiments presented in this thesis are formed by embedding iron oxide nanoparticles in porous monosized polymer beads and coated afterwards with a layer of polymer without charged groups.[83] Individual magnetite nanoparticles in the formed magnetic beads range 6-12 *nm*. Some of them cluster and form structures of up to 20 *nm*. The entire bead has a size of 1.05 μm and is coated by different end-groups such as carboxylic acid, streptavidin etc.

[1] Life Technologies GmbH, Frankfurter Straße 129B, 64293 Darmstadt, Germany

Discovery of streptavidin (Figure 2.7) was totally unexpected and happened during a screening of *Streptomyces* for antibiotics. The antibacterial effects could be reversed by high concentrations of biotin in the medium. A closer look revealed that the high molecular weight component was a biotin binding protein that had remarkably similar physical and chemical characteristics as avidin[84], including a 33% identity in the amino acid sequence.[85] In 1964, Chaiet and Wolf [86] published the first article about this titled "The properties of Streptavidin, a Biotin-Binding Protein Produced by Streptomycetes". This was the first time that a biotin-binding protein was isolated from a microbial source and not from egg white. Streptavidin has its name from the bacterial source of the protein, *Streptomyces avidinii*, and from egg white avidin. It is a tetrameric protein that consists 254 amino acids with the size of ($46 \times 93 \times 104\ \AA^3$)[87] and a molecular weight of about 60 *kDa* [2].[88]The exceptionally high binding affinity to biotin is in the same range as the binding affinity of avidin-biotin ($K_d \approx 10^{-15} mol/l$).[86] This is the highest known affinity without the formation of covalent bonds.[85] In order to understand these special properties and be able to use them for biotechnologic application, many groups have investigated the streptavidin-biotin system. The following section reviews the current state of the research on ligand-receptor bonds. Commercial streptavidin-coupled Dynabeads®[60] 1.05μm was used in this thesis for stimulating chemical oxidative stress."[75]

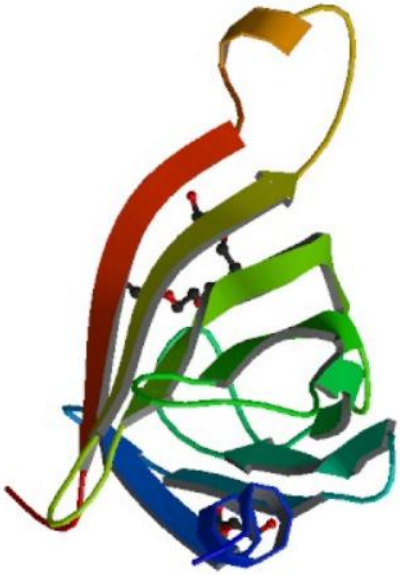

Figure 2.7: 3D structure of streptavidin, acquired with x-ray diffraction methods. [Taken from ref (88)]

[2] Dalton - unit of the molecular weight: 1Da = 1, 66054 $\times 10^{-24}$ g

Chapter 3: Materials & Methodology

This chapter describes the materials, instruments and methods utilized for various experiments on this work including: manipulation particle in the living cell experiments (magnetic particles, holding capillary,) Intracytoplasmic Sperm Injection (ICSI) capillary, Barley cell and fabrication methods for electrodes), heating experiments (glass capillary, preparation of the ThermoMicroCapillaries and isolation of *A.thalaina* cell and loaded in DCFH-DA) and chemical oxidative stress experiment (streptavidin magnetic particles, holding capillary, injection capillary and mask preparation to create holes with SU8- 3025, isolating the *A.thalaina* cell and *A.thalaina* vacuole fluid).

3.1 *Materials*

3.1.1 *Particles*

Two types of beads (Life Technologies)[3]were used in this thesis: Hydrophilic Dynabeads, 1.05 μm in diameter coated with carboxylic acid groups used for manipulation experiments and Streptavidin-coupled Dynabeads (1.05 μm & 2.8 μm) used in stimulation of the cell signals by chemical oxidative stress.

3.1.2 *Glass capillary*

Standard circular borosilicate glass capillaries without filament were used in heating experiments with the inner diameter (ID) of 0.78 *mm*, the outer diameter (OD) of 1 *mm* and total length of 70 *mm*. These capillaries were produced by Hilgenberg Company.[4]

3.1.3 *Holding and injecting ICSI capillary*

Various types of holding and injection capillaries (produced by BioMedical Instruments Company)[5] were tested in order to determine the most appropriate type and size for our experiments with the best specifications required.

[3] Life Technologies GmbH, Frankfurter Straße 129B, 64293 Darmstadt, Germany

[4] Hilgenberg GmbH ,Hilgenberg GmbH, Strauchgraben 2, 34323 Malsfeld, Germany

[5] BioMedical Instruments company Zur Schönen Aussicht 26, D-07551 Zöllnitz, Germany

In order to optimize the parameters of the holding capillary and injecting ICSI (Intracytoplasmic Sperm Injection) capillary for Barley cell, several experiments were carried out using various experiment set up as follows:

- Injection ICSI capillary with spike with 4 μm inner diameter (ID), 35˚ bending angle (B.A), 500 μm bending length (B.L)

- Holding pipette with 6.5 μm inner diameter (ID), 100 μm outer diameters (OD), 35˚ bending angle (B.A) and 500 μm bending length (B.L).

3.1.4 *Barley Mesophyll protoplast*

"Barley (*Hordeum vulgare)*[89] ecotype Franziska was seeded on MPI soil (project 187509, Cologne) with one Lizetan pill and the nutrient Osmocote Start (Scotts, USA). After 10 days in the climate chamber, a few Barley leaves were cut and stripped. The lower epidermis was peeled off and the open sides of the leaves placed in the enzyme solution[6]. After one and half hours being in 30˚C water bath, the enzyme solution was moved away and the protoplasts were washed off with sorbitol media. A gradient was prepared for separation of the mesophyll protoplasts from the epidermis protoplasts. The mesophyll and epidermis protoplasts in the sorbitol media were placed on top of percoll media and covered by a layer of betaine[7] media. After two consecutive centrifugation stages (5 minutes at 800 rpm followed by 10 minutes at 2400 rpm) the upper layer consist of the epidermis protoplasts mixed with percoll media[8] was separated. This mixture was transferred to a glass tube and covered with a layer of sorbitol media[9] and then three layers of a sorbitol media and betaine media with different mixing ratios (first layer ratio of (7:3), second layer ratio of (5:5) and next layer ratio of (3:7)) was added. This procedure was followed by adding a layer of betaine media as the top layer. Then this gradient was centrifuged for 15 minutes at 2300 rpm. The epidermis protoplasts were removed from the gradient and kept in ice with sorbitol media.[90] The procedure is essentially in accordance with the method

[6] Enzyme Solution (1,5% Cellulase R10 + 0,4% Macerozyme R10 + 0,4 M Mannitol+ 20 mM KCl + 20 mM MES pH 5,7 + 10 mM CaCl2+ 0,1% BSA Fraction V)

[7] betain media **(**400 mM glycin-betain+ 30 mM K-gluconat+ 20 mM HEPES-KOH pH 8 +0.1 % (w/v) BSA +1 mM DTT)

[8] Percoll media (Sorbit 450mM(4.099g/50 ml) +20mM MES(0.195g/50ml)+ 20mM KCl(0.074g/50ml) + 3mM $CaCl_2$(0.017/50ml))

[9] Sorbit media (Sorbit 450mM(20.49g/0.25l) +20mM MES(0.976g/0.25l)+ 20mM KCl(0.041g/0.25l) + 3mM $CaCl_2$(0.083/0.25l))

described by Kaiser and Heber (1983),[91] see (Figure 3.1)."[Written by Miriam Giesguth]

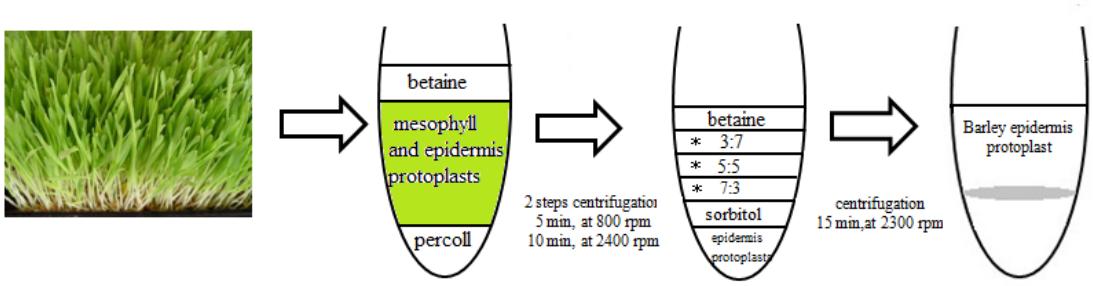

Figure 3.1: The Barley mesophyll protoplasts isolation process*

3.1.5 *A. thaliana mesophyll protoplasts with H_2DCF-DA*

"A. thaliana leaves were cut in stripes (0.5 *mm*) and vacuum infiltrated in digestion medium for 3 minutes. After incubation at room temperature on a platform, shaker at (40 *rpm*) for two and half hours the protoplasts were filtered through nylon net with 100 *μm* mesh size. The suspension was centrifuged at 115×*g* ("*g*" is traditionally named "relative centrifugal force" (RCF)) for 4 minutes, the supernatant discarded and the pellet suspended in 4 *mL* W5-solution[11]. After incubation on ice in a dark place for 60 minutes, the protoplasts were centrifuged at 115×g for 1 minute, the supernatant was discarded again, and the pellet suspended in 3 *mL* W5-solution with 2 *μM*, H_2DCF-DA. The protoplasts were loaded with the dye 2',7'-dichlorofluorescein for 10 minutes on ice in the dark followed by washing by 4 *mL* W5-solution and sedimentation for 4 minutes at 115×g. After incubation on ice in the dark for 45 minutes the protoplasts were washed again and suspended in 4 *mL* W5-solution. Protoplasts must be kept at 4 ˚*C* in the dark for future experiments. See (Figure 3.2)". [Written by Miriam Giesguth]

*mixing ratio of sorbitol media and betaine media

[11] W5 solution (154*mM* NaCl+ 125*mM* $CaCl_2$+5*mM* KCl+2*mM* MES pH5.7)

Figure 3.2: a) *A. thaliana* plant, b) *A. thaliana* protoplasts [Taken from ref (107)]

3.1.6 *Vacuoles isolation from A. thaliana*

"A. thaliana[92] protoplasts were suspended in 3 mL lysismedia[12]. They were incubated for 15-30 minutes at 38 ˚*C* in a water bath. Lysis of protoplasts was controlled with a microscope to determine completeness. This was followed by overlaying the lysismedia containing the vacuoles with a mixture between lysis and betain media in a ratio of (1:3). This was then overlaid with betain-media. (3*mL* Lysismedia with protoplasts, 2 *mL* mixture lysis media and betain media with ratio of (1:3) and 2*mL* betain media), 3 phases for density gradient centrifuged for 30 minutes at 200 *g* and 4 ˚*C*. After this step, vacuoles were in the middle phase and they could be removed."[Written by Miriam Giesguth]

3.1.7 *Preparation of coupled particle with DAAO*

In order to prepare coupled streptavidin beads with D-amino acid oxidase (DAAO) used in chemical oxidative stress experiment, 20 *µl* of streptavidin beads were mixed with 20 *µl*, 0.08 *µg/ML* DAAO and 10 *µl* Kpi buffer. This mixture was kept in 4 ˚*C* temperature for 30 minutes and then centrifuged at 500 rpm for 2 minutes. The buffer on top of the particles was collected by a pipette in next step. The coupled particles were then washed twice by 50 *µl* Kpi buffer by means of centrifuging at 500 rpm for 2 minutes.

[12] Lysis media (200 mM sorbitol + 10 % (w/v) ficoll+ 20 mM HEPES-KOH pH 8+ 20 mM EDTA pH 8 + 0.1 % (w/v) BSA +1 mM DTT)

In a final step, the buffer on top of the particles was collected and then 40 μl Kpi buffer was added. The suspension could be kept at -20 $^{\circ}C$ for 2 days. (Figure 3.3) shows the streptavidin-coupled particle with DAAO.

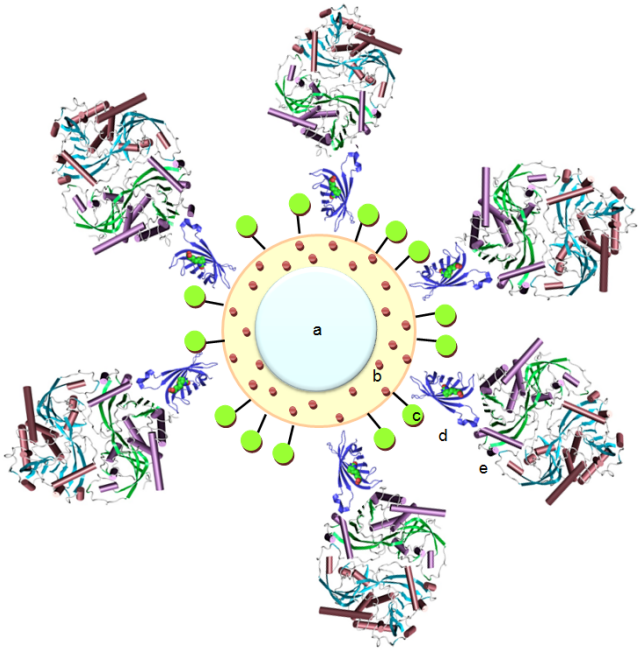

Figure 3.3: Streptavidin bead after coupling with DAAO enzyme. a) Polystyrene core, b) Iron magnetite central layer, c) Outer hydrophilic polymer surface d) Streptavidin and e) DAAO

3.2 *Methods*

3.2.1 *Methods for trapping the cells*

Several methods for trapping the cells were implemented in this work to discover the most appropriate solution. A brief description of each method is provided in following sections.

– Trapping the cells in Agarose gel

In the first method, it was intended to hold the cells in Agarose gel. Injection into the cells itself could be done by this method so this solution was used in chemical oxidative stress experiment. For manipulation of particles in living cell experiment, the cells had to be positioned exactly on top of the electrodes and

since the cell´s location in Agarose gel was out of operator control, positioning them with such accuracy was practically impossible; therefore this method could not be used for this experiment.

– Micro fluidic channel

The other solution for trapping the cells is the micro fluidic channel method. Several channel patterns were tried to find the best design for trapping a cell. This method was also used to prepare the holes for simulation of the cell condition for chemical oxidative stress experiment. Channel design was done by auto sketch software and the mask for the channel was prepared by laser lithography. First step in this process was cleaning the glass substrate with acetone and ethanol in ultrasonic bath for 15 minutes, and then coating 5 *nm* Tantalum (Ta) and 200 *nm* gold (Au) by DC magnetron sputtering. In the next step, positive resist AR-P 5350 was coated and baked at 90 $^{\circ}C$ for 30 minutes for laser lithography purposes. After transferring the channel pattern onto the substrate by a laser beam, the sample was developed in dilution of AR 300-35 and distilled water with a ratio of (2:1) for 5-7 seconds. Finally, the sample was cleaned by distilled water and dried by nitrogen gas. The sample shown in (Figure 3.4) was used as a mask to transfer the channel pattern onto a (SU-8 3025)[93] substrate.

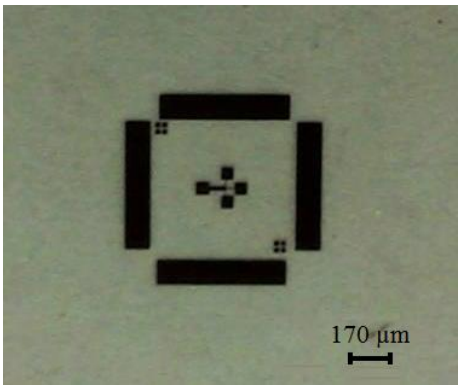

Figure 3.4: The mask designed for micro fluidic channel on a glass substrate, prepared by laser lithography procedure.

In order to prepare the micro fluidic channel, after cleaning the glass slide with acetone and ethanol in ultrasonic bath for 15 minutes, SU-8 3025 was coated on the substrate by means of spin coating method. Three steps of SU-8 3025 baking were required to create the channel. The first step was soft baking immediately after coating the SU-8 3025 by spin coater at 3000 *rpm*. The channel pattern was transferred by means of exposing the sample to UV light with optimized doses and light intensity. The sample was then post-baked as next step followed by

developing the sample by Dev 600 for 6 minutes, then washed with Isopropanol and distilled water, and hard-baked as final step. See (Figure 3.5).

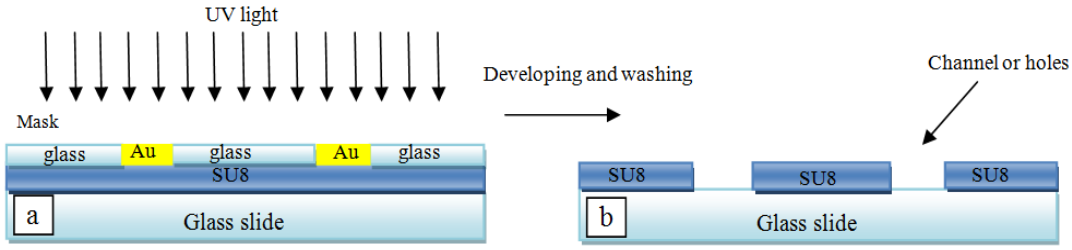

Figure 3.5: a) The mask on top of the sample (coated glass with SU-8 3025) is exposed to UV light, b) channel or holes after developing dev 600 and washing by isopropanol.

Exposure dose, light intensity and the thickness of SU-8 3025 were optimized for electrode surfaces (gold electrodes on glass substrate, covered by Ta_2O_5). The important point in trapping the cell is that the trapping zone should be exactly aligned on top of the electrodes. See (Figure 3.6).

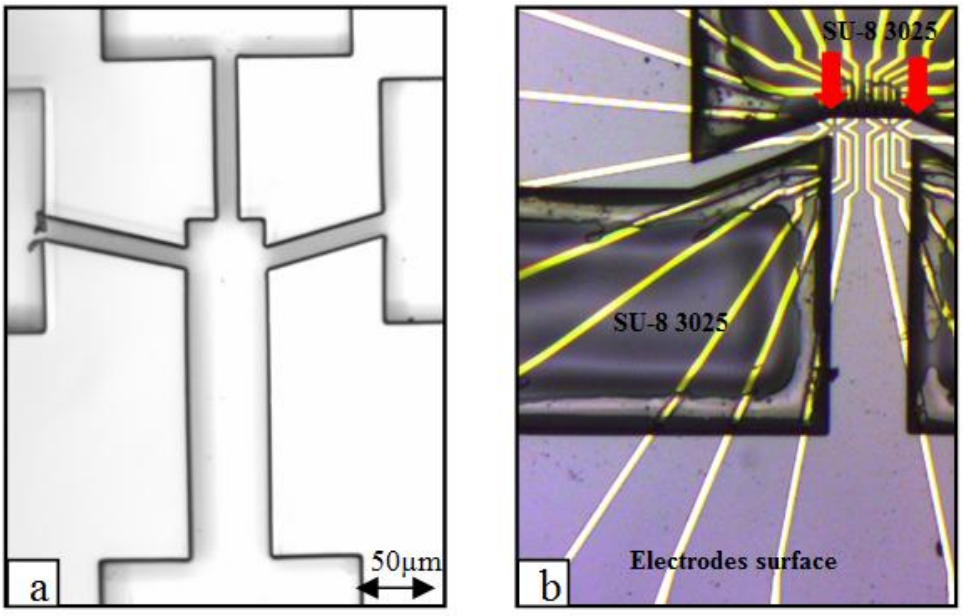

Figure 3.6: a) Micro fluidic channel structure on SU-8 3025 with a glass substrate b) Big squares and channels are suitable to lead the cells towards the trapping zones. The width of the narrow channel is 20 µm.

– Holding pipette (capillary) method

Holding pipette method was another method tested for trapping the cells. Two main parameters in trapping the cells by holding pipette are:

(a) The inner and outer diameter of the pipette

(b) The suction pressure.

Various holding pipette types were tested in order to find the optimum inner and outer diameter of the holding pipette with appropriate suction pressure for Barley cells. Schematic of the holding pipette is shown in (Figure 3.7).

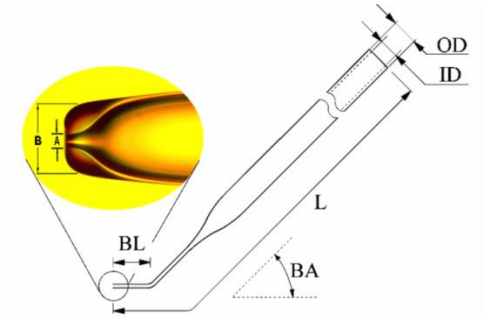

Figure 3.7: Holding Capillary (pipette) details, A: Inner diameter, B: Outer diameter, BA: Bending Angle, BL: Bending Length [Taken from ref (108)]

3.2.2 *Chip fabrication*

The construction of the electrodes is based on a chain of e-beam lithography, ion beam etching, removing and coating techniques for protection layer. Graphical schematics of these steps along with a brief description of relevant procedures are provided in (Figure 3.8).

The first step in fabrication of the electrodes was physical vapor deposition of metallic layer (10 *nm* Ta and 200 *nm* Au) on silica glass substrate utilizing a DC magnetron sputtering in presence of argon plasma. Negative resist AR-N 7500/18 (AllResist) was coated on the sample at 6000 *rpm* and annealed at 85 ˚*C* for 2 minutes. The sample was exposed to a 20 *kV* e-beam gun in 15 *mm* working distance of the Elphy Raith electron beam Lithography system (LEO Series 1530 Scanning Electron Microscope). [73,75,77]

The structure of the electrodes was patterned using a 120 μm aperture. The exposure dose value was optimized to prevent over exposure of the electrodes' structure. After developing the sample by developer AR 300-47 (AllResist) for 4

minutes, it was cleaned by water and dried by nitrogen gas. Then the sample was ready for the second lithography step followed by an ion beam etching procedure. It was done at a base pressure of at least 2×10^{-6} *mbar* and an argon pressure during the etching of 8×10^{-4} *mbar*.[73,75,77]

The ion source operates at a discharge voltage of 50 *V*, beam voltage of 400 *V*, accelerator voltage of 30 *V* and beam current of 6 *mA*. To ensure homogeneous etching, the sample holder is tilted by 30˚ and rotates slowly. The next step was removing the resist with the dilution of 1-Methyl-2-pyrrolidinone, Chromasolv plus from Aldrich for 15 minutes in an ultrasonic bath at a temperature of 60-80 ˚*C* and rinsed by ethanol. This was followed by sputtering 75 *nm* Ta_2O_5 as a protection layer using RF magnetron sputtering in combination of Oxygen and Argon. The final step was installing the sample on a ceramic IC socket and spraying a flexible, colorless and transparent resist (Schutzlack 70).[73,75,77]

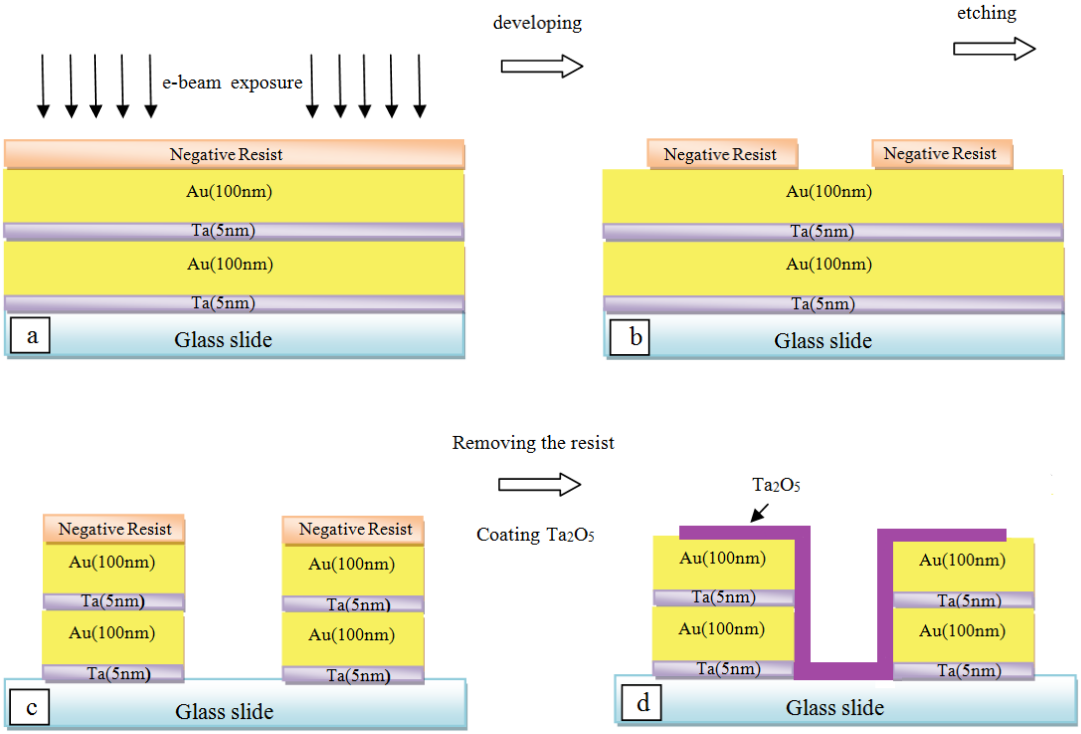

Figure 3.8: Lithography steps for preparation of electrodes

3.2.3 *Preparation of ThermoMicroCapillary (TMC)*

A standard circular glass capillary (borosilicate, 1 mm outer diameter, 70 *mm* long produced by Hilgenberg Co., Germany) was cleaned by acetone and ethanol and dried by nitrogen gas. It was then pulled into a capillary with 500 *nm* outer

diameter and then two opposite sides of the capillary were Ta coated by means of a mask. See (Figure 3.9).

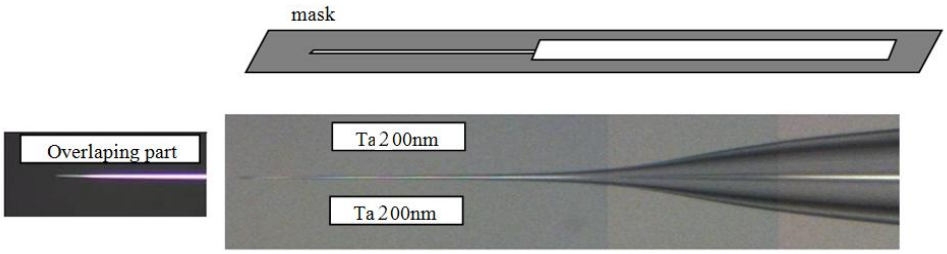

Figure 3.9: Coated capillary by 200nm Ta in two opposite sides as a heat generator

Since the capillary tip is very thin and sharp, Ta coating on both sides of the capillary overlapped on the tip. This overlapped section acts as an electric resistance resulting in heat generation on the capillary tip when an electric voltage is applied to two sides of the capillary. After Ta coating, the capillary was annealed in a computer programmable vacuum furnace at 300 $^{\circ}C$ temperature for 1 hour and then cooled for 30 minutes to provide more stable heat generation (constant temperature) during the experiment.

A special holder was designed to hold the capillary with two small ports in the body to insert Au wires (with Silver past) through the holder and connect them to the capillary. Two small screws were used on the capillary holder body to keep the capillary in place and tighten the Au wire joint to the capillary. (Figure 3.10) shows the ThermoMicroCapillary holder assembly including the capillary, holder & Au wires.

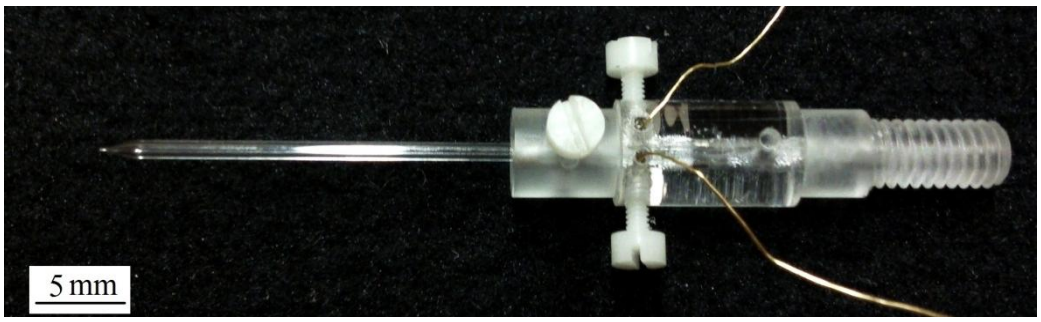

Figure 3.10: Special holder designed and fabricated for heat stress experiment to hold and apply electric voltage to the ThermoMicroCapillary

Chapter 4: Results

This chapter is presenting the detailed explanation of results of the three experiments described in the previous chapters.

Results related to the *manipulation of the particles into the living cell* experiment are listed in first part. Identifying the most appropriate system for holding the cell, outcome of cell injection, manipulation of the particles outside the cell, manipulation of particles into the living Barley cell and manipulation of the particles into the vacuole fluid are located in this section. The second part covers the experimental results of *cell stimulation by heat stress in* two sections; calibration of capillary as a stabile heat generator and local heat stress stimuli in *A. thaliana* cell. The final part is regarding the *local cell stimulation by chemical oxidative stress* experiment, including local chemical oxidative stress experiment out of the cell and local chemical oxidative stimulation inside the *A. thaliana* cell.

4.1 *Manipulation of magnetic particle inside a single cell*

4.1.1 *Holding the protoplast*

In order to study the cell it is required to sort or filter them first. Miniaturization methods provide the capability of appropriate tool fabrication in cellular dimension sizes such as holding pipettes used for trapping the cell. Their featured capabilities and excellent performance in holding and positioning the cells in any desired place on top of the electrodes make them the ideal solution for trapping the cell during the experiment.

The inner diameter (ID) of the holding capillary and the vacuum (suction) pressure are two critical parameters in cell trapping process. If the vacuum pressure is too high, the cell will be drawn into the capillary and if it is too low, the cell will not stick properly at the capillary tip. In the other hand, too large holding capillary ID causes the cell to be pushed into the holding capillary by the injection capillary during injection process, whereas too small ID of that does not provide sufficient contact surface (and therefore sufficient force) to hold the cell in position for injection purposes. These parameters were optimized at 100 μm OD (outer diameter), 35° B.A (bending angle) and 500 μm B.L. (bending length) and 6.5 μm ID (inner diameter) of holding pipette. (Figure 4.1) shows a cell trapped by such capillary dimensions properly in a pre-defined position without damaging the cell, while the vacuum (suction) and releasing pressures were under control.

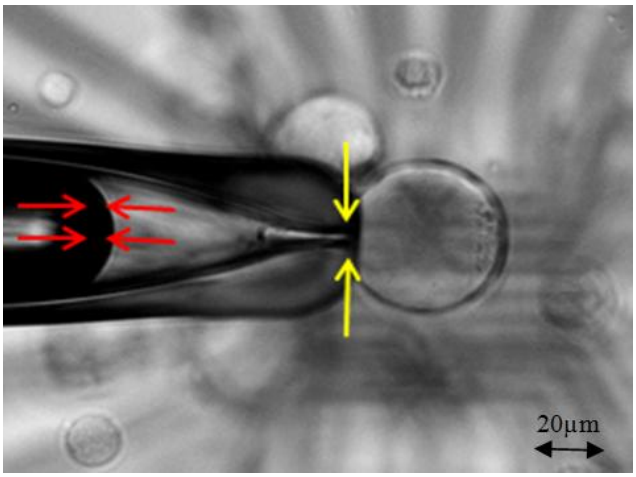

Figure 4.1: The Barley epidermis protoplast trapped by a holing capillary. Yellow arrows indicate the holding capillary ID and the red arrows represent the controlled pressure.

4.1.2 *Injecting into a single cell*

Three parameters play the major role for a successful cell injection: the injection capillary type (straight or bended), the bending angle and the bending length. Figure 4.2 shows both holding capillary (on the left hand side) and the injection capillary (on the right hand side) during an injection experiment with the similar 35˚ bending angle. An important point is that both the holding and injection capillaries should be leveled during the injection process in order to find the best injection point on the cell. The other point is that the inner diameter of the injection capillary was optimized based on the cell and the particle sizes. If the inner diameter of the injection capillary is too big, it will damage the cell membrane and burst the cell eventually, and if it is too small, the particles could not pass through the capillary into the cell. Optimized parameters for Barley cell injection experiment were gained as 4 μm inner diameter, 35˚ bending angle, and 500 μm bending length with dilution (1:100,000) of 1.05 μm dynabead. The final point is controlling the applied pressure in order to control the number of the particles being injected into the cell. Ideally, only one particle should be injected into a single cell by means of controlling the compensated pressure (*Pc)* during the injection. This pressure is depended on the density of the surrounding media and the dilution of the particles, and has to be changed on a case by case basis. Applied pressures during this work ranged from 143 *hPa* to 2000 *hPa*.

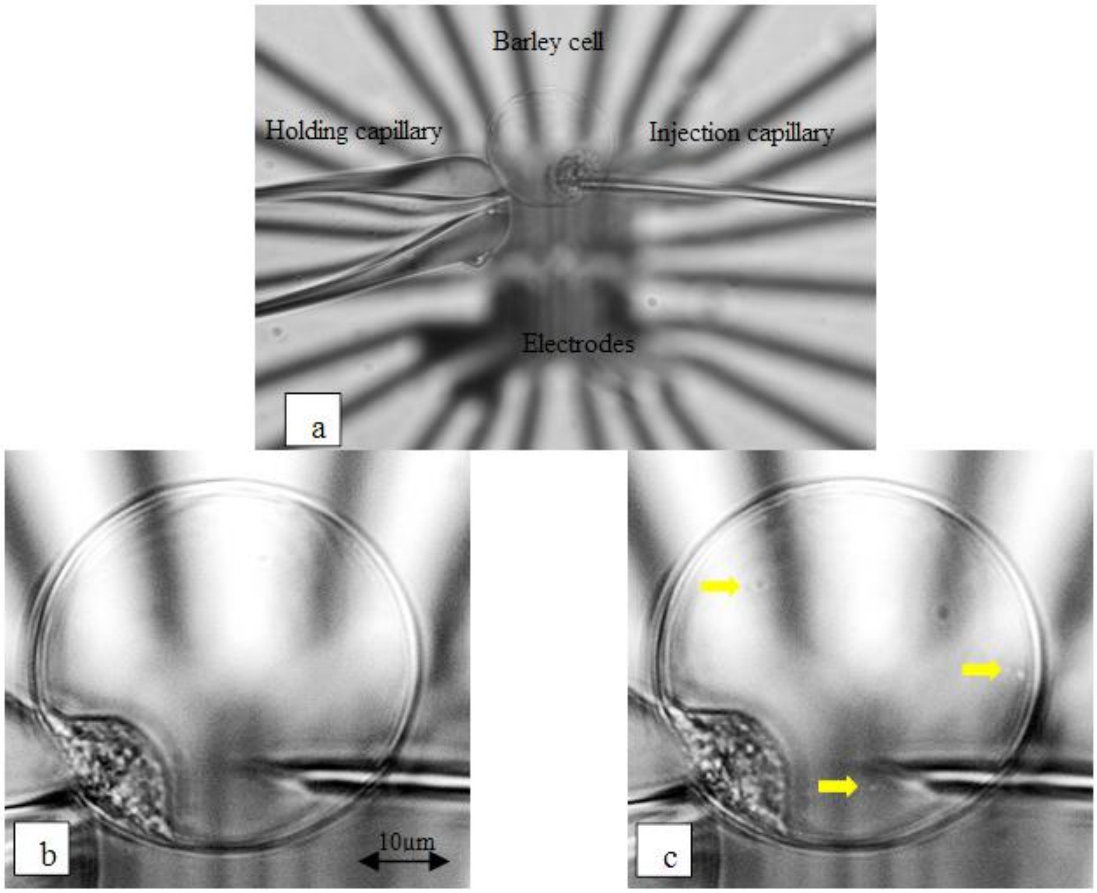

Figure 4.2: a) Barley cell trapped by a holding capillary (6.5 μm ID, left) and is being injected by an injection capillary (4 μm ID, right). b) Injection capillary inside the cell before injection. c) Yellow arrows showing the particles inside the injection capillary or already injected. Dilution of 1:100,000 of 1.05 μm myone dynabead used for the injection.

4.1.3 *Manipulation out of the cell*

In this experiment, the manipulation of a magnetic particle in water environment (outside of the cell) was carried out in order to a) Test the electrodes, and b) measure the water viscosity for normalization. (Figure 4.3) shows the actual electrodes after bonding on a ceramic IC socket and spraying resist (Plastik-70 Schutzlack)[13] on the center of the IC socket.

[13] Plastik-70 Schutzlack, Quick drying, colorless transparent insulating and protective coating based on acrylic resins. Produced by CRC Industries Europe BVBA, KONTAKT CHEMIE

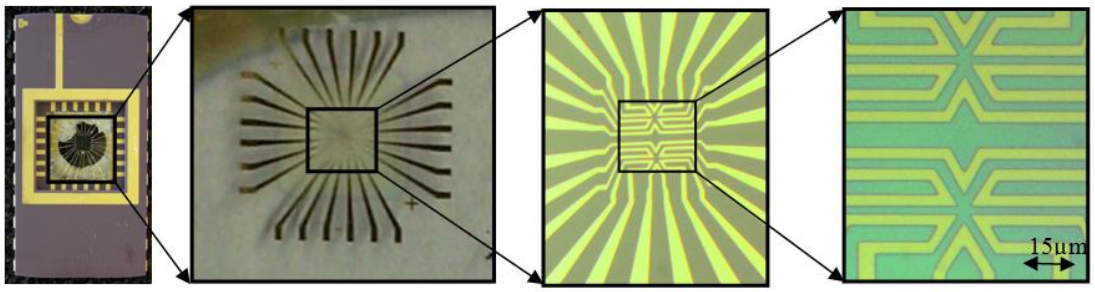

Figure 4.3: Actual electrodes after bonding on the ceramic IC socket and spraying the resist on top

An electric voltage needs to be applied to the electrodes to run a current through them for the creation of a magnetic field. The average resistance of the electrodes in this case was 40 Ω and the applied voltage was 1.2 *V*. Time-lapsed (Figure 4.4) shows different stages of this experiment over a 0.27 *s* period. In the first (Figure 4.4.a) an electric voltage was applied to one of the electrodes (I) to create a magnetic field around this electrode and attract the magnetized particle to that. Then the electric voltage was shifted to another electrode (II), therefore a new magnetic field was created and the magnetized particle was attracted and moved towards this electrode (Figures 4.4.b-h). The movement of the particle from electrode (I) towards electrode (II) was studied and the observations were analyzed to obtain the viscosity of water.

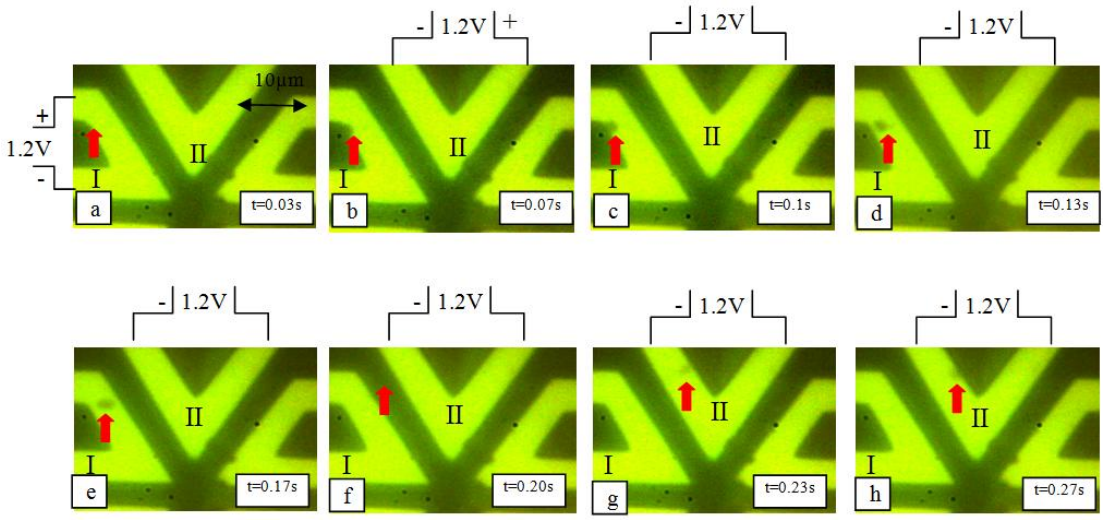

Figure 4.4: a) One magnetized particle attracted to electrode (I) after applying 1.2 V DC to the electrode. b-h) The electric voltage shifted to electrode (II), therefore the particle moved towards new electrode in 0.27 s. The experiment was carried out by a normal optical camera and dilution of 100 pg/L 1.05 µm dynabeads particles and the Susceptibility of bead is 1.377.[102] The average resistance of the electrodes was 40 Ω.

To calculate the viscosity of water accurately, this experiment was repeated four times. Results of these experiments are presented in (Figure 4.5) where the

particles' displacements on top of the electrodes versus time are shown by line series representing individual experiments. The difference between the values on displacement curves can be explained by the difference in distances between the selected electrodes also the difference in passing current through the individual electrodes because of their different resistance. These curves provide very useful data from the surrounding media of the particles. The viscosity of the environment can be obtained by calculating the velocity of the particle between two points and considering the effect of the magnetic force at that points. All measurements in this thesis are done with the GIMP software in pixel range and converted to μm by considering an object of known size in the image.

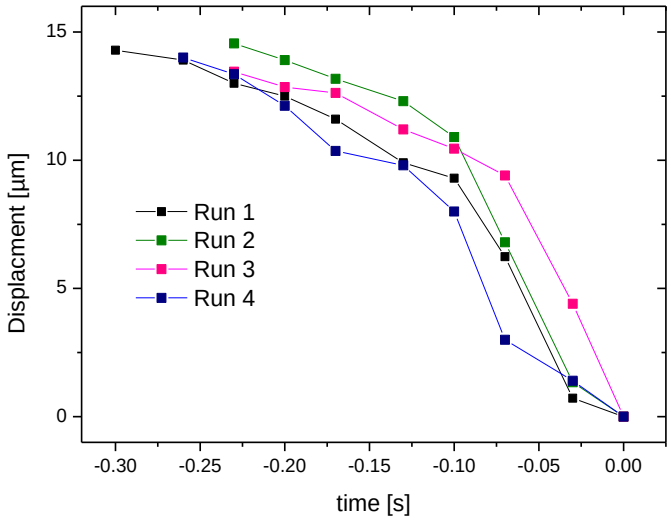

Figure 4.5: lines are showing the displacements of magnetic particles on top of the electrodes over time in water environment step by step.

4.1.4 *Manipulation inside the Barley*

A barley cell was selected as the living cell for manipulation of the magnetic particle due to its transparency (provides easier traceability of the particles inside the cell) and soft cell membrane (for easier penetration of the injection capillary into the cell).

(Figure 4.6) shows Barley protoplast held by a 6.5 μm inner diameter holding capillary (left side) and the particles (10 ng/L dilution of 1.05 μm dynabeads) injected into the cell. The Barley cell containing particles is located on top of the electrodes in (Figure 4.6.a). (Refer to (Figure 4.2) for information about particle injection). The microscope was focused on the electrodes to detect the magnetic particle movement. During the experiment, the magnetic particle was attracted to

the electrode (I) after applying 2.1 *V* DC to obtain I= 0.07 *A* (Figure 4.6.b), then the electric voltage was shifted to electrode (II) to change the magnetic field, resulting in the particle movement towards this electrode which took place in 0.42 *s*. The displacement of the particle is captured in (Figures 4.6.c-h).

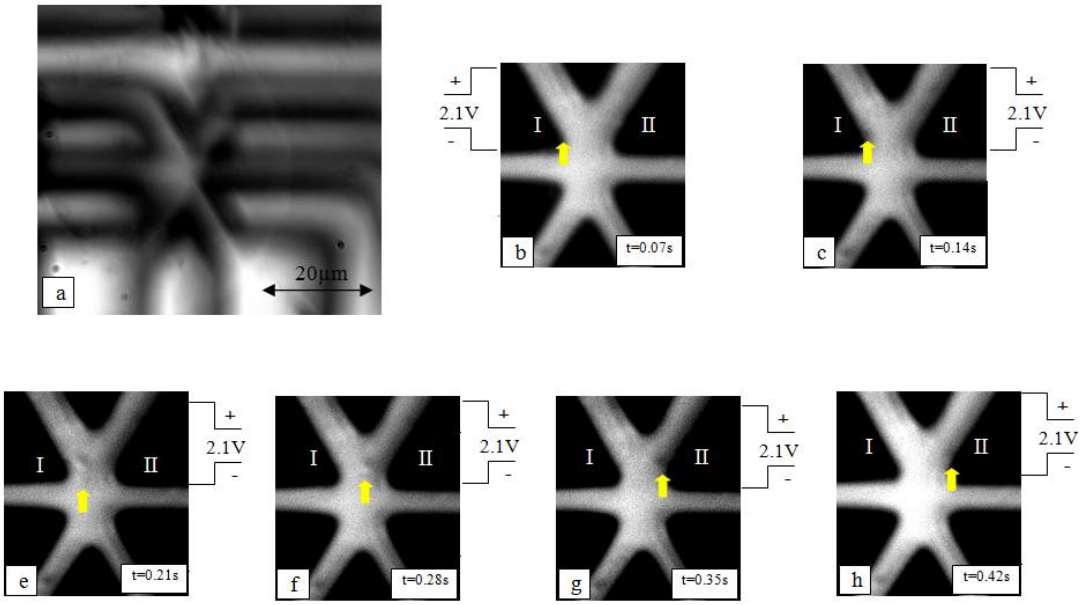

Figure 4.6: a) A Barley protoplast is positioned on top of the electrodes. Few particles (10 *ng/L* dilution of 1.05 *µm* dynabeads) are injected into the Barley epidermis protoplast while 754 *hPa* pressure was applied to inject the particles inside the cell. b-h) Magnetic particle movement from electrode (I) towards electrode II in 0.42 *s*. Average resistance of the electrode was 30 Ω.

The results of individual experiments with the above method are illustrated in (Figure 4.7) as curves representing the particle displacement inside the Barley cell with respect to time.

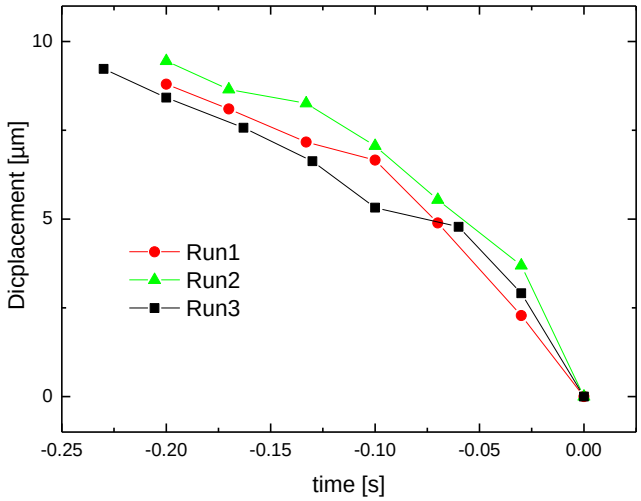

Figure 4.7: Displacement of the magnetic particles during the movement inside the Barley vacuole interior due to the magnetic field generated by the electrodes.

The results obtained from the displacement data, can be used to calculate the velocity and acceleration of the particles movement point by point, also determining the force acting on the bead along the movement path.

4.1.5 *Manipulation in Vacuole fluid of barley cell*

The manipulation of the magnetic particle was repeated in Vacuole fluid to determine viscosity of the vacuole fluid and to compare it with results for the Barley cell. Analyzing the results of these experiments assisted to study the effect of the cell membrane on the movement of the magnetic particles inside the Barley cell.

(Figure 4.8) shows a time-lapsed image from the movement of 1.05 μm magnetic particles in the vacuole fluid. To manipulate the particle, 2.1 V DC was applied to the electrodes with average resistance of 50 Ω. The magnetized particle traveled the distance between two electrodes in 0.3 s. Results from several experiments with vacuole fluid are presented in (Figure 4.9) as the displacement of the particle versus time.

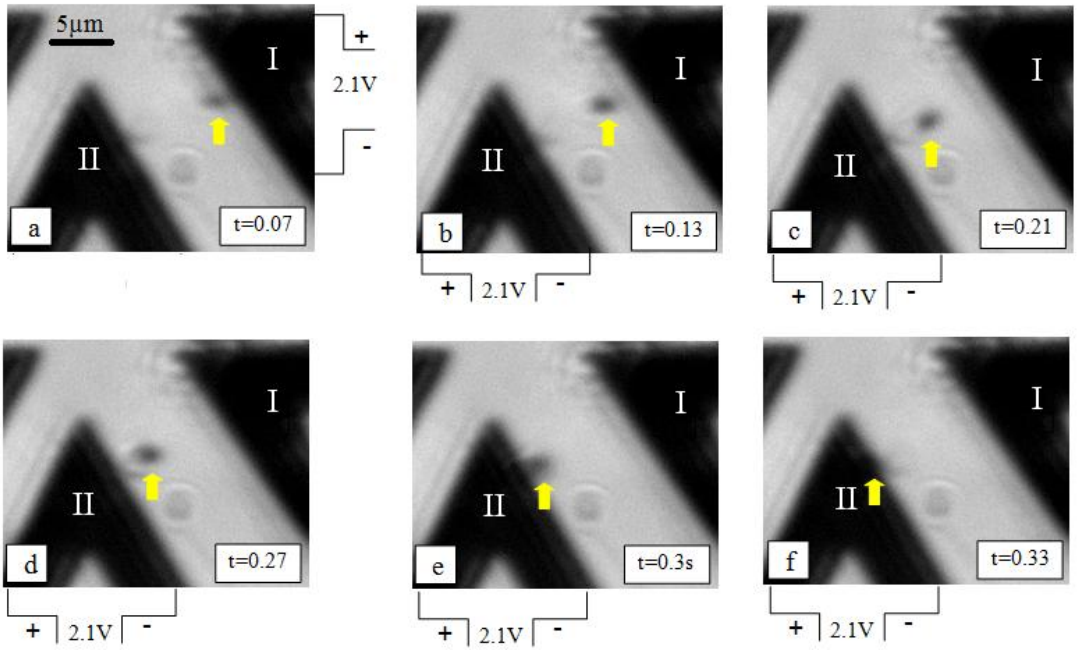

Figure 4.8: Traveling of the magnetic particle on top of electrodes in vacuole fluid environment.

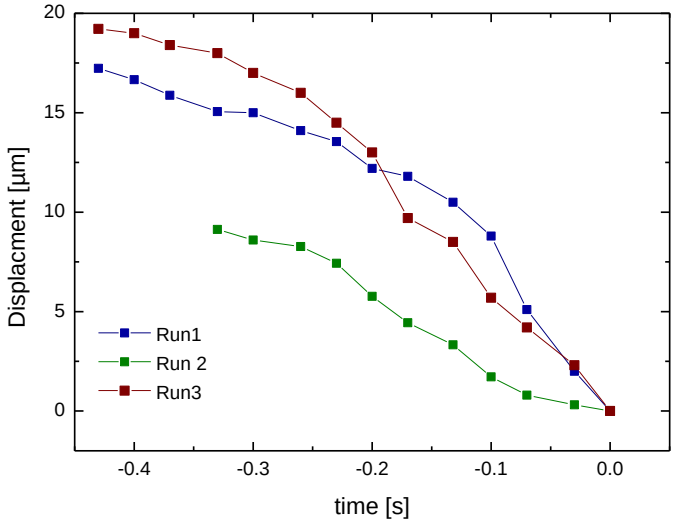

Figure 4.9: Displacement of magnetic particle in vacuole fluid of Barley versus time

The magnetic force is calculated from the displacement data, and total force acting on the particles is derived from the acceleration of the particle. From these together, the Stokes force is obtained. Finally the viscosity of the media is calculated from the velocity of the particle movement and the calculated Stokes force.

4.2 *Cell stimulation by heat*

4.2.1 *Calibration*

In order to perform the heating experiment in a single cell by TMC[14], it should be calibrated first to ensure steady state performance of the device as heat generator during the experiment. Calibration is performed by means of an infrared camera FLIR[15].

Two opposite sides of a normal pulled capillary with 500 *nm* outer diameter tip were coated by Ta (200 *nm*) by designed mask with narrow opening and then annealed at 300 $^{\circ}C$ for 1 hour. Due to the sharp tip of the capillary, the Ta coating of the capillary creates an overlapped area on the sharp tip of the capillary forming a metal bridge between two sides of the capillary. According to Joule's laws, when an electrical voltage is applied to both sides of this bridge, heat is generated due to the resistance of the metal. The resistance of the capillaries made for this experiment measured in the range of 3 $k\Omega$ to 8.38 $k\Omega$.

To generate heat, 20 *V* DC was applied to both sides of the capillary by means of Au wires connected to Ta coated sides. The temperature of the capillary tip raised due to the generated heat as expected. (Figure 4.10) capillary resistance was 8.38 $k\Omega$. The first two images show the capillary before applying the electric voltage at the initial temperature of 23.1 $^{\circ}C$. After applying a 20 *V* DC the temperature of the capillary tip increased to a maximum of 46.6 $^{\circ}C$ during 20 minutes, indicating that the TMC could generate a temperature difference of $\Delta T=23.5\ ^{\circ}C$. Once the electric voltage was terminated, the tip temperature rapidly decreased to 23.7 $^{\circ}C$.

[14] ThermoMicroCapillary

[15] FLIR Systems GmbH, Berner Strasse 81 D-60437 Frankfurt am Main Germany

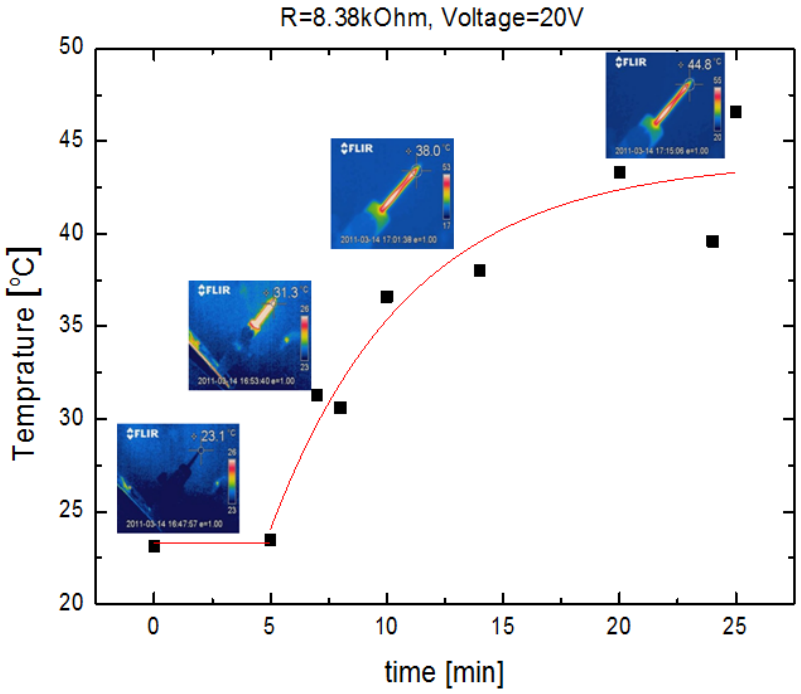

Figure 4.10: Time-lapsed image of heating capillary experiment with resistance of 8.38 kΩ after applying 20 *V* (DC).

To calibrate the TMC after annealing, three different electric voltages (10*V*, 15*V* and 20 *V* DC) were applied. The resistance of the TMC was TMC 3.2 *k*Ω. On each case, the heating capillary tip temperature was measured during the experiment to monitor the tip temperature behavior as a function of the electric voltage and time. (Figure 4.11) illustrates results of all three experiments combined in one graph.

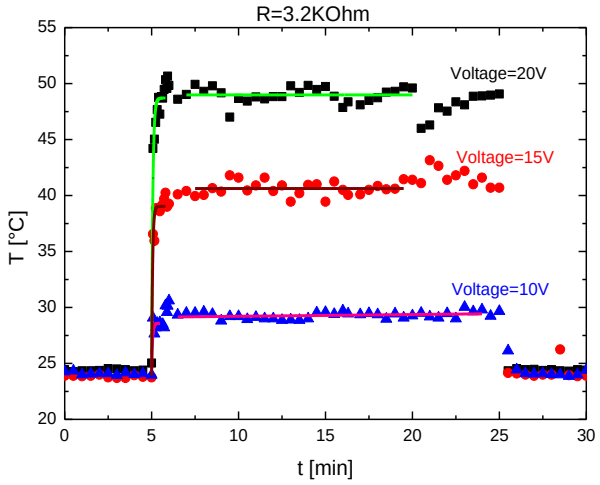

Figure 4.11: The plots illustrating the temperature rise in the TMC tip with applying different voltages over time. The resistance of the TMC was 3.2 *k*Ω.

4.2.2 *Heat stress in A. thaliana*

4.2.2.1 Negative control experiment

To study the heat stress, a negative control experiment was carried out. For this experiment, protoplasts were incubated in 2′,7′-dichlorofluorescein and a 500 *nm* tip size TMC coated by 200 *nm* Ta inserted into an *A. thaliana* cell without applying any voltage, and then emission of fluorescence was monitored by fluorescence microscopy. The main purpose of the control experiment at room temperature was to study the reaction of the cell against the mechanical stress due to penetration of the capillary without applying any voltage. As it is shown in (Figure 4.12), no stress was detected by inserting the TMC into the cell during 25 minutes of experiment duration. The exposure time was kept constant for taking all images during the experiment.

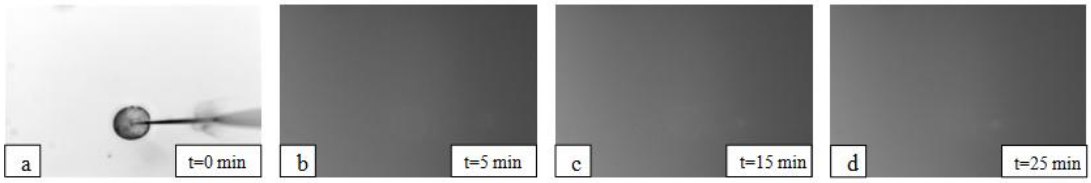

Figure 4.12: TMC inserted into an *A. thaliana* cell incubated with 2′,7′-dichlorofluorescein fluorescence at room temperature. No voltage was applied to the TMC. During 25 minutes of experiment period, no stress detected in the cell.

The relative intensity of the protoplast was obtained by converting the fluorescence intensity into a grey scale and integrating the whole image area of the protoplast with a graphic program (GIMP 2.6).

Heat stress initiates reactions inside the cell, which results in ROS production. Changes in DCF fluorescence were measured. (Figure 4.13) indicating the fluorescence intensity of the cell for negative control experiment.

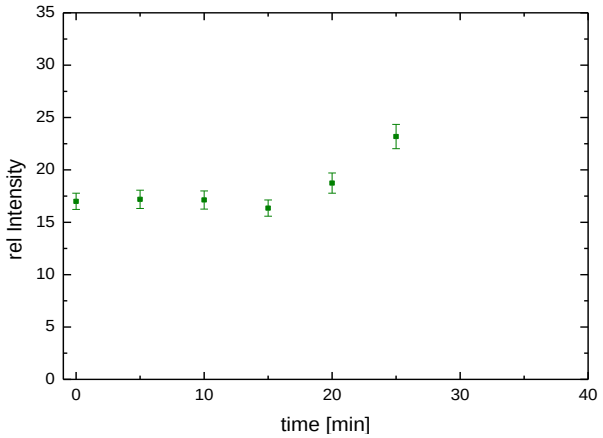

Figure 4.13: Data points corresponding to the negative control experiment show negligible changes in DCF florescence intensity as a repost of heat stress.

4.2.2.2 Heat stress in A. thaliana cell

The main experiment performed by penetrating the TMC into an *A. thaliana* cell incubated with 2′,7′-dichlorofluorescein fluorescent dye is described here.

(Figure 4.14) shows a TMC with 3 *k*Ω inserted into an *A. thaliana* cell. Just a few seconds after applying a voltage to the TMC, the tip temperature started to rise. Initial temperature of the tip was measured at 27.7 ˚*C* and it rapidly raised to 44.8 ˚*C* in 26 seconds after applying 20 *V* DC.

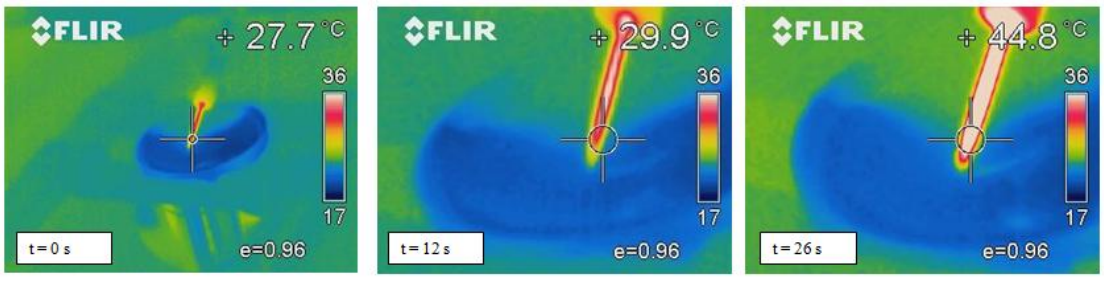

Figure 4.14: Heat stress experiment after inserting TMC into the cell and applying 20 *V* (DC).

The electric voltage was applied to the TMC for 10 minutes and during this period, the ROS content of indicating fluorescence reached its maximum. The intensity of the ROS over time decreased after stopping the electric voltage. (Figure 4.15) shows snapshots of the heat shock response experiment of *A. thaliana* protoplasts visualized as oxidative stress-induced green fluorescence

emitted from 2′,7′-dichlorofluorescein in 70 minutes. Heat stress response experiment was repeated for three times in three days.

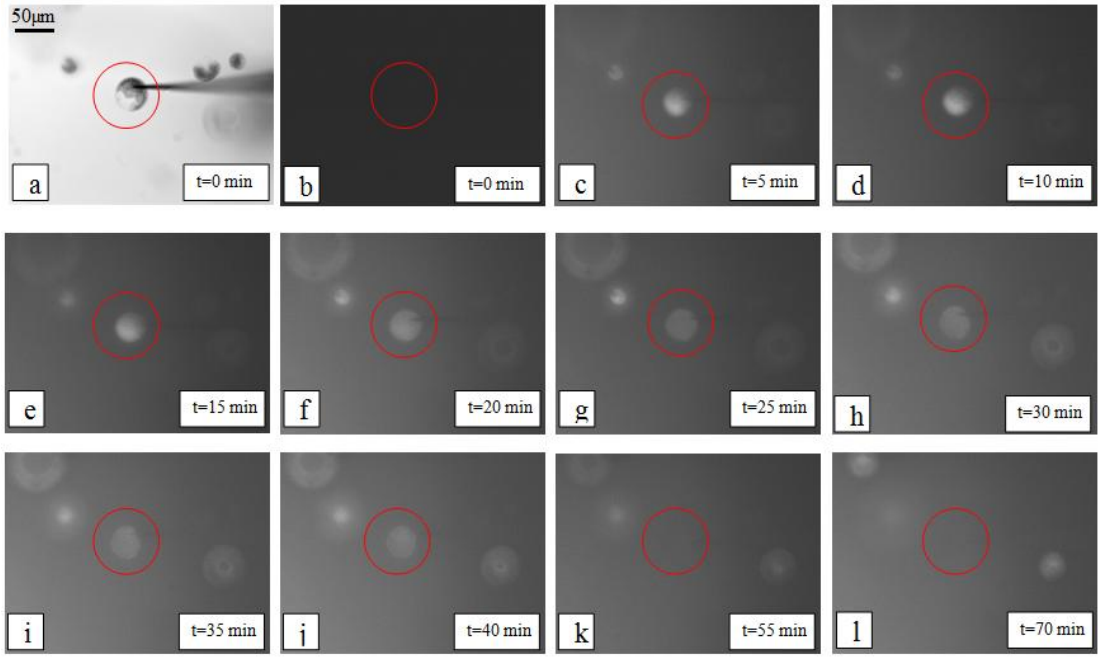

Figure 4.15: Time-lapse images of a single *A. thaliana* protoplast in presence of the heat stress produced by TMC (R=3 kΩ).

The heat shock response in cells was studied in dependence of the orthogonal distance from the heat source. (Figure 4.16) shows the measured value of ROS-indicating fluorescence for three cells in three different positions.

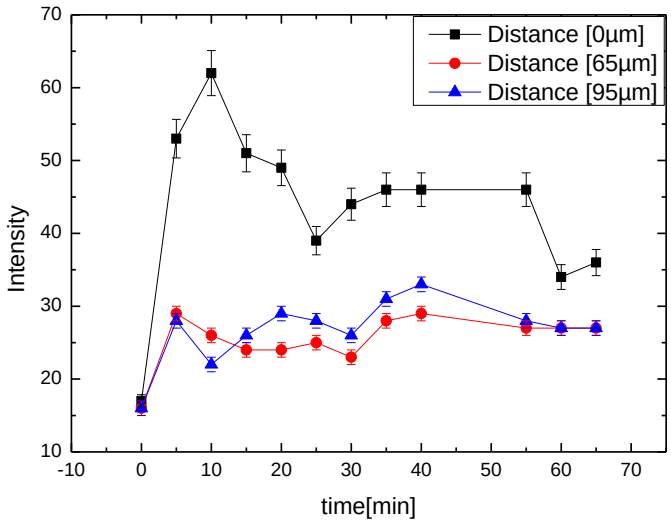

Figure 4.16: Relative intensity measured for three cells in different positions respect to the orthogonal distance from the TMC

4.3 *Local stimulation by chemical oxidative stress*

4.3.1 *Local stimulation outside the cell*

To simulate the cell condition, several holes with 100 μm and 300 μm diameter were prepared from SU-8 3025 on a glass substrate, by means of UV lithography as it is shown in (Figure 4.17).

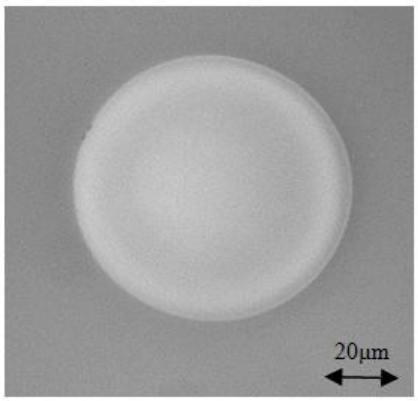

Figure 4.17: SU-8 3025 hole created by UV lithography method.

Several pre-tests were carried out in order to study the chemical oxidative stress out of the cell in these holes in addition to positive and negative control experiments to validate the experimental results.

The chemical oxidative stress experiment was performed in a micro hole (100 *µm* in diameter). A (2:1) ratio mixture of 10 *mM* D-alanine and 2 *µM* H_2DCF-DA was added and followed by addition of 2.8 *µm* streptavidin beads coupled with 0.08 *µg/ml* D-amino acid oxidase (DAAO) into the hole. The formation of H_2O_2 as a result of reactions between DAAO and 10 *mM* D-alanine was monitored by camera. Time lapsed images in (Figure 4.18) show the results of this experiment.

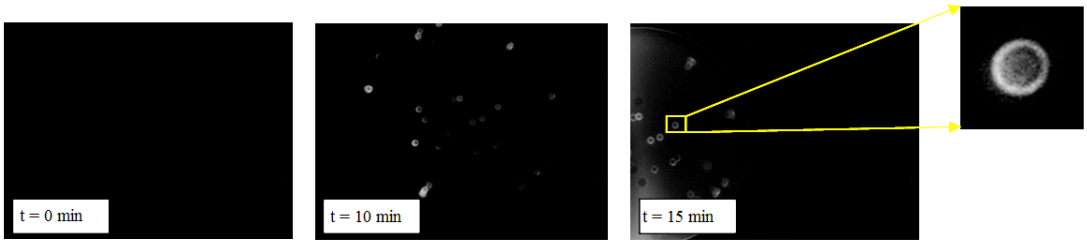

Figure 4.18: Generation of H_2O_2 around the bead surface of a 2.8 *µm* functionalized particle as a result of reactions between DAAO and D-alanine

4.3.2 *Local stimulation in A. thaliana vacuole fluid*

The next step was to repeat the experiment described above using *A. thaliana* vacuole fluid. Two positive control experiments were carried out in this stage.

4.3.2.1 Positive control experiments

– First positive control was carried out in a 100 *µm* diameter hole containing 2 *µl* mixture of *A. thaliana* vacuole fluid, 2 *µM* H_2DCF-DA and 10 *mM* D-alanine with a ratio of (2:1:1). See figure (Figures 4.19 .a). Then 2 *µl* of 50 *mM* H_2O_2 was added to the assay mixture inside the hole. 5 minutes later, reactive oxygen species (ROS) formed due to oxidative stress were detectable by DCF fluorescence. (Figures 4.19 .b-f) indicate the whole experiment period including the initiation of the reaction, maximum exposure and termination of the reactions.

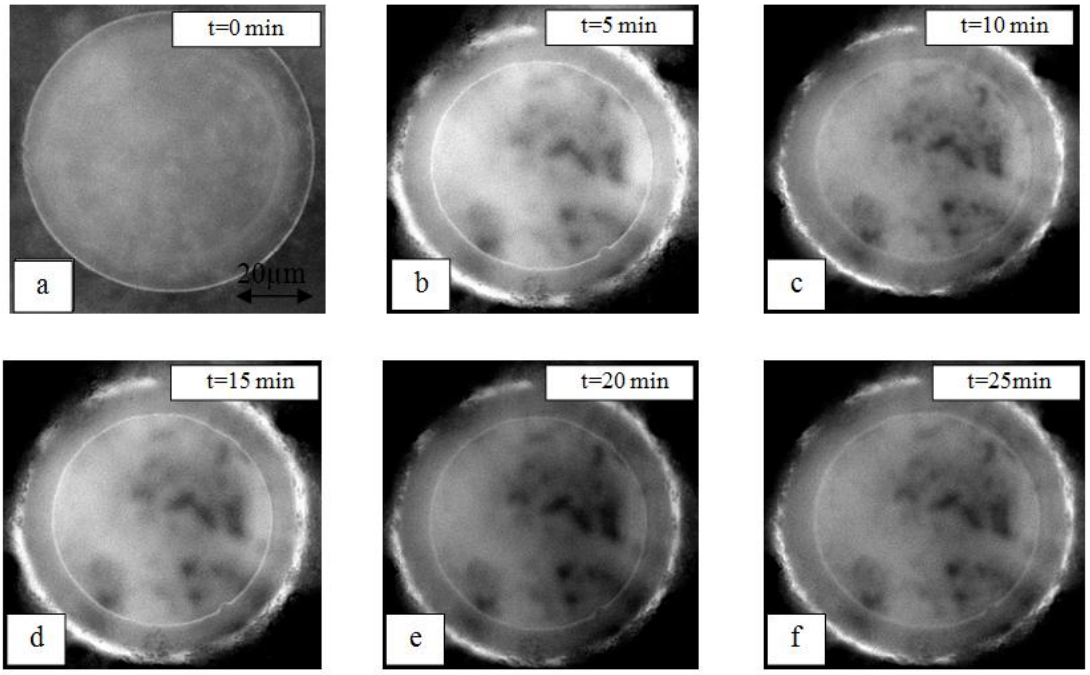

Figure 4.19: Positive control experiment performed by adding 50 *mM* H_2O_2 to the mixture of *A. thaliana*, H_2DCF-DA and D-alanine. Intensity of light emitting increased because of creating DCF inside the hole, (b) after 5 minutes and decay during the time (f).

– The next positive control experiment was accomplished by adding 1 μl DAAO 0.08 $\mu g/ml$ to the suspension of *A. thaliana* vacuole fluid with 2 μM H_2DCF-DA and 10 *mM* D-alanine in the 100 μm hole. As it is shown on (Figure 4.20), it took 10 minutes to observe initiation of H_2O_2 formation detectable by changing the intensity of DCF fluorescence due to reaction between DAAO and D-alanine.

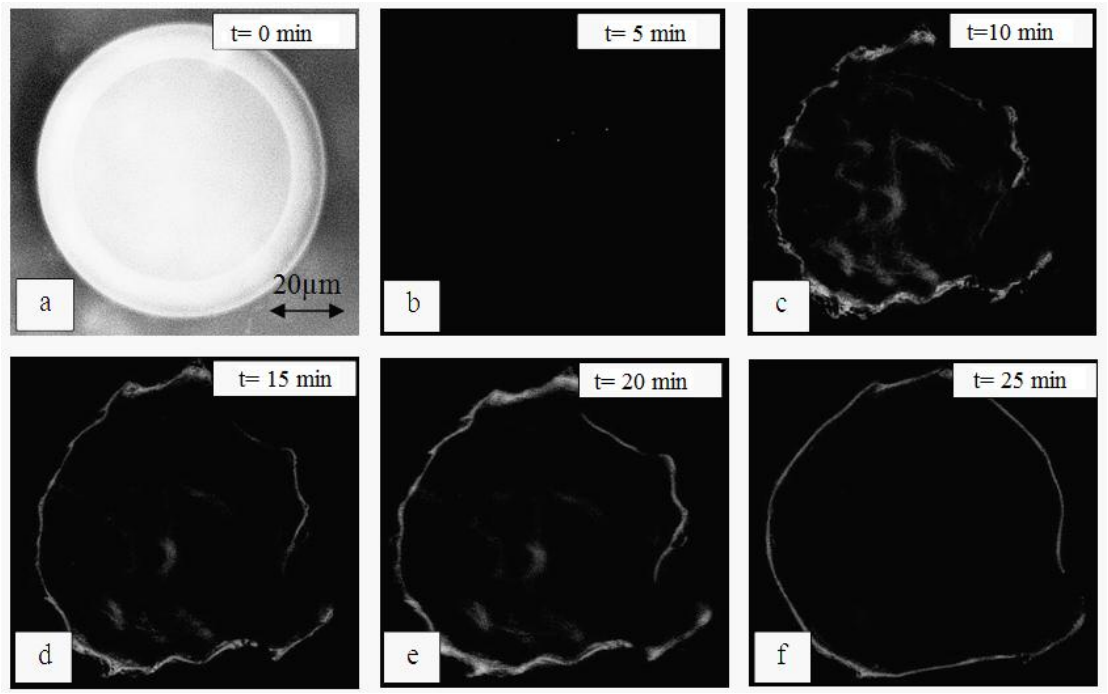

Figure 4.20: Positive control experiment to detect the reaction between DAAO and D-alanine.as it shown in the pictures after 10 minutes (c) DCF light emitting started because of ROS generation and decay during the time (f).

4.3.2.2 Local stimulation on vacuole fluid of A. thaliana

The final test was to exert the functionalized particle with 0.08 *µM/ml* DAAO to stimuli local chemical oxidative stress in a hole. A 1.05 *µm* streptavidin particle with dilution of (1:100) was coupled with 0.08 *µg/ml* DAAO. A 100 *µm* diameter hole was filled by 1 *µl* mixture of *A. thaliana* vacuole fluid, 2 *µM* H_2DCF-DA and 10 *mM* D-alanine at a ratio of (2:1:1) and then the coupled particles were added to the mixture inside the hole. According to the time lapsed images in (Figure 4.21), the fluorescence was observed 15 minutes after adding the coupled particle inside the hole.

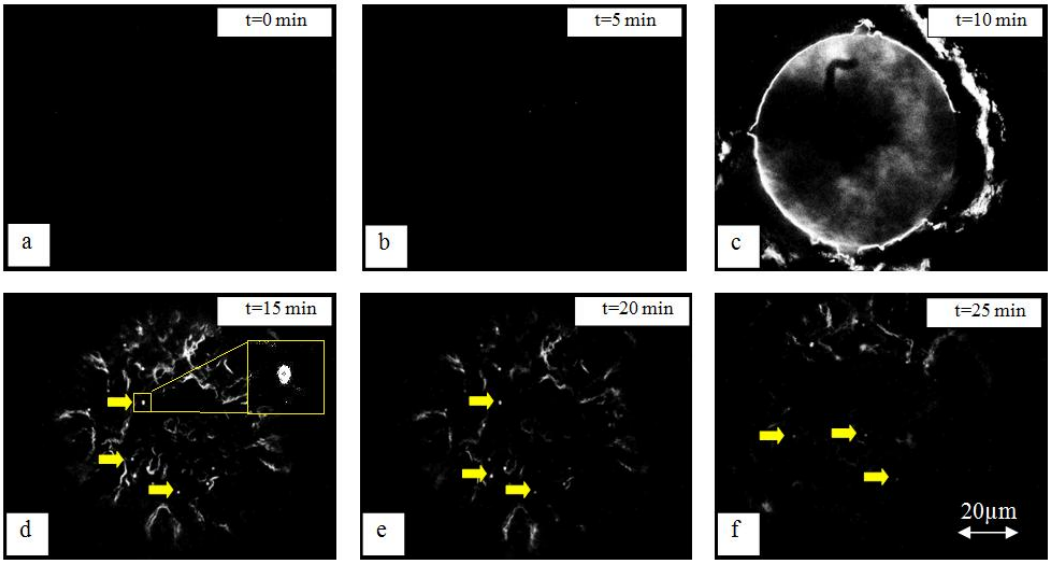

Figure 4.21: Local oxidative stress generated around the bead surface in *A. thaliana* vacuole fluid environment after 15 minutes (d) . (1.05μm streptavidin functionalized particle used to detect the ROS generation)

4.3.3 *Local stimulation inside the cell*

Local chemical oxidative stress was studied in *A. thaliana* cells with 1.05 μm streptavidin functionalized particle. Two positive and negative control experiments were carried out.

4.3.3.1 Positive control experiments

– As the positive control experiment, a 300 μm diameter hole was designed to trap a few cells immersed in W5 buffer solution. *A. thaliana* cells were preloaded in 2 μM H_2DCF-DA and trapped in a 300 μm diameter holes. 1 μL of 50 mM H_2O_2 was added to top of the trapped protoplasts in the hole carefully (because they can easily escape from the hole). Time-lapsed images of the process are presented in (Figure 4.22) illustrating that immediately after adding H_2O_2, ROS generation started because of oxidative stress in the cells (follow the same color rows during the time which are showing the changing the intensity of DCF fluorescence as a result of ROS generation).

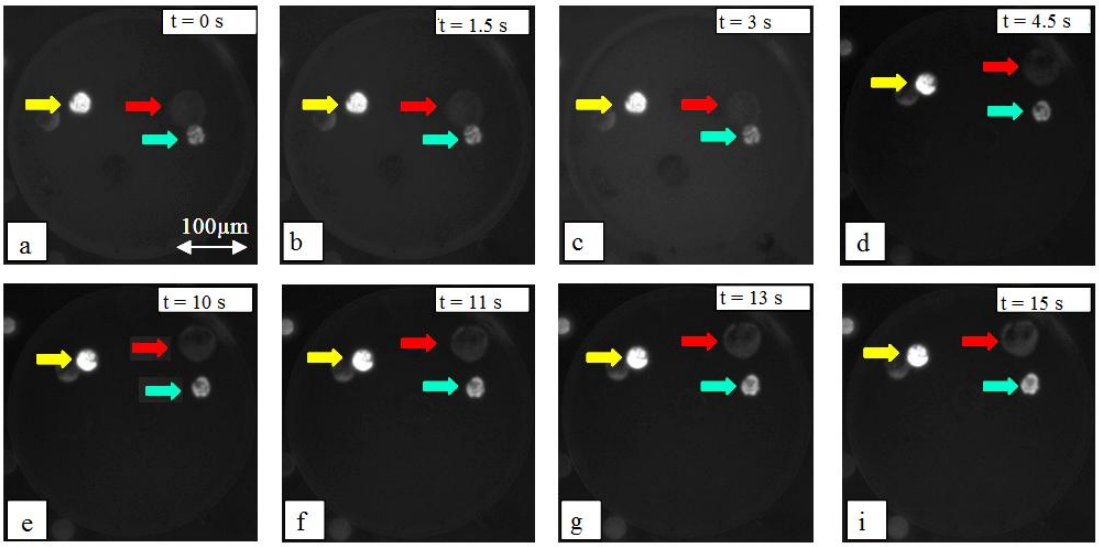

Figure 4.22: H_2O_2 added on top of the cells reloaded in H_2DCF-DA as a positive control experiment to detect the DCF emitting light. Same color of arrows shows the changing the intensity emitted from the cell during the time

– The second positive control experiment was carried out by injecting DAAO into the cell. For this experiment, *A. thaliana* cells were incubated with 2 *µM* H_2DCF-DA and 10 *mM* D-alanine and then embedded in Agarose gel. A dilution (1:10,000) of 0.08 *µg/ml* DAAO and Kpi was injected into the cell by the injection capillary ID:1.47 *µm*. The reaction between DAAO and D-alanine after injection of DAAO was monitored which is shown in (Figure 4.23. a-h) as the changes in DCF fluorescence represent the oxidative stress.

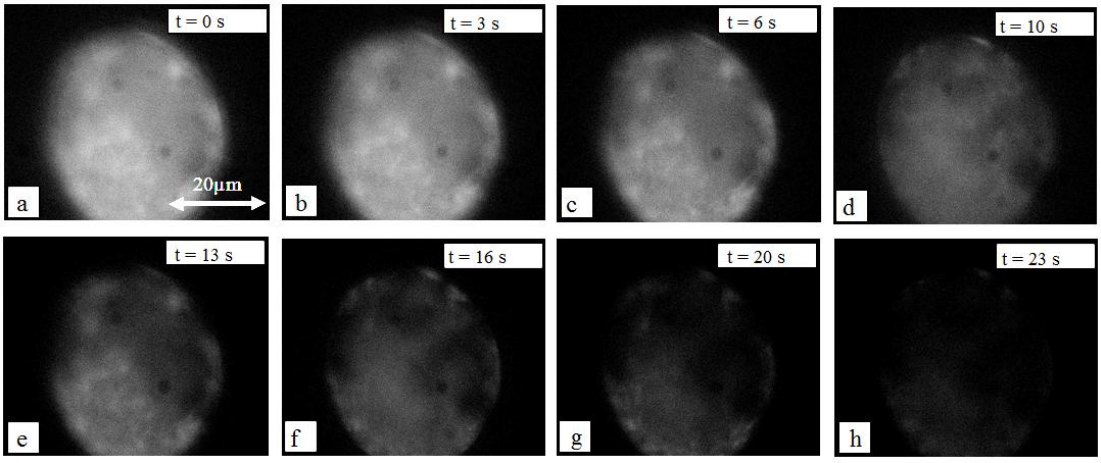

Figure 4.23: Injection of DAAO inside the cell reloaded in H_2DCF-DA and D-alanine as positive control experiment. As it shown in the pictures (a-h) the intensity of light changes because of the reaction of DAAO and D-alanine inside the cell and decay during the time.

4.3.3.2 Negative control experiment

– As a negative control experiment, pre-loaded *A. thaliana* cells in 2 μM H_2DCF-DA were monitored for a period of 20 minutes to detect any reaction due to oxidative stress in room temperature, but as it is clear in (Figure 4.24) no stress was detected.

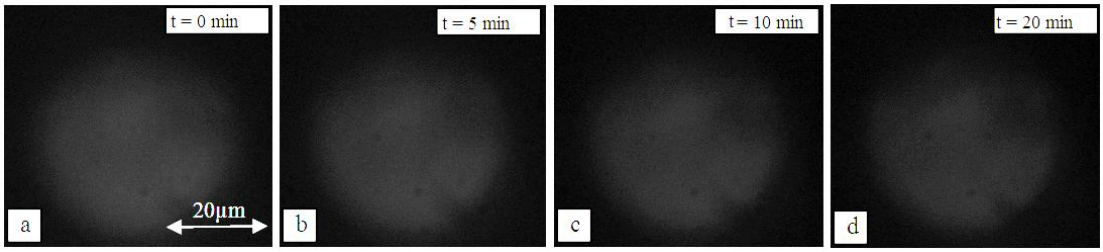

Figure 4.24: Negative control experiment to detect the environment stress. No signal detected during the 20 minutes.

– The second negative control experiment was performed by injecting a dilution of (1:100,000) 1.05 μm uncoupled streptavidin particles into *A. thaliana* cells which were incubated with 2 μM H_2DCF-DA and 10 mM D-alanine and then embedded in Agarose gel. The purpose of this test was to detect any toxicology stress due to either injection of the particles into the cells or any chemical reaction of the bead inside the cell or mechanical stress due to penetration of the injection capillary. (Figure 4.25) shows the time-lapsed images of the cell during the experiment, indicating that no stress was observed after injecting uncoupled particle inside the cell.

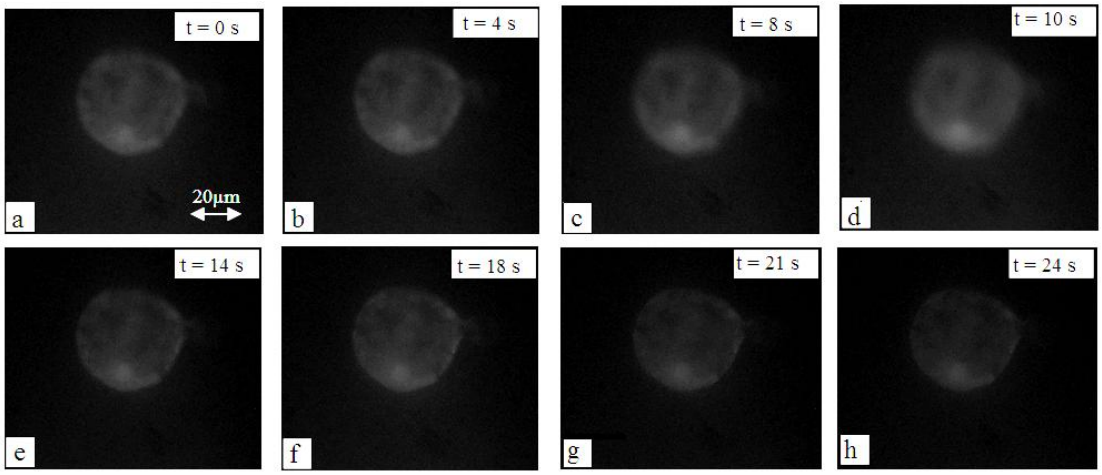

Figure 4.25: Injection of 1.05 μm uncoupled particle inside the cell to detect the light emitting because of oxidative stress as a negative control. No signal detected after injecting the particle inside the cell reloaded in H_2DCF-DA and D-alanine.

4.3.3.3 Local chemical oxidative stress into the cell

Upon completion of the positive and negative control experiments, the final step was injecting the functionalized particles into the cell to induce chemical oxidative stress locally. This step was designed in the two different following methods.

– Holding the cells by Agarose gel

1.05 μm particles coupled with 0.08 $\mu g/mL$ DAAO in (100,000) dilution were filled in a 1.47 μm injection capillary and injected into *A. thaliana* cells by applying 456 *hPa* pressure. The cells were incubated with 2 μM H_2DCF-DA and 10 *mM* D-alanine, and then embedded in Agarose gel. The enzyme activity started in the surrounding area of the particle as a signal of ROS generation.

– Holding the cells by holding capillary

A. thaliana cell were incubated with H_2DCF-DA and then immersed in W5 solution. The cells were trapped by a holding pipette with 6.5 μm inner diameter.1.05 μm particles coupled with 0.08 $\mu g/mL$ DAAO in (1000, 000) dilution were filled into the injection ICSI capillary with 4.5 μm inner diameter. Then the functionalized particles were injected into the cell and then 10 *mM* D-alanine was added to the top of the cell. After diffusing D-alanine into the cell, ROS formation started at the surface of the particle as a result of chemical oxidative stress. All these process are shown in (Figure 4.26) during the experiment period. Local oxidative stress of *A. thaliana* protoplasts visualized as oxidative stress induced green fluorescence emitted from 2′,7′-dichloro-fluorescein (DCF).

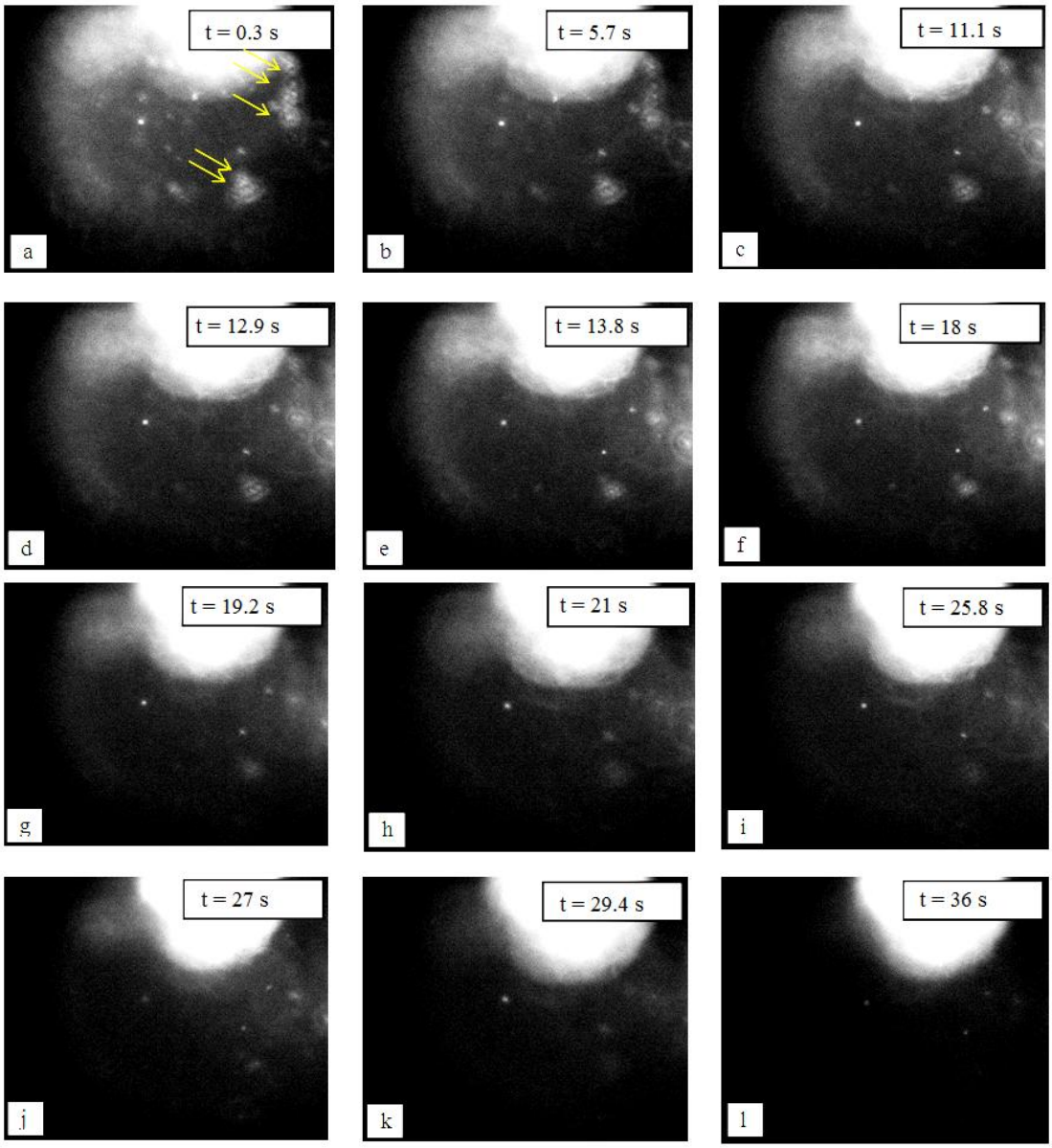

Figure 4.26: Local chemical oxidative stress induce into the *A. thaliana* cell by means of injection of the functionalized particles. Detecting the chemical oxidative stress (ROS) appears as ring around the particles.

Chapter 5: Discussions

This chapter covers the discussions about the various methods utilized for different experiments during the research work. It also highlights special features of various experiments performed during this work compared to other works in this area.

5.1 *Manipulation of particles*

5.1.1 *Holding the protoplast*

Three different methods were implemented for trapping various cells in this work. Due to special needs of each experiment, any of these trapping methods would have their own list of benefits and limitations for that specific application making them more appropriate for one specific application while the same method may not be suitable for other experiments.

As an example from the previous paragraph, trapping the cells in Agarose gel was the most appropriate solution for the chemical oxidative stress experiment, since the target cell could be easily selected, the experiment devices such as microscope could be easily focused on the target and the functionalized particle could be injected into the cells in any direction, in addition to providing the possibility of repeating the experiment several times in the same Petri dish containing target cells. The same advantages are valid for Agarose gel cell trapping method in heat stress experiment as well in addition to providing flexibility in inserting the TMC into the cells in any direction.

Against the heat stress and chemical oxidative experiments, cell trapping by Agarose gel did not quite fit the manipulation of the particle experiments because in this case the cells must have been located on top of the electrodes exactly. In Agarose the operator had no control on the cell positions and the probability of the cell being exactly on top of electrodes is too low. Note that in this method, the cell suspension is dropped onto the electrodes and then Agarose gel is added on top, which minimizes probability of the cell being exactly on top of the electrodes. Even if one cell (in the whole drop) could be trapped, since the other cells are not in desired position, the whole experiment set-up had to be changed in order to repeat the experiment.

Trapping the cells by a micro fluidic channel was not as satisfactory as expected. As it is shown in (Figure 5.1), although the channel width was 2-3 times smaller than the cell diameter (channel width of 20 μm versus cell diameter of 50-100 μm), the cells could still not be positioned on top of electrodes mainly due

to flexibility of the cell membranes causing them to escape from the trapping zone.

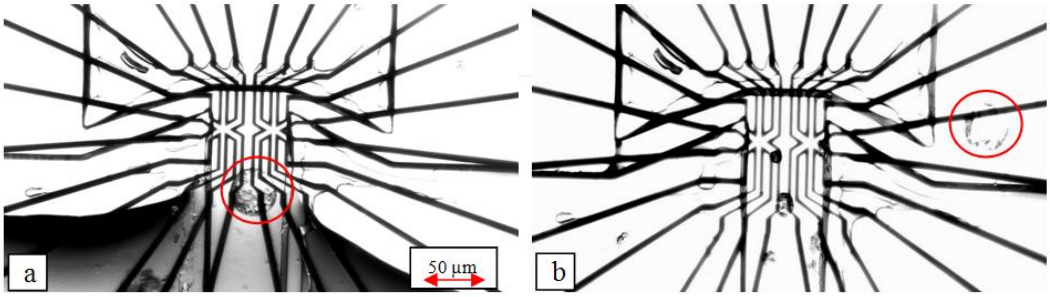

Figure 5.1: a) An *A. thaliana* epidermis protoplast in a micro fluidic channel moving to the trapping zone, b) The cell escaped from the channel due to the flexibility of the cell membrane

Eventually, the holding capillary turned out as the most appropriate method for manipulation experiment, which provided an easy solution for taking the cells and moving them to the top of the electrodes.

Utilizing the holding capillary method enabled us to easily select any cell on top of the electrodes and then drive the trapped cell into the desired location on top of the electrodes in all three dimensions. Another significant advantage of this method compared to the Agarose gel trapping method was the possibility of repeating the experiment several times without changing the experimental set-up.

An important factor in utilizing the holding capillary method is the optimization of the parameters (such as inner and outer diameter, bending angle and bending length of capillary, suction pressure etc.) according to the cell sizes. Refer to images in (Figure 5.2), too large holding capillary size (Figure 5.2.a) or high suction pressure inside the holding capillary sucks the cells into the capillary while too small size (Figure 5.2.b) or too low suction pressure results in inappropriate trapping and holding feature required for the injection purposes.

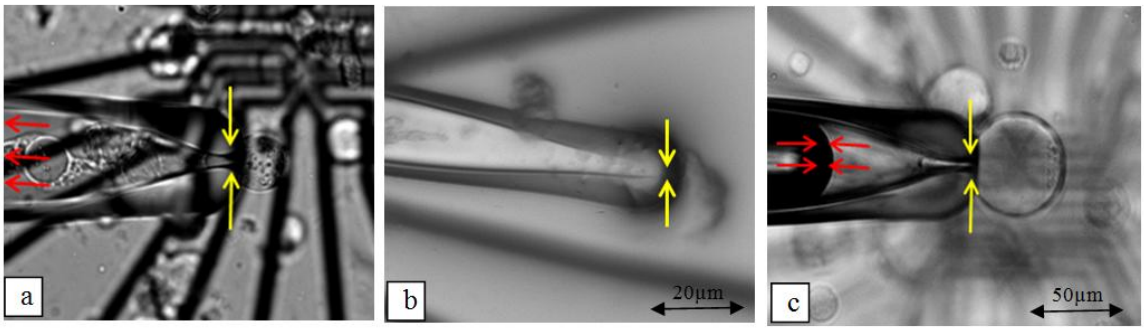

Figure 5.2: a) Inappropriate capillary size for holding the cells: due to large inner diameter and applying high suction pressure some of the cells are sucked into the pipette. b) Capillary with small inner diameter is blocked as soon as entering to suspension c) Appropriate capillary size with sufficient suction pressure. Parameter of holding capillary were optimized as (BA=35˚, ID=6.5 μm, B=0.5 mm, BL=500 μm)

5.1.2 *Injection into the cell*

An ordinary pulled capillary is not suitable for injecting the particles into the Barley cells for manipulation experiment. As it is shown in (Figure 5.3.a) if a normal capillary was used for injection, the cell could easily escape firstly because of the injection axis (which is not in the same axis of holding capillary) and therefore any mechanical forces coming from the injection capillary would push the cell away from the holding capillary and secondly because of the round shape of the injection capillary tip. In order to overcome these issues, a bent capillary with a spike should be used and positioned at the same level and axis of the holding capillary (Figure 5.3.b). This requires the bending angle of injecting and holding capillaries to be the same. Additionally, the tip size of the injection capillary should be optimized. In one hand, it should be large enough to accommodate and carry the particle from the capillary to the cell and on the other hand, it should not be too large. Otherwise, it would burst the cell membrane during penetration. (Figure 5.3.b) represents the optimized solution, which is a capillary with an opening diameter of 4 μm with spike and positioned in the same level and axis of the holding capillary.

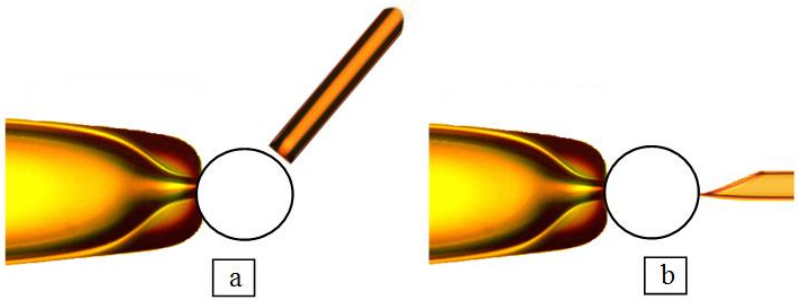

Figure 5.3: a) Normal injection capillary b) Proper situation for injection experiment using a bend capillary with spike ID: 4 µm and BA: 35˚. [Taken from ref (109)]

Injection into the *A. thaliana* cell embedded in Agarose gel for generating chemical oxidative stress done by normal pulled capillary (ID: 1.43 μm) while the cell was fixed in position and stabilized in all sides by Agarose gel.

One of advantages of this method is the capability of controlling the number of injected particles into the cell by means of the ICSI capillary and of optimizing the Pc pressure to inject only one particle (Figure 5.4). Other methods such as spraying and bombardment do not offer such a useful feature in controlling the number of the injected particles in addition to other limitations such as very long duration (in some case 30 minutes to 2 days) for the particle injection process inside the cell like phagocytoses[1,94] method.

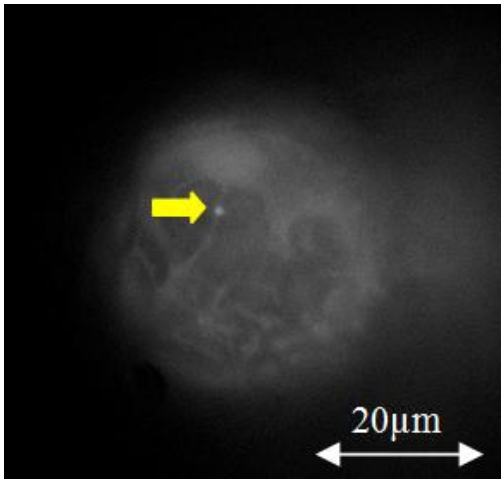

Figure 5.4: Injection of a 1.05 μm particle into the cell

5.1.3 *Electrical isolating layer to protect the electrodes*

Electrodes are prepared by an e-beam lithography process. The cell suspension will be dropped on top of the electrodes and the holding and injection capillaries will move around the electrodes during the experiment. The electrodes should be fabricated with a strong protection against water environment in addition to their resistance to scratching. Initially Ta_2O_5 was sputtered as the top layer of the electrodes acting as electrical isolation layer but during the experiment, it was discovered that as soon as the electrical voltage is applied this resist would decompose; and also the upper layer would be scratched by the capillaries. See (Figure 5.5)

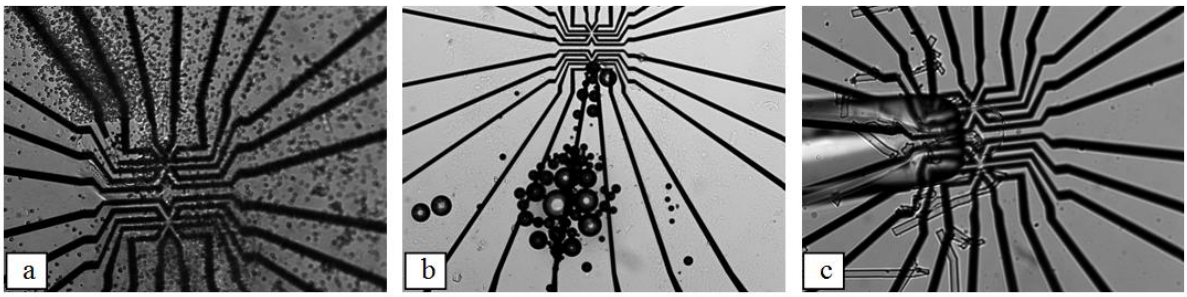

Figure 5.5: Sputtering Ta_2O_5 as electrical isolation layer was not good enough to protect the electrodes. a) Decomposition of the isolating layer after applying voltage to the electrodes b) Boiling water around the electrodes c) protection layer scratched by a movement of the capillary on top of the electrodes

These issues were resolved by spraying a special type of plastic resist[16] into the mid-section of the sample after bonding on an IC socket in addition to Ta_2O_5 sputtering. The resist is a colorless, flexible and transparent media.

5.1.4 *Determination of Viscosity*

To determine the viscosity of a medium we need to analyze the movement of a bead in a surrounding media. (All manipulation experiments to determine the viscosity of fluid were done in a controlled room temperature 23˚C, with ±2 ˚C temperature tolerance. Also a control experiment was set up to ensure temperature of the fluid does not change considerably during the experiment. For further information, refer to Appendix 2), (Figure 5.6) represents a schematic of the sample set-up and the forces acting on the particle. The total force acting on the particle is derived from the relative velocity of the particle during the movement point by point, considering the particle mass.[95]

[16] Plastik-70 Schutzlack, Quick drying, colorless transparent insulating and protective coating based on acrylic resins. Produced by CRC Industries Europe BVBA, KONTAKT CHEMIE

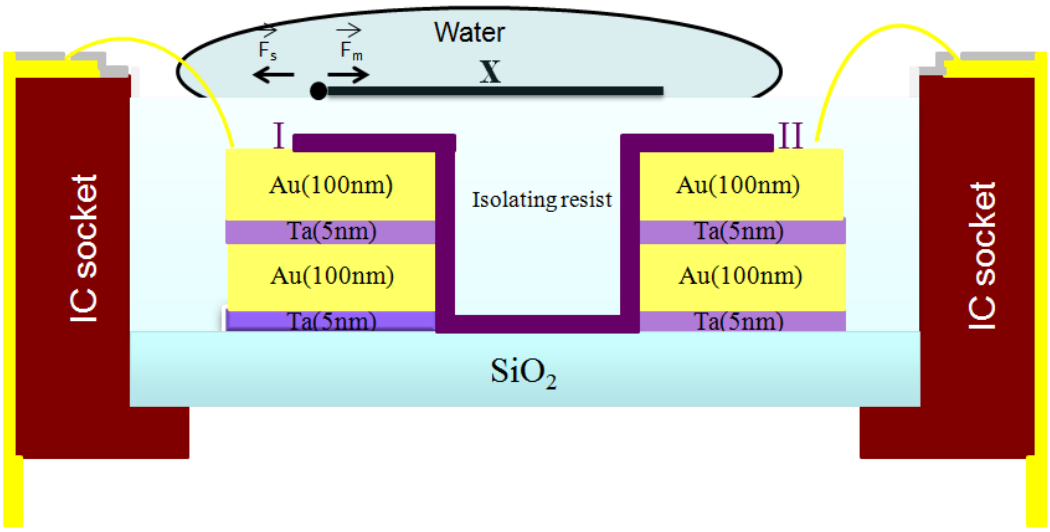

Figure 5.6: Schematic of forces acting on a bead in the magnetic field

The magnetic force for straight electrodes has been calculated by the Whiteside group in 2007.[96] This equation (eqn (7)) needs a constant coefficient to match to V type electrodes which was found by geometrical consideration (eqn (8)) (C= 0.21).

Using this magnetic force from (eqn (9)) and Stokes force from (eqn (11)), the viscosity of water[97] was determined but the result was not in accordance with the literature value (Figure 5.7). To resolve this issue (eqn (11)) and (eqn (9)) were introduced into (eqn (10)) to obtain (eqn (12)) as below: (by rearranging the equation as X and $\dot{X}$ and considering the constant coefficients of X and $\dot{X}$ in equations as K_1, K_2, K_3)

$$m\frac{d^2x}{dt^2} = \frac{K_1}{x^2} + \frac{K_2}{x^3} + K_3\frac{dx}{dt} \qquad (12)$$

Solving (eqn (12)) by a finite differential method[98] resulted in (eqn (13)) considering the step size of (h=0.03s). h is the time step for imaging during the experiment. (For more details see appendix. 3)

$$x(t+h) = \frac{\frac{K_1}{x^2(t)} + \frac{K_2}{x^3(t)} - \left(\frac{2m}{h^2} - \frac{K_3}{h}\right)x(t) - \frac{m}{h^2}x(t-h)}{\left(\frac{m}{h^2} - \frac{K_3}{h}\right)} \qquad (13)$$

The series of data points achieved with this equation gives us a curve which helps us to optimize the C value for resolving the issue. Two data series are represented in (Figure 5.7); the dotted values represent the experimental data for the displacement of the particles versus time and the solid line represents the x

values calculated by the numerical method (eqn (13)) with a constant coefficient of C=0.21. It is clear that the fit is not representing the experimental data.

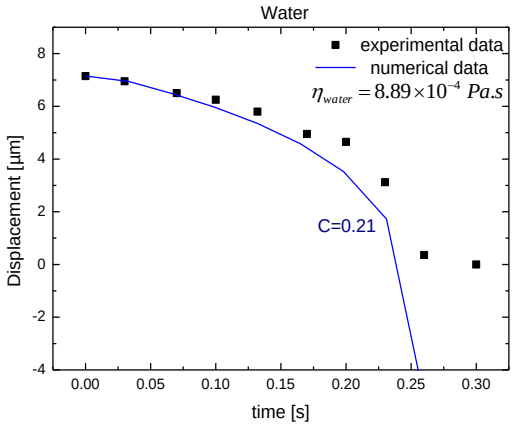

Figure 5.7: Experimental data and numerical calculation for displacement of a particle in water environment by considering the viscosity of water as known value according to the literature.

One explanation for the difference between these two graphs is the calculation of the constant coefficient C. The magnetic field and therefore the magnetic forces generated around the V type electrode are not only function of the wire geometries (C) but also the current density passing through the wire. As such, magnetic forces around the electrodes could not be determined accurately based on geometrical consideration.

Several C values were introduced to (eqn (13)) to find the best fit considering the standard value for water viscosity. The best value for C was found as C=0.19 (Figure 5.8). (The water viscosity is 8.9×10^{-4} *Pa.s* at 25 ˚C and 1×10^{-3} *Pa.s* at 20 ˚C)[98]

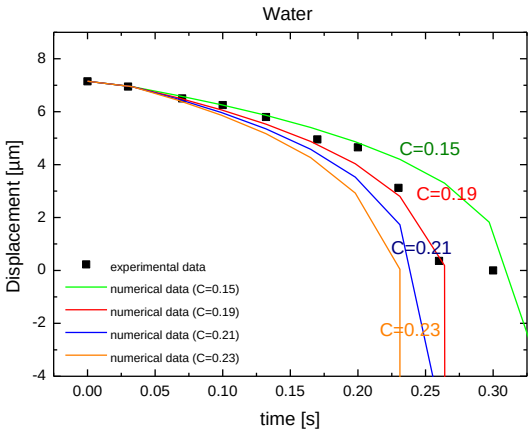

Figure 5.8: Optimization of C value for the best fit between numerical and experimental data

Additionally, the viscosity of Barley vacuole interior and Vacuole fluid of Barley cell were calculated assuming C=0.19. (Figure 5.9) shows the finding procedure using the numerical method and the experimental data points to determine the viscosity of Barley and Vacuole fluid.

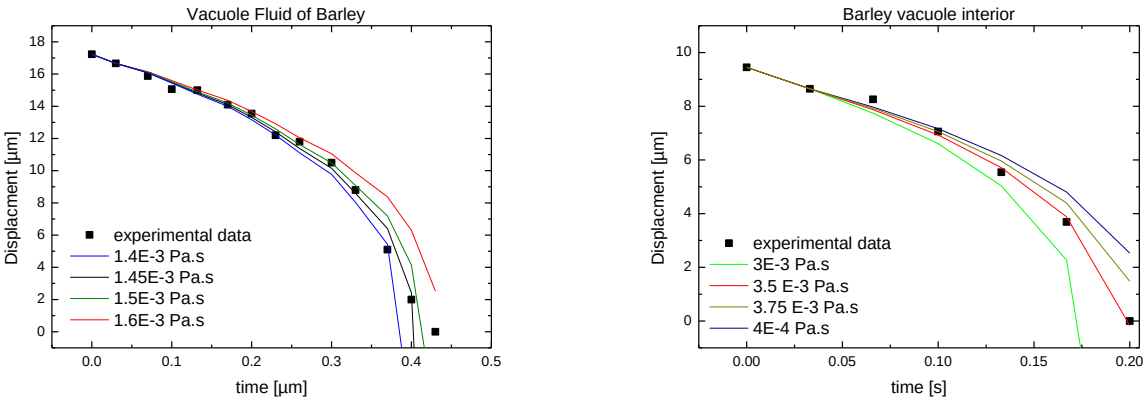

Figure 5.9: Finding the best fit using the numerical method (eqn (13)) and the experimental data to determine the viscosity of Barley and Vacuole fluid (C= 0.19).

The experiment was repeated several times for Barley, Vacuole fluid and water, and the average value of the viscosity for each fluid was determined as it is shown in (Figure 5.10).

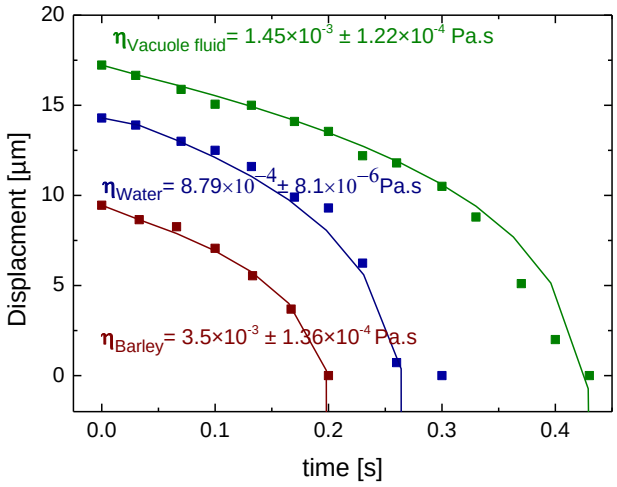

Figure 5.10: Calculated average viscosity of various fluids by numerical method modified by experimental data.

Also the average viscosity value for Barley, water and Vacuole fluid calculated from the experimental data for the first few points of displacement curves are presented in (Figure 5.11). The viscosity of water determined by our experimental ($\eta = 8.78\times10^{-4} \pm 3.07\times10^{-5}\ Pa.s$) was very close to the literature value $\eta = 8.89\times10^{-4}\ Pa.s$. It was assumed that because of the cell membrane effect the viscosity of Barely is larger than the vacuole fluid.

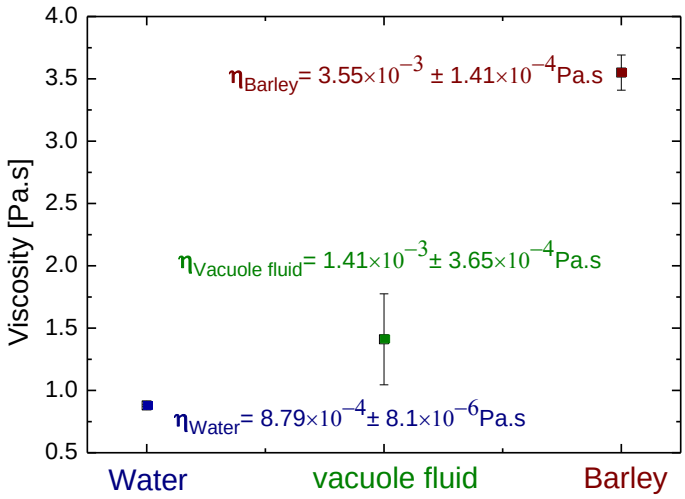

Figure 5.11: Comparison of viscosity values for Barley, Vacuole fluid and water

This means that movement of the particle in a Barley cell is slower than in Vacuole fluid due to the cell conditions and the effect of the cell membrane pressure on molecules and particle inside. Calculations and experimental data verify this statement. Comparison of the results from these two methods is presented in (Table 5.1).These results indicates reasonable agreement between numerical method and experimental methods.

Table 5.1: Comparison of the calculated viscosity values for different fluids by means of numerical and experimental method

Medium	Numerical method (Pa.s)	Experimental method (Pa.s)
Water	8.89×10^{-4}	$8.79\times10^{-4} \pm 8.1\times10^{-6}$
Vacuole liquid	$1.45\times10^{-3} \pm 1.22\times10^{-4}$	$1.41\times10^{-3} \pm 3.65\times10^{-4}$
Barley	$3.5\times10^{-3} \pm 1.36\times10^{-4}$	$3.55\times10^{-3} \pm 1.41\times10^{-4}$

Also diffusion constants (eqn (14)) could be calculated using the viscosity values obtained for various molecules with different molar masses. (See table 5.2)

$$D = \frac{kT}{6\pi\eta R_H} \tag{14}$$

Where k (m^2. kg. s^{-2}. K^{-1}) is the Boltzman constant, T (K) is the absolute temperature, η ($Pa.s$) is the viscosity of the environment and r (m) is the radius of bead.

Also characteristic diffusion time can be determined by (eqn (15)).

$$< x^2 >= 2Dt \tag{15}$$

$< x^2 >$ (m^2) is the average square of the distance traveled by the bead, D ($m^2.s^{-1}$) is the diffusion coefficient and t (s) is the time.

Table 5.2 presents the calculated diffusion time for the interior vacuole of Barley.

Table 5.2: Diffusion constants and diffusion times calculated for various molecules in the interior vacuole of Barley.

	Molar mass [g/mol]	Density [g/cm^3]	Hydrodynamic Radius [m]×10^{-10}	Diffusion constant [$m^2\ s^{-1}$]×10^{-10}	Diffusions time [s]
Ca^{+2}	40.078	1.54	2.18	3.14	1.43
Malic acid	134.09	1.6	3.21	2.13	2.11
10kDa	10000	1.2	1.49	4.6	9.7
20kDa	20000	1.2	1.88	3.65	12.33
50kDa	50000	1.2	25.5	0.26	16.74
100kDa	100000	1.2	32.1	0.21	21.1

The local active forces produced by an electrode on a 1.05 μm bead varies from 2 nN at the center of the V type electrode to 0.5 pN at 20 μm distance from the center which is the farthest distance the particle could be manipulated by

electrodes. The calculation of the magnetic force generated by the electrodes in this thesis was much stronger than that used in other works.[2,7] As an example compared to magnetic tweezers (permanent magnet) that generate 150 pN[1] or 900 pN[2] or 12 pN[99] to move a 1.05 μm bead.

The distance of the particle movement to a predefined position achieved in this work, ranged at least four times to forty times longer than that of previous works many other methods do not provide the capability of fixing the particles in a position which enable the researcher to fix the particles at desired position. The other advantage of this work is offering multiple positioning points for fixing and trapping the particles inside the cell, due to 12 electrodes provided on the IC socket. In addition, particles could be manipulated at a speed of 3.03×10^{-5} ($m\ s^{-1}$) between two electrodes which is 100 times faster than other literature values.[2]

The main advantages of the methods used here compared to previous works are a cell manipulation with wide flexibility in selecting various cell types, holding the cells in any desirable position, controlling the number of the injected particles in a short time, generating strong forces by means of current carrying wires, possibility of fixing the particles in multiple positions for analysis and triggering local effects into the living cell.

5.2 *Heating experiment*

5.2.1 *Calibration of the thermo capillary*

The stability of TMCs for local heating of single cells to elicit molecular responses was studied. For heating experiment, Joule heating was selected.

After coating two opposite sides of a pulled capillary by 200 *nm* Ta, different voltages were applied to them in order to study the heat generation behavior of the capillary. Resistance of capillary was 3.2 $k\Omega$. The results in (Figure 5.12), suggest a linear relationship between the maximum temperature difference generated by TMC and the applied voltage.

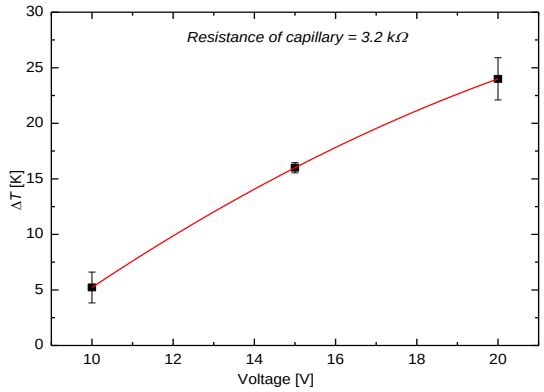

Figure 5.12: Calibration of TMC by applying different voltages (polynomial fit function used to find the best fit because of relation of temperature and voltage ($T = T_0 + \propto_1 V + \propto_2 V^2$))

In order to calibrate the TMC as a stable heat generator, the mass of the capillary can be calculated by two different methods. The first method is calculating the mass by the generated thermal energy in the TMC and in the second method mass the capillary mass is calculated based on its geometry and the properties of glass.

The generated thermal energy in TMC by applying 20 *V* DC is calculated by (eqn (16)) as below where $\frac{\Delta T}{t}$ is the slope of the TMC (R= 3.2 *k*Ω) temperature rise curve per time (Figure 4.11).

$$C_V m \Delta T = VIt \qquad (16)$$

$$\frac{\Delta T}{t} = \frac{VI}{C_V m}$$

Where C_v is the heat capacity of glass ($kJ\ kg^{-1}\ ^{\circ}C^{-1}$), m is the mass of the TMC (*kg*), V is the electrical voltage (*V*), I is the electric current (*A*) and t is the time (*s*)

$$m = \frac{20^2 kg}{733 \times 3.2 \times 10^3 \times 8} = 2.109 \times 10^{-5}\ kg$$

The mass of the TMC by this total thermal energy method is calculated as:

$$m = 2.109 \times 10^{-5}\ kg.$$

To implement the second method, the density of glass ρ=2.65 $\times 10^3$ ($kg\ m^{-3}$) multiplied by the volume of the capillary calculated from the length of capillary coated by Ta (L=26 *mm*), the inner diameter of ID=0.78 *mm* and outer an diameter of OD=1 *mm* is introduced in (eqn (17))

$$m = \rho V = \rho\pi(r_{OD}{}^2 - r_{ID}{}^2)L \qquad (17)$$

$$m = 2.119 \times 10^{-4}\ kg$$

The mass value calculated by first method is much less than the second method, indicating that the heat generation is mostly limited to the TMC tip not the whole TMC body.

A critical point in fabricating a proper TMC is the Ta coating on two opposite sides of the TMC with sharp edges and making an appropriate connection the between Au wires and the Ta coat on the TMC. Another point is measuring the high resistance of the Ta coating in the range of megaohm (*M*Ω) due to oxidation of Ta on TMC after annealing. This issue was resolved by scratching the Ta coated surface in order to remove Ta_xO from the surface before connecting the Au wires.

5.2.2 ***Heat stress detection***

In order to study the heat stress inside the cells, the formation of Reactive Oxygen Species (ROS) was detected. To monitor the heat stress induced ROS generation the cells were incubated in membrane permeable dye dichloro fluoresceindiacetate (DCF-DA). ROS oxidized DCF-DA to the highly fluorescent 2′,7′-dichlorofluorescein (DCF). Consequently, the ROS production because of heat stress stimulated metabolic disorder in the plant cell system was indicated by appearance of green fluorescence inside the cells. This result confirmed that DCF-DA could be readily used to study the increase of ROS in heated protoplasts.

In addition, TMCs allow measuring energy requirements and thresholds for triggering heat stress signaling in a single cell and studying the propagation of heat stress signaling from the effect site to the site of response.

20 *V* DC was applied to a TMC inserted into the *A. thaliana* cell for 10 minutes. During this period, the ROS indicating fluorescence reached its highest intensity. A control experiment was done with the same cell and the same

conditions but without applying an electrical voltage to TMC. The control experiment indicate only small rise in fluorescence during 25 minutes of the monitoring period.

In (Figure 5.13) green dots represent the light intensity detected during the control experiment. It can be concluded that the intensity of florescent light due to heat stress is insignificant and therefore there is no ROS generation. The black dots denote the cell's response during a 70 minutes experiment period after inserting the TMC and applying electric voltage. ROS indicating fluorescence increased over time, reached its maximum, and then reduced after terminating the electric voltage.

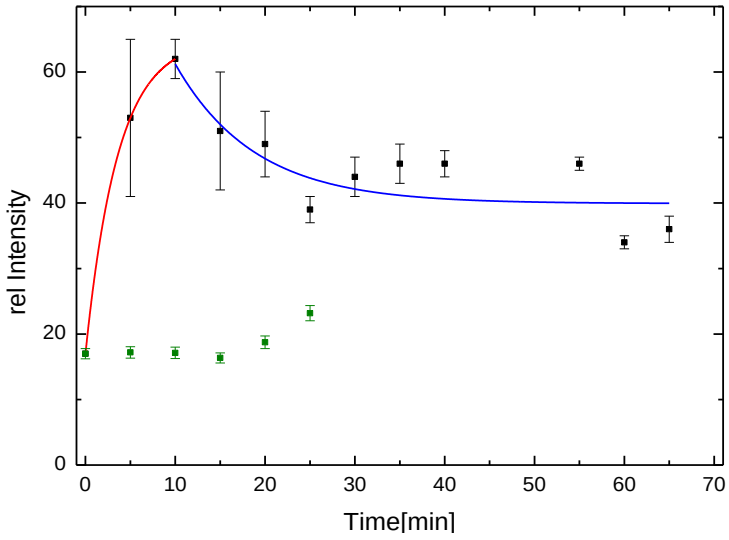

Figure 5.13: Black dots indicate the light intensity, due to ROS generation in *A. thaliana* cell after applying heat stress and the green dots correspond to the control experiment, which shows slow increasing in fluorescence within 25 minutes.

Two aspects were studied in the heat stress cell signaling experiment: first the effect of orthogonal distance of the TMC from the cell on the heat shock response and, second the effect of the heat value generated by the TMC which depends on the TMC resistance.

Regarding the heat shock response, several experiments were carried out by TMCs with various resistances to study the heat shock response of the cell against the heat in different orthogonal distances from capillary. (Figure 5.14) shows the results of heating experiment. These points are related to the highest intensity of each cell in presence the TMC curve and normalized (Figure 4.16). According to these data, lower resistance capillaries generate higher temperatures resulting in

maximum intensity of the heat shock response. Highest ROS formation was achieved by a capillary with a resistance of R=3 *k*Ω.

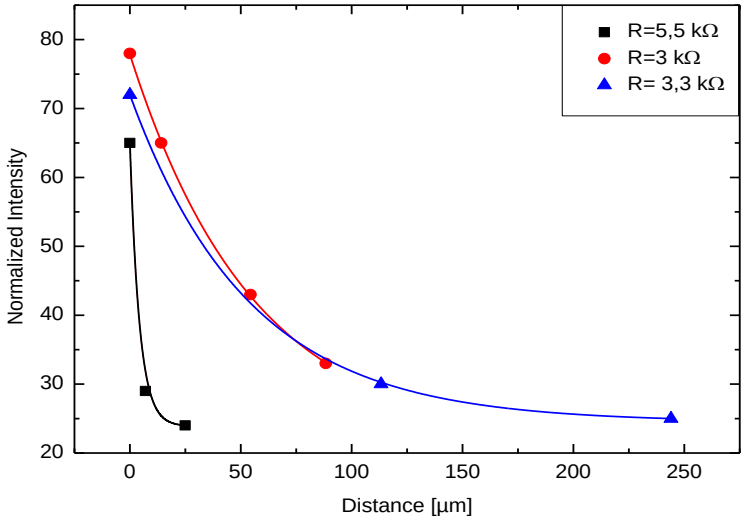

Figure 5.14: Normalized fluorescent intensity of ROS generation versus orthogonal distances of TMCs from *A. thaliana* cell

5.3 *Oxidative stress*

To investigate the chemical oxidative stress in *A. thaliana* cells, several control experiments carried out. The results of chemical oxidative stress in different experiments were indicated by ROS generation. This reaction is measured by light intensity of the DCF fluorescent emission.

As it is shown in (Figure 5.15) the highest ROS intensity generation is related to the first positive experiment by adding the H_2O_2 on top of the cell suspension, and controlling the cell in room temperature to study the environmental stress had lowest intensity. The second positive control experiment does not have such high intensity compared to the chemical oxidative stress experiment because inside the cell the reaction of DAAO and D- alanine only occurs around the particles, therefore the ROS generation is limited to this spot whereas in the main experiment, the reaction (and therefore ROS generation) is spread throughout the hole. Overall, in the positive experiments have higher intensity compared to negative control experiment which proves cell reaction because of chemical oxidative stress (ROS generation around the particle). The exposure time was kept constant for all experiment.

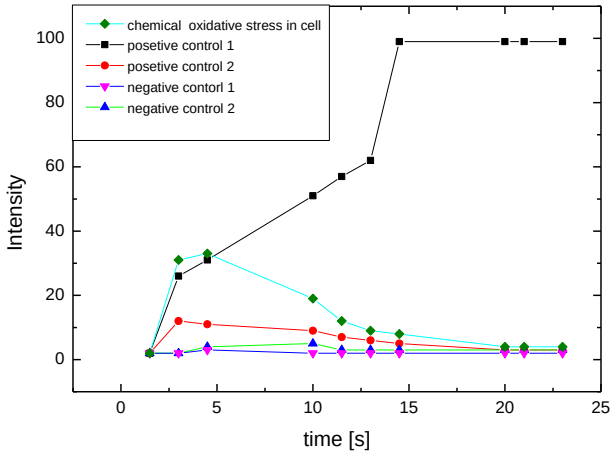

Figure 5.15: Intensity measurements due to chemical oxidative stress around the particle in the cell

A few coupled particles with DAAO were injected into a cell that was incubated in 2 μM H_2DCF-DA and 1 mM D-alanine are shown in (Figure 5.16). Due to the reaction of D-alanine with D-amino acid oxidase, a bright ring around the particles was observed.

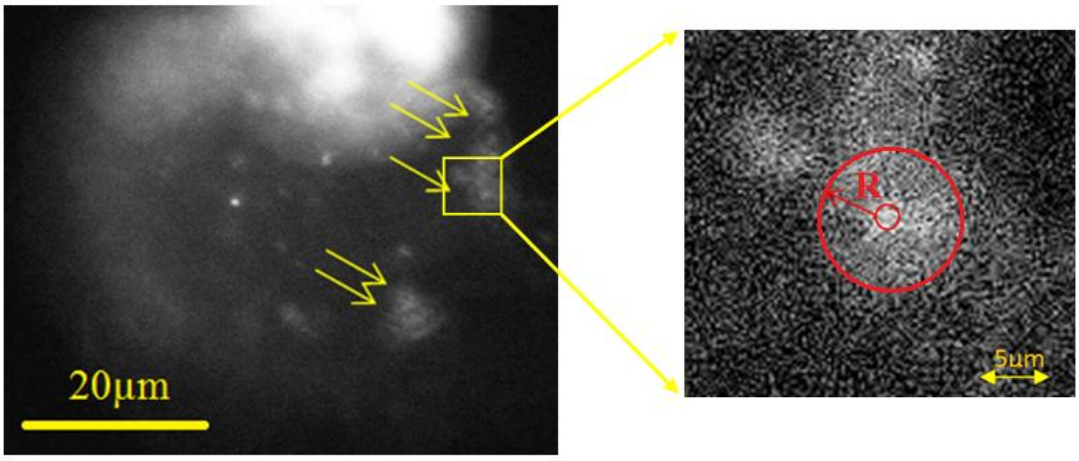

Figure 5.16: ROS formation around the particle because of DAAO and D-alanine reaction. Small red circle shows the boundary of particle and the big red circle shows the ring (chemical oxidative stress boundary around the particle).

This phenomenon explains the fact that ROS formation and therefore florescent light emitting (DCF), continues as long as D-alanine exists inside the cell. To validate this statement, the maximum number of DAAO molecules surrounding a streptavidin particle 1.05 μm was calculated by dividing the surface area of the streptavidin particle by the cross section area of DAAO molecules (eqn (18)) as follows:

$$Area_{particle} = 4\pi r^2 = 4 \times 3.14 \times (0.525 \times 10^{-6})^2\ m^2 = 3.46 \times 10^{-12} m^2 \quad (18)$$

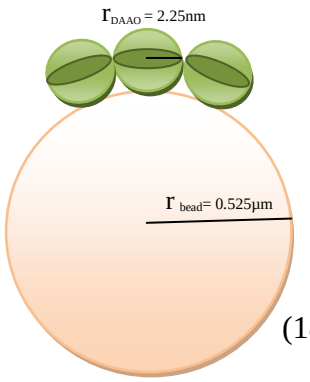

Figure 5.17: Calculating number of DAAO molecules surrounding the 1.05 μm streptavidin bead

The cross sectional area of each DAAO molecule was calculated as A_{DAAO}=16 nm^2, considering the DAAO molecule volume of V_{DAAO}=48nm^3.[100,101] Therefore approximately 200,000 DAAO molecules can be coupled to each particle (Figure 5.17).

The amount of D-alanine= 8×10^9 molecules that react with DAAO per minute in a cell were estimated by considering the turnover rate of D-alanine[102] with one DAAO molecules per minute (K_{cat}=43,000 /min). The total amount of 10 mM D-alanine molecules in a 50 μm cell was calculated as following (eqn (19)):

$$Amount\ of\ D-alanine\ moleclules\ inside\ the\ 50\ \mu m\ cell$$

$$= 10 \times 10^{-3} \frac{mol}{l} \times 6.022 \times 10^{23} \frac{1}{mol} \times 1000 \frac{l}{m^3} \times \frac{4}{3} \times \pi \times (25 \times 10^{-6})^3$$

$$= 4 \times 10^{10}\ \text{molecules} \quad (19)$$

So the amount of D-alanine in a cell will be consumed in five minute for one particle. In our experiment, we have more than ten particles so in few second the D-alanine will be consumed.

The discussion above describes the reason for the appearance of a bright ring around the particles for a short period. According to (Figure 5.18) bright rings, around six different particles were monitored and the ring radius (R) (see (Figure 5.16)) of them was measured over time. See (Figure 4.26)

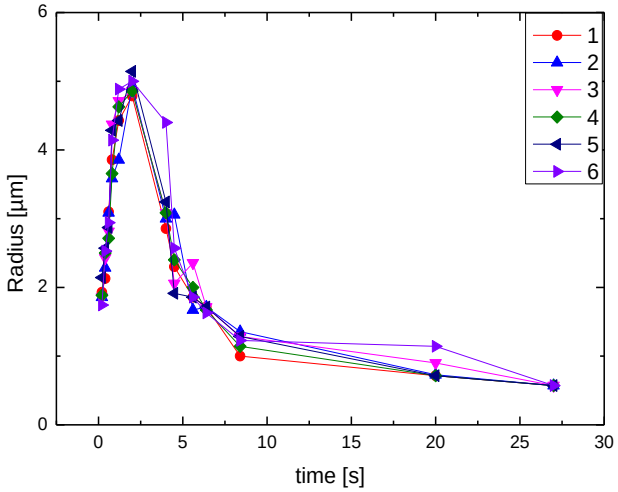

Figure 5.18: Bright ring radius measurements around 6 different particles inside the cell. All particles' ring radius changed similarly as the limited amount of D-alanine molecules inside the cell was equally disturbed between the particles.

Additionally, the diffusion constant D could be calculated by fitting the (eqn (15)) to the first part of experimental data till reaching the maximum intensity from chemical oxidative stress. Figure 5.19 illustrates the increase of the ring radius related to ROS formation around the particle over time. Data from the fit function of the curve could be used to determine the diffusion characteristic for *A. thaliana* cell.

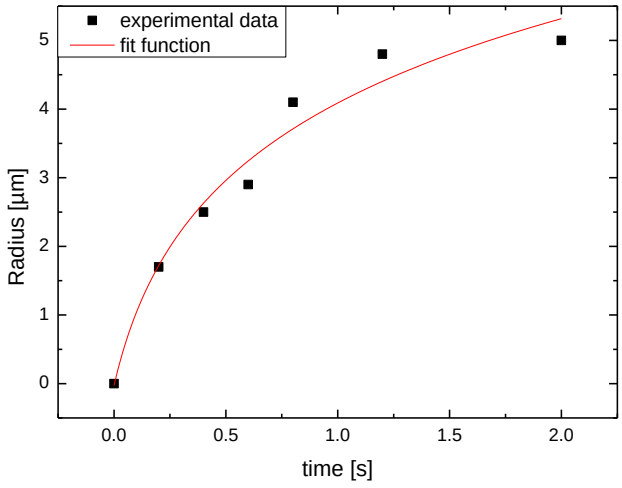

Figure 5.19: Increasing radius of bright ring around the particle because of ROS generation.

Diffusion time determined considering the fit function (eqn (15)) to experimental data as: D= 7.96×10^{-12} (m^2 s^{-1})

Summary

Manipulation experiments led us to calculate the diffusion constant in the interior of a Barley vacuole which can be attributed to the diffusivity in membrane adjacent fluids or dissolved carbohydrates. The calculated diffusion constants are important since by means of this parameter, the travel time of a particle with a certain molecular mass inside the cell can be determined.

Direct injection of single magnetic particles into the cells by microinjection rather than endocytosis allows for particle functionalization with antibodies, enzymes or specific surface groups and their site-specific placement inside the cell. It also provides the possibility of particle injection into other cell types, such as flexible fungus cells or into stiffer protoplasts containing chloroplasts in an easier and better controlled manner instead of the injection by particle a gun, there is no danger of bursting or damaging the cells.

In addition, direct injection of a single magnetic particle into a cell offers new opportunities for better understanding of the cell processes in signaling, toxicity, binding or catalysis. As an example, chemical oxidative stress induced by injecting the functionalized particle inside the cell gives the possibility to find the diffusion coefficient in the vacuole interior of an *A. thaliana* cell. A further achievement is the positioning the functionalized particle in a desired position and inducing the chemical oxidative stress inside the cell.

Another main issue of the present work is generating cell signals via generating heat stress locally inside the cell by TMCs in a controlled manner in order to find the heat stress signaling initiation point and studying the heat distribution inside the cell. These features make TMCs ideal for various cell or tissue studies such as heat capacity and heat transfer in a specific cell environment. TMCs are also used for monitoring temperature in optically dense soft materials. This experiment will be further developed by generating the heat stress by injecting the magnetic particles and attracting them with electrodes and heating with additional of electrodes at specific point inside the cell.

The summary of whole work in three different parts represented:

Manipulation of the magnetic particles inside a living cell

A silica glass slide was cleaned by acetone and ethanol and used as a substrate for the preparation of the electrodes. A metallic coat (Ta 10 *nm* & Au 200 *nm*) was deposited on the substrate by means of the Physical Vapor Deposition (PVD) method utilizing a DC magnetron sputtering in presence of Argon plasma and then

negative resist AR-N 7500/18 (ALLResist) was coated for e-Beam lithography. The sample was exposed to a 20 *kV* e-beam gun in the working distance of 15 *mm* from an Elphy Raith electron beam Lithography system (LEO Series 1530 Scanning Electron Microscope).

The structures of the electrodes were patterned with a 120 μm aperture. The exposure dose was optimized to prevent over-exposure of the electrodes' structure. After developing the sample by developer AR 300-47 (ALLResist) for 4 minutes, it was cleaned in water and dried by nitrogen gas. Then the second lithography step was applied followed by an ion beam etching procedure. The ion source operates at a discharge voltage of 50 *V*, beam voltage of 400 *V*, an accelerator voltage of 30 *V* and a beam current of 6 *mA*. Next the resist was removed by a dilution of 1-Methyl-2-pyrrolidinone, Chromasolv plus from Aldrich Co. in an ultrasonic bath at a temperature of 60 ˚*C* to 80 ˚*C* for 15 minutes and then rinsing by ethanol. Then 75 *nm* of Ta_2O_5 was sputtered as a protection layer by means of RF magnetron sputtering in combination of oxygen and argon. Finally the sample was installed on a ceramic IC socket and a flexible, colorless and transparent resist (Schutzlack 70) was sprayed on top to provide further protection for the electrodes.

For testing the sample, water environment was selected to manipulate 1.05 μm myone magnetic particles. The movement of the particle was studied and the results analyzed. For normalization, the viscosity of water was calculated by this experiment as $\eta_{Water} = 8.79\times10^{-4} \pm 8.1\times10^{-6}\ Pa.s$ and then compared to standard value of water viscosity in other literatures $\eta_{Water} = 8.89\times10^{-4}\ Pa.s$.

For manipulation experiments in Barley cells, a holding pipette was used to trap the cell on top of electrodes. The optimized parameters for the holding pipette to hold the Barley cell were found as ID: 6.5 μm, OD: 100 μm, bending length: 500 μm and bending angle: 35˚. The injection ICSI (Intracytoplasmic sperm injection) capillary used to inject 1.05 μm particles into the Barley cells. The parameters of the injecting capillary were optimized as ID: 4 μm, bending angle: 35˚and bending length 500 μm. For manipulation purposes, a dilution (1:100,000) used to inject the particle into the cell while applying 143 *hPa* pressure.

Manipulation in the Barley cells carried out and the movement of particles studied and the viscosity of the Barley determined $\eta_{Barley} = 3.55\times10^{-3} \pm 1.41\times10^{-4}\ Pa.s$ as a result. Also a characteristic diffusion time was calculated for various molecules.

Manipulation experiment repeated in vacuole fluid to study the effect of cell membrane on movement of the particle inside the living cell. Viscosity of vacuole fluid, calculated as $\eta_{vacuolefluid} = 1.41\times10^{-3} \pm 3.65\times10^{-4}\, Pa.s$

Heat stress

For heating experiment, a standard borosilicate glass capillary (without filament) was utilized with inner diameter of ID: 0.78 *mm*, outer diameter of OD: 1 *mm* and a total length of 70 *mm*. To prepare the Thermo Micro Capillary (TMC), they should be cleaned with acetone, ethanol and dried with nitrogen gas and then pulled to reach 500 *nm* outer diameter. Capillaries coated by a thin layer (200 *nm*) of Ta on two opposite sides with an overlapped area on the capillary tip, which acts as an electrical resistance so that it generates heat when an electrical voltage is applied. After coating, the capillary was annealed in 300 ˚*C* for 1 hour to provide more stability during the heating experiment. The resistance of the capillaries used in this thesis ranged from 3 *k*Ω to 8.38 *k*Ω.

Different voltages (10*V*, 15*V* & 20 *V* DC) were applied to the capillary and the tip temperature was monitored to calibrate the TMC. A maximum temperature difference generated by capillary was observed as ΔT=23.5 ˚*C*.

Stimulating cell signals by heat stress was performed by penetrating the TMC into an *A. thaliana* cell which was incubated in 2′,7′-dichlorofluorescein fluorescent dye. With TMC resistance of 3 *k*Ω and an applied voltage of 20*V* DC, heat shock response of *A. thaliana* protoplasts visualized as oxidative stress induced green fluorescence emitted from 2′,7′-dichlorofluorescein during 70 minutes. The relative intensity of the protoplast was obtained by converting fluorescence intensity into a grey scale and integrating the whole imaging area of the protoplast. As a negative control experiment, these steps were repeated without applying a electric voltage to the TMC. No signal was detected for the negative control experiment.

Chemical oxidative stress

To stimulate cell signals by oxidative stress, experiments were carried out in three steps. The first was simulating the cell condition to oxidative stress in a hole that contains 2 *μM* DCF-DA and a dilution of 2.8 *μm* coupled streptavidin particles with 0.08 *μg/ml* DAAO and the detecting the oxidation stress by adding 10 *mM* D-alanine which initiates the reaction after 10 minutes.

1.05 μm streptavidin particles were used in the second step in a dilution of (1:100) coupled with DAAO (0.08$\mu g/ml$). 1 μL D-alanine was added to the composition and after 15 minutes the coupled particles inside the hole started to glow because of H_2O_2 formation around the particles. The intensity of light around the particle decreased over time.

The last step of the experiment was detecting the local ROS formation inside the *A. thaliana* cell. Preloaded *A. thaliana* cells in 2 μM H_2DCF-DA were used in this test. After injecting the (1:10,000) dilution of coupled streptavidin particles with 0.08 $\mu g/ml$ DAAO into the cell, 10 mM D-alanine was added to top of the cell. After defusing the D-alanine into the cell and chemical reaction generated H_2O_2 around the particles. The intensity of light increased because of oxidative stress up to a maximum value and then decreased again.

Future plans

The aim of this thesis is activating cell signals locally by means of heat or chemical stress using a magnetic or functionalized particle or TMC´s. The results can be used to determine the viscosity of the vacuole interior and to deduce characteristic diffusion constants through a vacuole for various molecules and proteins.

Positioning the 1.05 μm magnetic particle in a specific location inside the living cell was done by means of special designed microelectrodes. Future plans for this part are using nano-particles for the experiment with a narrow ICSI capillary to minimize the damage to the cells during the experiment and to provide an injection that is more accurate and more information from the cells. As it is shown in Figure 1, the manipulation was done by 100 *nm* fluorescent particle on top of electrodes.

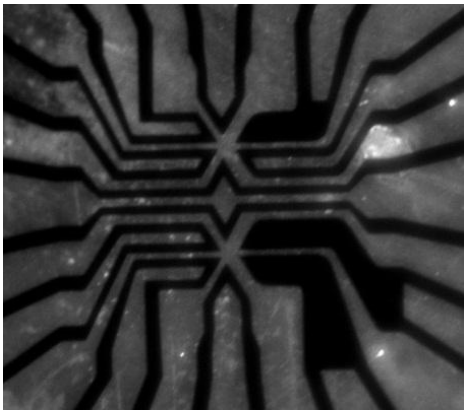

Figure 1: Manipulation 100 *nm* red florescent particles on top of electrodes

The stimulation of cells to obtain the heat stress signals was performed by heating a TMC. The next step to develop this experiment is generating cell signals locally using a magnetic particle, which is positioned and heated by magnetic electrodes to induce the heat inside the cell in a specific location. Another development is using the specific design for electrodes with Ni-Cr to generate heat and position the cell on top of the electrodes using a holding capillary to get the signals.

Chemical oxidative stress of *A. thaliana* cell was studied by injecting coupled streptavidin particle with DAAO into the cell and adding D-alanine on top. A further development is anticipated to localize chemical oxidative stress inside the cells by positioning the functionalized magnetic particles in specific locations by means of magnetic electrodes and then adding D-alanine to initiate the reaction.

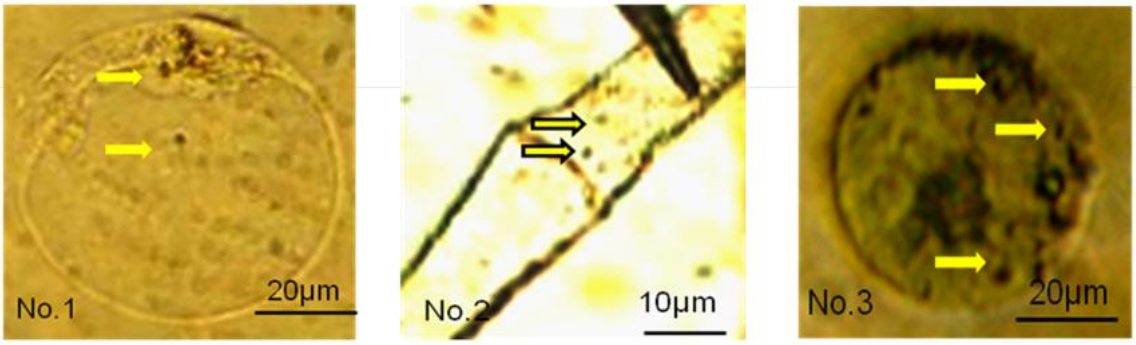

Figure 2: Injection of 1 μm particles inside three different cells immobilized in Agarose. No.1 is Barley epidermis protoplast (Hordeum vulgare), No.2 is Fungus (Mucor mucedo) and No.3 is Mesophyll protoplast

Figure 2 shows the injection of 1.05 μm magnetic particles into three different cells (Fungus, *A. thaliana* epidermis protoplast and Mesophyll protoplast of Barley). However due to flexibility of the methods presented in this thesis, further development plans can be designed and executed with various types of cells other than those presented here. Certainly manipulation experiment by magnetic electrodes can be performed for these systems as well. Additionally, viscosity and characteristic diffusion times for such systems can be determined or the reaction of these cells against chemical and heat stresses can be studied.

Appendices

Appendix1: C factor in the force equation (eqn (1))

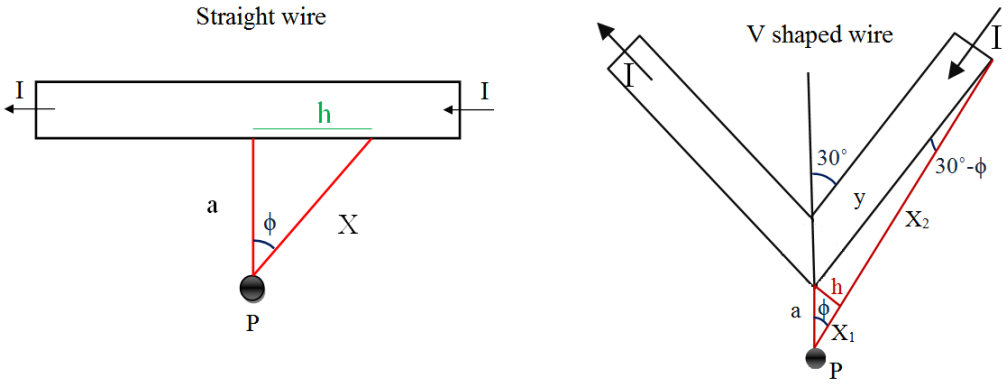

Fig. 1: Position of the magnetic particle in relation to the electrode

$$c = \frac{F_{mag.V\ shaped}}{F_{mag.\ straight}} \tag{1}$$

According to (Fig 1.a and b) the relation between X and ϕ is calculated by basic trigonometric equations, eqn (2) to eqn (5).

$$\sin(\varphi) = \frac{h}{a} \tag{2}$$

$$\cos(\varphi) = \frac{X_1}{a} \tag{3}$$

$$\sin(30° - \varphi) = \frac{h}{y} \tag{4}$$

$$\cos(30° - \varphi) = \frac{X_2}{y} \tag{5}$$

Using previous equations, X_1, X_2 and X3 are calculated as follows:

$$X_1 = a{\cdot}\cos(\varphi) \ , \ X_2 = \frac{a{\cdot}\cos(30-\varphi){\cdot}\sin(\varphi)}{\sin(30-\varphi)} \quad \text{and} \quad X_3 = \frac{a}{\cos\varphi}$$

Replacing X_1, X_2 and X_3 in (eqn (1)), results an estimate value for C:

$$c = \frac{F_{mag.V\ shaped}}{F_{mag.\ stright\ shaped}} = \frac{2\int_0^{\frac{\pi}{6}} \frac{1}{(x_1 + x_2)^3(\varphi)}\, d\varphi}{2\int_0^{\frac{\pi}{2}} \frac{1}{{x_3}^3(\varphi)}\, d\varphi}$$

$$c = \frac{2\int_0^{\frac{\pi}{6}} \frac{1}{\left(a \cdot \cos(\varphi) + \frac{a \cdot \cos(30-\varphi) \cdot \sin(\varphi)}{\sin(30-\varphi)}\right)^3 (\varphi)}\, d\varphi}{2\int_0^{\frac{\pi}{2}} \frac{1}{\left(\frac{a}{\cos(\varphi)}\right)^3}\, d\varphi} = 0.2145$$

Above C value was used in finite differential equation (numerical method) to calculate x value point by point, but the curve resulted by these points did not fit the experimental data point. C value then was modified to find the best fit matching both the numerical method data and experimental data. As it shown in (Fig 5.8) best value for C is (C= 0.19).

Appendix 2: Control experiment for fluid temperature monitoring during the experiments

Temperature is one of the important factors having direct effect on the viscosity. Viscosity of a fluid reduces dramatically as the temperature rises. As an example, the viscosity of water at different temperatures is represented in (Fig 2).

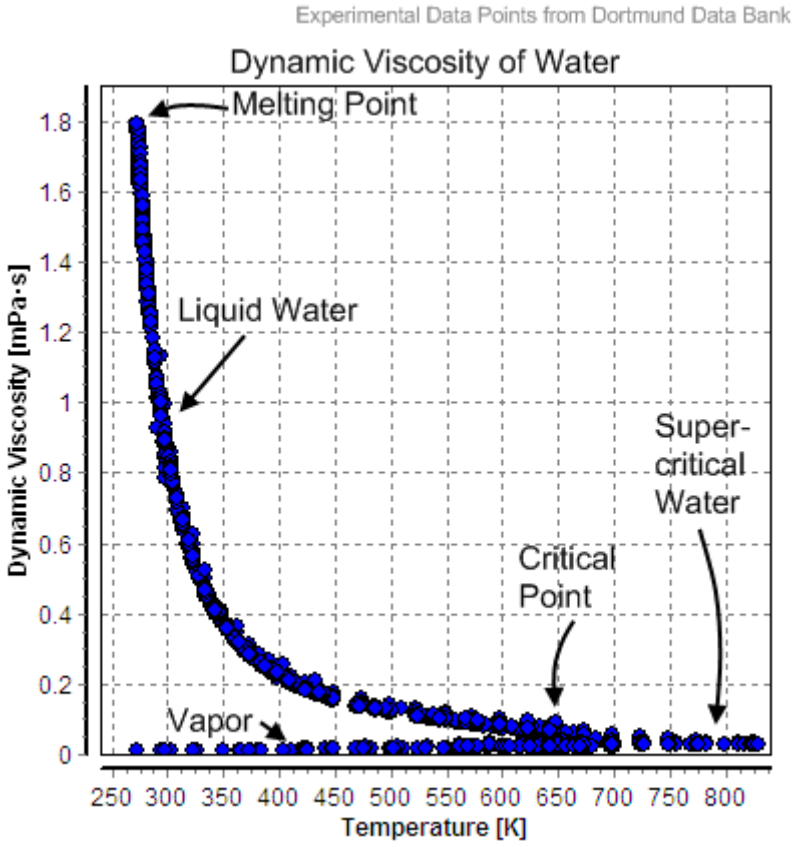

Fig .2: Dynamic Viscosity of Water. [Experimental data are taken from Dortmund Data Bank]

To ensure temperature of media does not change due to the microscope light or other heat sources during manipulation experiment, and hence to guarantee the accuracy of the measurements for viscosity calculations, a control experiment set up to monitor the temperature of media during manipulation, in presence of microscope light and room condition. A NiCr-Ni thermo-element was utilized to

measure the temperature difference. One side of the micro capillary was coated with NiCr and the other side with Ni. These two coatings were connected to a Nano-voltmeter measuring the potential difference during the control experiment. Although the duration of the manipulation test is less than one minute, fluid temperature in control experiment monitored for 14 minutes. (See Fig 3)

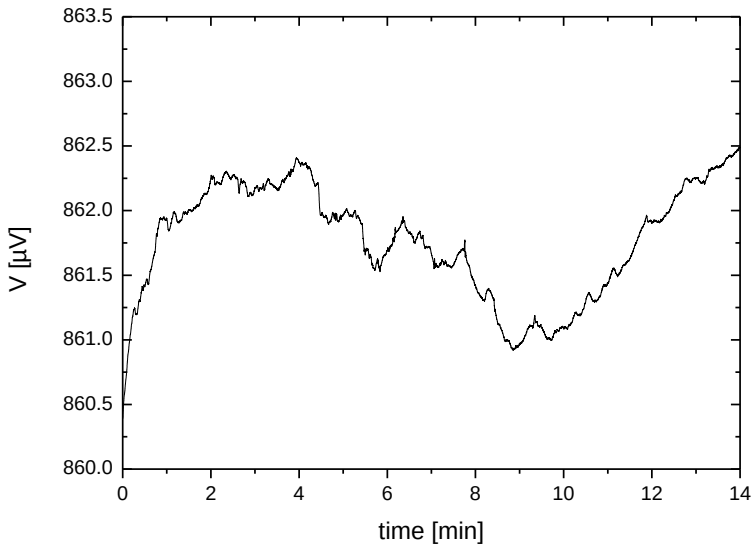

Fig 3: Output voltage of a thermocouple NiCr-Ni versus time

Using the control experiment data (Fig. 3) and considering the Seebeck coefficient of NiCr-Ni, S= 40µV temperature rise of the media calculated as below (eqn (6)):

$$S = \frac{\Delta V}{\Delta T} \tag{6}$$

$$40\mu V\ K^{-1} = \frac{2\mu V}{\Delta T}$$

$$\Delta T = 0.05\ ^{\circ}C$$

According to this experiment, no significant temperature rise observed during 14 minutes experiment period. This proves that the temperature of the media during manipulation experiment and therefore the viscosity of the media are constant during the manipulation experiment.

Appendix 3: Finite differential method:

Assuming the function whose derivatives are to be approximated is properly-behaved, by Taylor's theorem,

$$f(x_0 + h) = f(x_0) + \frac{\dot{f}(x_0)}{1!}h + \frac{\ddot{f}(x_0)}{2!}h^2 + \cdots + R_n(x)$$

Where n! denotes the factorial of n and Rn (x) is a remainder term, denoting the difference between the Taylor polynomial of degree n and the original function. Again using the first derivative of the function f as an example, by Taylor's theorem,

$$f(t_0 + h) = f(t_0) + \dot{f}(t_0)h + R_1(t)$$

Setting, t_0=a and (t-a) =h we have,

$$f(t + h) = f(t) + \dot{f}(t)h + R_1(t)$$

Dividing across by h gives:

$$\frac{f(t + h)}{h} = \frac{f(t)}{h} + \dot{f}(t) + \frac{R_1(t)}{h}$$

Solving for f'(a)

$$\dot{f}(t) = \frac{f(t + h) - f(t)}{h} - \frac{R_1(t)}{h}$$

So that for $R_1(t)$sufficiently small

$$\dot{f}(t) \approx \frac{f(t + h) - f(t)}{h}$$

Consequently by using this method $\ddot{f}(x_0)$ will be found as below:

$$\ddot{f}(t) \approx \frac{f(t-h) - 2f(t) + f(t+h)}{h^2}$$

By replacing the $\ddot{f}(t)$ and $\dot{f}(t)$ in (eqn (12)),

$$m\ddot{f}(t) = \frac{K_1}{x^2} + \frac{K_2}{x^3} + K_3\dot{f}(t)$$

(eqn (13)) obtained as below:

$$x(t+h) = \frac{\frac{K_1}{x^2(t)} + \frac{K_2}{x^3(t)} - \left(\frac{2m}{h^2} - \frac{K_3}{h}\right)x(t) - \frac{m}{h^2}x(t-h)}{\left(\frac{m}{h^2} - \frac{K_3}{h}\right)}$$

References

[1]de Vries A. H. B., Krenn B. E., Drie R. V., Kanger J. S., Micro Magnetic Tweezers for Nanomanipulation Inside Live Cells, Biophysical Journal, 88: 2137-2144, (2005)

[2]Chin C. D., Linder V. and Sia S. K., Commercialization of micro fluidic point-of-care diagnostic device, Lab Chip, 12: 2118-2134, (2012)

[3]Wu C., heat shock transcription factors: Structure and Regulation, Annual Review of Cell and Developmental Biology, 11: 441-469, (1995)

[4]Allakhverdiev S. I., Kreslavski V., Klimov V. V., Los D.A., Carpentier R., Mohanty P., Heat stress: an overview of molecular responses in photosynthesis, Photosynth Research Journal, 98: 541-50, (2008)

[5]Baniwal S. K., Heat stress response in plants: a complex game with chaperones and more than twenty heat stress transcription factors, Journal of Bioscience, 29: 471-487, (2006)

[6]Turner J. G., Ellis Ch., Devoto A., The jasmonate signal pathway, Plant Cell, 14: 153-164, (2002)

[7]Maksymiec W., Signaling responses in plants to heavy metal stress, Acta Physiologiae Plantarum, 29: 177-187, (2007)

[8]Sinha A. K., Jaggi M., Raghuram B. and Tuteja N., Mitogen-activated protein kinase signaling in plants under abiotic stress, Plant Signaling & Behavior, 6: 196-203, (2011)

[9]Boyer J. S., Plant productivity and environment, Science, 218: 443-448, (1982)

[10]Berry J. A. and Bjorkman O., Photosynthetic response and adaptation to temperature in higher plants, Annual Review of Plant Physiology, 31: 491-543, (1980)

[11]Ohara-Imaizumi M., Yoshida M., Aoyagi K., Saito T., Okamura T., Takenaka H., Akimoto Y., Nakamich Y., Takanashi-Yanobu R., Nishiwaki C., Kawakami H., Kato N., Hisanaga Sh., Kakei M., Nagamatsu Sh., Deletion of CDKAL Affects Mitochondrial ATP, Generation and First-Phase Insulin Exocytosis, PLoS ONE, 5, e15553, (2010)

[12]Aro E. M., Virgin I., Andersson B., Photoinhibition of photosystem II: inactivation, protein damage and turnover, Biochimical and Biophysical Acta, 1143: 113-134, (1993)

[13]Carpentier R., Effect of high-temperature stress on the photosynthetic apparatus. Handbook of plant and crop stress, Marcel Dekker Inc, New York, Second Edition, eBook ISBN: 978-0-8247-4672-8, 337-348, (1999)

[14]Al-Khatib K., Paulsen G. M., Enhancement of thermal injury to photosynthesis in wheat plants and thylakoids by high lightintensity, Plant Physiology, 90: 1041-1048, (1989)

[15]Adir N., Zer H., Shochat S., Ohad I., Photoinhibition a historical perspective, Photosynth Research, 76: 343-370, (2003)

[16]Nishiyama Y., Yamamoto H., Allakhverdiev S. I., Inaba M., Yokota A., Murata N., Oxidative stress inhibits the repair of photo-damage to the photosynthetic machinery, EMBO Journal, 20: 5587-5594, (2001)

[17]Takahashi S., Murata N., How do environmental stress esaccelerate photo inhibition? Trends in Plant Science, 13: 178-182, (2008)

[18]Suzuki N., Mittler R., Reactive oxygen species and temperature stresses: a delicate balance between signaling and destruction, Plant Physiology, 126: 45-51, (2006)

[19]Baniwal S. K., Bharti K., Chan K. Y., Fauth M., Ganguli A., Kotak S., Mishra S. K., Nover L., Port M., Scharf K. D., Tripp J., Zielenski C. D., Koskull-Döring P.V., Heat stress response in plants: a complex game with chaperones and more than twenty heat stress transcription factors, Journal of Biosciences, 29: 471-487, (2004)

[20]Mittler R., Oxidative stress, antioxidants and stress tolerance, Trends in Plant Science, 7: 405-10, (2002)

[21]Gill S.S., Tuteja N., Reactive oxygen species and antioxidant machinery in abiotic stress tolerance in crop plants, Plant Physiology and Biochemistry, 48: 909-930, (2010)

[22]Asada K., The water-water cycle in chloroplasts: scavenging of active oxygen and dissipation of excess photons, Annual Review of Plant Physiology and Plant Molecular Biology, 50: 601-39, (1999)

[23]Kim J. A., Agrawal G. K., Rakwal R., Han K. S., Kim K. N., Yun Ch. H., Heu S., Park S. Y., Lee Y. H., Jwa N. S., Molecular cloning and mRNA expression analysis of a novel rice (Oryza sativa L.) MAPK kinase, OsEDR1, an ortholog of Arabidopsis AtEDR1, reveal its role in defense/stress signaling pathways and development, Biochemical and Biophysical Research Communications, 300: 868-876, (2003)

[24]Bukhov N. G., Carpentier R., Heterogeneity of photosystem II reaction centers as influenced by heat treatment of barley leaves, Plant Physiology, 110: 279-285, (2000)

[25]Liszkay K., A Singlet oxygen production in photosynthesis, Journal of Experimental Botany, 56: 337-346, (2005)

[26]Asada K., Production and scavenging of reactive oxygen species in chloroplasts and their functions, Plant Physiology, 141: 391-396, (2006)

[27]EL-Shitinawy F., Ebrahim M. K. H., Sewelam N., EL-Shourbagy M. N., Activity of photosystem 2, lipid peroxidation, and the enzymatic antioxidant protective system in heat shocked barley seedlings, Photosynthetica, 42: 15-21, (2004)

[28]Krupa Z., Siedlecka A., Maksymiec W., Baszyn´ski T., In vivo response of photosynthetic apparatus of Phaseolus vulgarisL. to nickel toxicity, Journal of Plant Physiology,142: 664-668, (1993)

[29]Casella S., Frassinetti S., Lupi F., Squartini A., Effect of cadmium, chromium and copper on symbiotic and free-living Rhizobium leguminosarium biovar trifolii, FEMS Microbiology Letters, 49: 343-347, (1988)

[30] Mishra K. P., Fluorescence studies on radiation oxidative damage to membranes with implications to cellular radiosensitivity, Indian Academy of Science, (Chem. Sci.), 114: 705–711, (2002)

[31] Curtin J. F., Donovan M., Cotter T. G., Regulation and measurement of oxidative stress in apoptosis, Journal Immunol Methods, 265: 49-72, (2002)

[32]Lidstrom M.E. and Meldrum D. R., Life-on-a-chip, Nature Reviews Microbiology, 1: 158-164, (2003)

[33]Jordan P., Leach J., Padgett M., Blackburn P., Isaacs N., Goksör M., Hanstorp D., Wright A., Girkin J., Cooper J., Creating permanent 3D arrangements of isolated cells using holographic optical tweezers, Lab Chip, 5: 1224-1228, (2005)

[34]Albrecht D. R., Tsang V. L., Sah R. L., Bhatia S. N., Photo- and electropatterning of hydrogel-encapsulated living cell arrays, Lab Chip, 5: 111-118, (2005)

[35]Braschler T., Johann R., Heule M., Metref L., Renaud P., Gentle cell trapping and chip by in situ alginate hydrogel formation, Lab Chip, 5: 553-559, (2005)

[36]Johann R. M., Cell trapping in microfluidic chips, Analytical and Bioanalytical Chemistry , 385: 408-412, (2006)

[37]Voldman J., Gray M. L., Toner M., Schmidt M. A., A microfabrication-based dynamic array cytometer, Analytical Chemistry, 74: 3984-3990, (2002)

[38]Chou C. F., Zenhausern F., Electrodeless dielectrophoresis for micro total analysis systems, IEEE Engineering in Medicine and Biology Magazine, 22: 62-67, (2003)

[39]Holmes D., Green N. G., Morgan H., Dielectrophoretic flow-through separation systems: Comparison of experimental and numerical simulations, IEEE Engineering in Medicine and Biology Magazine, 22: 85-90, (2004)

[40]Wiklund M., Spégel P., Nilsson S., Hertz H. M., Ultrasonic-trap-enhanced selectivity in capillary electrophoresis, Ultrasonics, 41: 329-333, (2003)

[41]Lilliehorn T., Simu U., Nilsson M., Almqvist M., Stepinski T., Laurell T., Nilsson J., Johansson S., Trapping of microparticles in the near field of an ultrasonic transducer, Ultrasonics, 43: 293-303, (2005)

[42]Hertz H. M., Standing-wave acoustic trap for nonintrusive positioning of microparticles, Journal of Applied Physics, 78: 4845-4849, (1995)

[43]Hochmuth R. M., Micropipette aspiration of living cell, Journal of Biomechanics, 33: 15-22, (2000)

[44]Chiou P. Y., Ohta A. T., Wu M. C., Massively parallel manipulation of single cells and microparticles using optical images, Nature, 436: 370-372, (2005)

[45]Kimura T., Sato Y., Kimura F., Iwasaka M., Ueno S., Micropatterning of Cells Using Modulated Magnetic Fields, Langmuir, 21: 830-832, (2005)

[46]Khademhosseini A., Yeh J., Eng G., Karp J., Kaji H., Borenstein J., Farokhzad O. C., Langer R., Cell docking inside microwells within reversibly sealed microfluidic channels for fabricating multiphenotype cell arrays, Lab Chip, 5: 1380-1386, (2005)

[47]Tanyeri1 M., Johnson-Chavarria E. M. and Schroeder Ch. M., Hydrodynamic trap for single particles and cells, Applied Physics Letters, 96, 224101-1_224101-3, (2010)

[48]Zhang Y., Yu L. C., Single-cell microinjection technology in cell biology, bioessays, 6: 606-610, (2008)

[49]http://www.sutter.com/contact/faqs/Introduction%20to%20Microinjection.pdf

[50]http://www.sutter.com/contact/faqs/pipette_cookbook.pdf

[51]Safarik I. and Safarikova M., Use of magnetic techniques for the isolation of cells, Journal of Chromatography B: Biomedical Sciences and Applications , 722: 33-53, (1999)

[52]Ito A., Shinkai M., Honda H. and Kobayashi T., Medical application of functionalized magnetic nanoparticles, Journal of Bioscience and Bioengineering, 100: 1-11, (2005)

[53]Pamme N., Magnetism and micro fluidics, Lab Chip, 6: 24-38, (2006)

[54] Lee H., Purdon A. M. and Westervelt R. M., Manipulation of biological cells using a microelectromagnet matrix, Applied Physics Letter, 85: 1063-1065, (2004)

[55] Furdui V. I., Kariuki J. K. and Harrison D. J., Microfabricated electrolysis pump system for isolating rare cells in blood Micromech, Journal of Micromechanics and Microengineering, 13: 164-170, (2003)

[56]Xia N., Hunt T. P., Mayers B. T., Alsberg E., Whitesides G. M., Westervelt R. M. and Ingber D. E., Combined microfluidic-micromagnetic separation of living cells in continuous flow, Biomedical Microdevlopment, 8: 299-308, (2006)

[57]Inglis D. W., Riehn R., Austin R. H. and Sturm J. C., Continuous microfluidic immunomagnetic cell separation, Applied Physics Letter, 85: 5093-5095, (2004)

[58]Islam D., Lindberg A. A., Clin J., Detection of Shigella dysenteriae type 1 and Shigella flexneri in feces by immunomagnetic isolation and polymerase chain reaction, Microbiology, 30: 2801-2806, (1992)

[59]Choi J. W., Oh K. W., Thomas J. H., Heineman W. R., Halsall H. B., Nevin J. H., Helmicki A. J., Henderson H. T. and Ahn C. H., An integrated microfluidic biochemical detection system for protein analysis with magnetic bead-based sampling capabilities, Lab Chip, 2: 27-30, (2002)

[60]Gijs M. A. M., Magnetic bead handling on-chip: new opportunities for analytical applicationsMicrofluid, Nanofluid, 1: 22-40, (2004)

[61]Siegel A. C., Shevkoplyas S. S., Weibel D. B., Bruzewicz D. A., Martinez A. W. and Whitesides G. M., Cofabrication of Electromagnets and Microfluidic Systems in Poly(dimethylsiloxane), Angewandte Chemie International Edition,45: 6877-6882, (2006)

[62]BioMag, Bangs Laboratories,Inc.,
http://www.bangslabs.com/sites/default/files/bangs/docs/pdf/PDS_547.pdf

[63]COMPEL, Bangs Laboratories, Inc.,
http://www.bangslabs.com/sites/default/files/bangs/docs/pdf/PDS_705.pdf

[64]SPHERO, Spherotech, Inc.,
www.spherotech.com/para_par.htm

[65]Jackson J. D., Classical Electrodynamics, 3nd ed, united state America. John. ISBN: 0-471-30932-X, (1998)

[66]Purcell E. M., Electricity and Magnetism, 2nd ed. New York, NY: McGraw-Hill, ISBN: 9780070049086, (1984)

[67]Bleaney B. I. and Bleaney B., Electricity and Magnetism, Oxford University Press, Oxford, England, New York, USA, ISBN: 9780198511724, (1989)

[68]Shevkoplyas S., Siegel A. C., Westervelt R. M., Prentissc G. M. and Whitesides G. M., The force acting on a superparamagnetic bead due to an applied magnetic Field, Lab Chip, 7: 1294-1302, (2007)

[69]Batchelor G. K., An Introduction to Fluid Dynamics, Cambridge University Press, Cambridge, England, ISBN-10: 0521663962, (2000)

[70]Vernon-Parry K. D., Scanning electron microscopy: an introduction, III-Vs Review,13: 40-44, (2000)

[71]Kelly P. J. and Arnell R. D., Magnetron sputtering: a review of recent developments and applications, Vacuum, 56: 159-172, (2000)

[72]Grove W. R., On the electro-chemical polarity of gases, Philosophical transactions of the Royal Society of London, 142: 87ff, (1852)

[73] Panhorst M., On-chip manipulation and positioning of biomolecules with magnetic beads, PhD thesis, Bielefeld University, (2005)

[74]Waser, Rainer (ed.), Nanoelectronics and information technology, Advanced electronic materials and novel devices, Willey-VCH Verlag, ISBN: 978-3-527-40927-3, (2003)

[75]Venkatesh A. G., Novel Platform for DNA Alignment and Studying DNA-Protein Interaction in Realtime, PhD thesis, Bielefeld University, (2011)

[76]Reichmanis E., et al. , Lithographic Resist Materials Chemistry, Annual Review of Materials Science, 23: 11-43, (1993)

[77]Albon C., Integration of tunneling magnetoresistive sensors for high resolutive magnetic particle detection, PhD thesis, Bielefeld University, (2009)

[78]El-Ghandoor H., Synthesis and Some Physical Properties of Magnetite (Fe_3O_4) Nanoparticles, International Journal of Electrochemical Science, 7: 5734-5745, (2012)

[79]Hu L. and Hach D., One step grafting of monomethoxy poly(ethylene glycol) during synthesis of maghemite nanoparticles in aqueous medium , Physicochemical and Engineering Aspects, 330: 1-7, (2008)

[80]Hoet P. H. M., Brüske-Hohfeld I., Salata O. V., Nanoparticles – known and unknown health risks, Journal of Biotechnology, 2: 12, (2004)

[81]Buschow K. H. J., Handbook of Magnetic Materials, Elsevier B. V. Vol. 16, ISBN:10: 0444518509, (2006)

[82]Sellmyer D. and Skomski R., Advanced Magentic Nanostructures, Springer, ISBN:10: 0387233091, (2005)

[83]Fonnum G., Johansson C., Molteberg A., Morup S., Aksnes E., Characterisation of Dynabeads® by magnetization measurements and Mössbauer spectroscopy, Journal of Magnetism and Magnetic Materials, 293: 41-47, (2005)

[84]Green M. N., Avidin, Advances in Protein Chemistry, 29: 85-133, (1975)

[85]Hendrickson W., Pähler A., Smith J. L., Satow Y., Merritt E. A., and Phizackerley R., Crystal structure of core streptavidin determined from multiwavelength anomalous diffraction of synchrotron radiation, Proceedings of the National Academy of Sciences, USA Biophysics, 86: 2190-2194, (1989)

[86]Chaiet L. and Wolf F. J., The properties of streptavidin, abiotin-binding protein produced by streptomycetes, Archives of Biochemistry and Biophysics, 106: 1-5, (1964)

[87]RCSB Protein Data Bank.
http://www.rcsb.org/pdb/

[88]Berneis K., La Belle M., Blanche P. J. and Krauss R. M., Analysis and quantitation of biotinylated apob-containing lipoproteins with streptavidin-cy3, Journal of Lipid Research, 43: 1155-1159, (2002)

[89]Badr A., Müller K., Schäfer-Pregl R., El Rabey H., Effgen S., Ibrahim H. H., Pozzi C., Rohde W. and Salamini F., On the Origin and Domestication History of Barley (Hordeum vulgare), Molecular Biology and Evolution, 17: 499-510, (1983)

[90]Dietz K. J., Characterization of the epidermis from barley primary leaves, Planta, 187: 425-430, (1992)

[91]Kaiser G., Heber U., Photosynthesis of leaf cell protoplasts and permeability of the plasma lemma to some solutes, Planta, 157: 462-470, (1983)

[92]Meinke D. W., Cherry J. M., Dean C., Rounsley S. D., Koornneef M., Arabidopsis thaliana: A Model Plant for Genome Analysis, Science, 282: 662-682, (1998)

[93]SU-8 3000, www.microchem.com

[94]Bausch A. R., Möller W. and Sackmann E., Measurement of Local Viscoelasticity and Forces in Living Cells by Magnetic Tweezers, Biophysical Journal, 76: 573-579, (1999)

[95]Fonnuma G., Johanssonb Ch., Molteberga A., Morupc S., Aksnes E., Characterisation of Dynabeadss by magnetization measurements and Moessbauer spectroscopy, Journal of Magnetism and Magnetic Materials, 293: 41-47, (2005)

[96]Shevkoplyas S. S., The force acting on a superparamagnetic bead due to an applied magnetic Field, Lab Chip, 7: 1294-1302, (2007)

[97]Kestin J., Sokolov M. and Wakeham W. A., Viscosity of liquid water in the range 8 ˚C to 150 ˚C, Journal of Physical and Chemical Reference Data,7: 941-948, (1978)

[98]LeVeque R. J., Finite Difference Methods for Ordinary and Partial Differential Equations, ISBN: 978-0-898716-29-0, (2007)

[99]Gosse Ch. and Croquette V., Magnetic Tweezers: Micromanipulation and Force Measurement at the Molecular Level, Biophysical Journal, 82: 3314-3329, (2002)

[100]D-amino-acid oxidase Gene card.
http://www.genecards.org/cgi-bin/carddisp.pl?gene=DAO

[101]Erickson H. P., Size and Shape of Protein Molecules at the Nanometer Level Determined by Sedimentation, Gel Filtration and Electron Microscopy, Biological Procedures Online, 11: 32-51, (2009)

[102]Pollegioni L., Kinetic Mechanism of D-Amino Acid Oxidases from Rhodotorulagracilis and Trigonopsis variabilis, Journal of biological Chemistry 19: 13850-13857, (1993)

[103]Hultgren A., Tanase M., Chen C. S., Meyer G. J., Reich D. H., Cell manipulation using magnetic nanowires, Journal Of Applied Physics, 93: 7554-7556, (2003)

[104]Held P., An introduction to Reactive Oxygen Species, white Paper, Principle Scientist, Applications Dept., Bio Tek Instruments, Inc.

[105]http://www.bscb.org/?url=softcell/cellsignal

[106]Evgeniy Eruslanov E., Kusmartsev S., Identification of ROS Using Oxidized DCFDA and Flow-Cytometry, Methods in Molecular Biology, 594: 57-72, 2010

[107]Schubert J. R., Detektion der Hitzestressantwort an einzelnen Protoplasten von Arabidopsis thaliana, Bachelor-Arbeit, Bielefeld University, (2010)

[108]http://www.biomedical-instruments.de/index.php/products-side-menu/41-pipettes/pipettes-for-animal-research/321-biomedical-instruments-holding-pipettes

[109]http://www.biomedical-instruments.de/index.php/products-side-menu/47-pipettes/pipettes-for-animal-research/icsi-pipettes/2-biomedical-instruments-icsi-pipettes-with-spike

[110]Chinnusamy V., Schumaker K., Zhu J. K., Molecular genetic perspectives on cross-talk and specificity in abiotic stress signalling in plants, Journal of Experimental Botany, 55: 225-236, (2004)

[111] Sreenivasulu N., Sopory S. K., Kavi Kishor P. B., Deciphering the regulatory mechanisms of abiotic stress tolerance in plants by genomic approaches, Gene 388: 1-13, (2007)

[112]Eaton-Rye J. J., Baishnab C. T., Thomas D. Sh., (Eds.), Photosynthesis, Plastid Biology, Energy Conversion and Carbon Assimilation Series: Advances in Photosynthesis and Respiration, Vol. 34, ISBN 978-94-007-1579-0, (2012)

[113]Nover L., Heat stress response: a complex game with chaperones and transcription factors, Goethe University Frankfurt, (2000)